170

MARTIN MARIETTA ENERGY SYSTEMS LIBRARIES
3 4456 0361457 8

CENTRAL RESEARCH LIBRARY
DOCUMENT COLLECTION

ORNL-2835
Reactors - Power
TID-4500 (15th ed.)

GAS-COOLED REACTOR PROJECT

QUARTERLY PROGRESS REPORT

FOR PERIOD ENDING SEPTEMBER 30, 1959

CENTRAL RESEARCH LIBRARY
DOCUMENT COLLECTION
LIBRARY LOAN COPY
DO NOT TRANSFER TO ANOTHER PERSON
If you wish someone else to see this document, send in name with document and the library will arrange a loan.

OAK RIDGE NATIONAL LABORATORY
operated by
UNION CARBIDE CORPORATION
for the
U.S. ATOMIC ENERGY COMMISSION

~~LIBRARY REFERENCE COPY~~

Printed in USA. Price $3.00. Available from the

Office of Technical Services
Department of Commerce
Washington 25, D.C.

LEGAL NOTICE

This report was prepared as an account of Government sponsored work. Neither the United States, nor the Commission, nor any person acting on behalf of the Commission:

A. Makes any warranty or representation, expressed or implied, with respect to the accuracy, completeness, or usefulness of the information contained in this report, or that the use of any information, apparatus, method, or process disclosed in this report may not infringe privately owned rights; or

B. Assumes any liabilities with respect to the use of, or for damages resulting from the use of any information, apparatus, method, or process disclosed in this report.

As used in the above, "person acting on behalf of the Commission" includes any employee or contractor of the Commission, or employee of such contractor, to the extent that such employee or contractor of the Commission, or employee of such contractor prepares, disseminates, or provides access to, any information pursuant to his employment or contract with the Commission, or his employment with such contractor.

ORNL-2835

Reactors — Power
TID-4500 (15th ed.)

Contract No. W-7405-eng-26

GAS-COOLED REACTOR PROJECT
QUARTERLY PROGRESS REPORT
For Period Ending September 30, 1959

Staff
Oak Ridge National Laboratory

DATE ISSUED

NOV 25 1959

OAK RIDGE NATIONAL LABORATORY
Oak Ridge, Tennessee
operated by
UNION CARBIDE CORPORATION
for the
U. S. ATOMIC ENERGY COMMISSION

3 4456 0361457 8

CONTENTS

SUMMARY .....

PART 1. DESIGN INVESTIGATIONS

1. REACTOR PHYSICS 3

Power-Density Distribution in EGCR 3

Power-Density Distribution in Seven-Rod Cluster Fuel Elements 8

Power-Density Achievable in Gas-Cooled Reactors with Ceramic Fuel Elements 13

Physics of Fuel Element Clusters 19

Fast-Neutron Reactions in BeO 23

2. REACTOR DESIGN STUDIES 24

Structural Investigations 24
Study of Fuel Cladding Behavior Under Arbitrary Temperature Distributions 24
Creep Behavior of Fuel Element Cladding 30
Tests of Threaded-Pin-Type Graphite Column Joints ... 33
Tests of Metal-Clad Graphite Bodies 36

Thermal Performance of Fuel Elements 38
Thermal Analysis 38
EGCR Fuel Element Vibrations 42
Parametric Study 43

Helium Purification System for the EGCR 44

EGCR Hazards Evaluation 46

Design Study of Advanced Steam Generators 49

3. EXPERIMENTAL INVESTIGATIONS OF HEAT TRANSFER AND FLUID FLOW 54

Resistance-Heated-Tube Heat-Transfer Experiment 54

Mass-Transfer Measurements 59

Velocity Distribution in Septafoil Channels 63

PART 2. MATERIALS RESEARCH AND TESTING

4. METALLURGY 73

Fuel Materials Development 73
Fabrication of UO_2 73
High-Temperature Compression Testing of UO_2 73
Thermal Conductivity of UO_2 74
Fission-Product-Release Studies 74

Mechanical Properties of Fuel Capsule Material 75
Tube-Burst Tests 75
Modified Tube-Burst Tests 76
Strain-Cycling Tests 80
Collapsing Behavior 80
Effect of Mid-plane Spacers 81

Effect of Gaseous Environments on Properties of Type 304 Stainless Steel 82
Reactions of Type 304 Stainless Steel with Impurities in Helium 82
Creep Tests in Various Gaseous Environments 84

Manufacturing Development 86
End-Closure Evaluation 86
Mid-plane Spacer 86
Fuel Element Hangers 87
Helium Leak Testing of Fuel Capsules 87

Inspection of Fuel Capsule Tubing 88
Eddy-Current Inspection 88
Capsule Tubing Evaluation 94

Pressure Vessel Studies 96
Pressure Vessel Welding 96
Inspection of Pressure Vessel Welds 97

Beryllium Investigations 100
Welding and Brazing 100
Beryllium-Tubing Evaluation 100
Procurement of Beryllium Tubing 101
Gas-Metal Reactions of Beryllium 102

5. IN-PILE TESTING OF COMPONENTS AND MATERIALS 104

Fuel Capsule Irradiation Program 104
Full-Diameter Prototype Fuel Capsules 104
Reduced-Size Prototype Fuel Capsules 107
Minature Capsule Fission-Gas-Release Experiments 109

Fission-Gas-Release Studies 113
Instantaneous Fission-Gas-Release Experiment 113
Postirradiation Fission-Product-Release Studies 116
Stable Fission Gas Release 116

Examinations of Irradiated Capsules 116
Hot Cell Examinations at GEVAL 116
Modifications of ORNL Cell 6 119

Closed-Cycle-Loop Irradiation Facility in ORR 120

Thermocouple Irradiation Studies 120

Radiation Effects on Structural Materials 120
Steels 120
Beryllium 124

6. OUT-OF-PILE TESTING OF MATERIALS AND COMPONENTS 125

Materials Compatibility Tests 125
Static Helium Tests 125
Low-Pressure Thermal-Convection Loop Tests 128
High-Pressure Thermal-Convection Loop Tests 131
Forced-Circulation Loop Tests 132

Evolution of Gases from Graphite 132

Transport of Gases Through Graphite 142

Purification of Cooling Gas 143

Measurement of High Temperatures 146
Attachment of Thermocouples for Measurement of Surface Temperatures in High-Velocity Cooling Gas 146
Stability of Rhenium-Tungsten Thermocouples 149
Chromel-Alumel Thermocouple Drift Problem 150
Theoretical Effects of Transmutation on Thermocouples 150

Automatic Continuous Analysis of Helium from Test Loops 151

7. DEVELOPMENT OF TEST LOOPS AND COMPONENTS 153

ORR Gas-Cooled In-Pile Loops 153
GCR-ORR Loop No. 1 153
GCR-ORR Loop No. 2 154

Special Gas Compressors and Electric Motors 157
Grease-Lubricated Centrifugal Compressors 157
Regenerative Compressors 159
Compressors with Gas-Lubricated Bearings 161
Electric Motors for High-Temperature Service 162

GAS-COOLED REACTOR PROJECT QUARTERLY PROGRESS REPORT

SUMMARY

Part 1. Design Investigations

1. Reactor Physics

A four-group, two-dimensional, diffusion-theory calculation of the power-density distribution in the EGCR was made in order to reduce the uncertainties in the results of previous calculations. In the previous calculations the core was represented as a homogeneous medium with the control rods and the stainless steel experimental tubes represented as heterogeneities in the homogeneized core material. For the new calculations, all the heterogeneous characteristics of the EGCR core, including the eight experimental tubes, were included explicitly. Several results of significance to the design of the EGCR were obtained. In addition to the calculations for the entire EGCR core, a series of supercell calculations was made in which an experimental tube was placed at the center of a three-by-three array of fuel channels, and a calculation was made of the effect of an empty fuel channel on the power-density distribution.

A comparison was made of calculated neutron flux distributions in seven-rod fuel clusters and the preliminary experimental results obtained in the Physical Constants Test Reactor at Hanford. The comparison verified the model used for the P-3 calculations. Neutron flux ratios for the EGCR lattice cell were calculated for fuel enrichments of 2.0 and 2.6%.

Studies were made of the power densities attainable in gas-cooled reactors operated with ceramic material as both fuel and moderator. The results of the studies indicated that power densities of 100 to 200 w/cm^3 are possible with uranium-bearing graphite and that power densities of 50 to 100 w/cm^3 are achievable with uranium-bearing beryllium oxide. Considerations which may limit the power generation are thermal stresses in the fuel material, ability of the gas to transfer heat from the fuel

element surface and to remove the heat, and the effect of the rate of gas temperature rise on the length of the core. The data obtained in this study indicate that the maximum power densities are achieved with fuel element sections as thin as possible and cooling passages as small as possible.

Extensive studies were conducted to determine how the multiplication factor of a gas-cooled reactor varies with the number of rods in the fuel element cluster, cladding thickness, cladding material, inter-rod spacing, lattice pitch, solid and cored rods, fuel enrichment, and fuel-to-moderator ratio. The results show that greater subdivision of the fuel requires higher enrichment for a given fuel lifetime in the case of stainless steel cladding on UO_2. With beryllium cladding, however, a very small increase in enrichment is necessary when the number of rods in the cluster is increased from 7 to 61. Probabilities of fast-neutron reactions in beryllium and in beryllium oxide were determined.

2. Reactor Design Studies

A theoretical study is being conducted of the deflections (bowing) and stresses in fuel element cladding based on arbitrary temperature distributions. Results of linear theory calculations and series solutions are being compared. An analytical study is also being made to determine the magnitude of bowing as dictated by the creep characteristics of the material.

Tests were run to determine the load-carrying ability of the threaded-pin-type graphite column joints proposed for the EGCR. In the tests, pure moment loadings were applied to the graphite blocks, and deflections were measured at the joint. The pins did not appear to be notch sensitive; a brittle type of failure always occurred; and the elongation at rupture was negligible.

A test program was initiated for studying the behavior of metal-clad graphite bodies. The mode of collapse of the cladding onto the graphite bodies and the number of thermal cycles required to cause

failure will be determined. Fabrication of the test equipment and the first metal-clad graphite body were completed.

An analytical model for investigating temperature structure and thermal stability of a seven-rod fuel element cluster was developed that takes into account the effect of heat conduction around the circumference on the actual temperature and the effect of this temperature variation on the displacement or bow of the element. Results of calculations made with the use of this model were used in the above-described study of the deflection and stresses in the fuel element cladding.

Calculations have been made of the natural frequencies and an amplitude of vibrations in the EGCR fuel element clusters. This investigation is part of an over-all study of the aerodynamic stability of the element.

A parametric study was completed from which the following three dependent variables can be evaluated for a helium-cooled reactor fueled with UO_2 clad with stainless steel: (1) diameter of the coolant channel, (2) pressure drop across the core, and (3) pumping power. The charts prepared in this study facilitate a rapid evaluation of the thermal performance of the reactor.

A detailed analysis was made of the helium purification system needed for limiting graphite burnup and carbon mass-transfer in the EGCR. The recommended purification system incorporates the following units and operations: (1) a catalytic converter, a cooler condenser, a silica-gel adsorber, a Linde molecular sieve adsorber, and a filter and compressor unit. The proposed purification system does not include provisions for the planned removal of radioactive impurities, such as krypton or xenon, or for the removal of minor impurities, such as nitrogen and argon.

Discussions with members of the Hazards Evaluation Branch revealed concern about several points in the EGCR Hazards Report as submitted previously, and assistance was given to Kaiser Engineers and Allis-Chalmers Manufacturing Company in the preparation of a supplemental report. The points covered in the supplemental report included (1) the gaseous contamination within the containment vessel following the maximum credible

accident, (2) the total exposure as a function of distance from the containment shell following the maximum credible accident (including justification of the self-shielding in the calculation of direct exposure from the activity released to the containment shell), (3) the sources of water within the containment shell, and (4) the discharge of activity from relief valves.

In a design study of advanced steam generators, data were obtained with which to evaluate the effects of fin height and tube diameter on the pressure vessel. For a reactor output of 1320 Mw, it was found that, to achieve the minimum over-all vessel height, the fin height should be about 1/8 in. and that bare tubes give nearly as small a vessel height. Data are presented to show the effects of the fin height on the over-all weight of both the fin matrix and the cylindrical length of pressure vessel required, together with the cost of the tubing and the cost of the tubing plus that of the pressure vessel. A review of the data indicates that there is little advantage to be gained from use of fins and that the lowest cost and lightest weight unit can be obtained with bare tubes.

3. Experimental Investigations of Heat Transfer and Fluid Flow

The study of heat transfer in the septafoil geometry was reoriented toward establishing the criteria for the thermomechanical stability of the tubes in a seven-tube bundle when a nonuniform circumferential temperature distribution exists. To this end, the heat-transfer apparatus was redesigned to include a spacer at the mid-plane of the cluster so that the tube surface temperature distributions can be measured for fixed and known amounts of tube bowing. In preliminary experiments, with the tubes restrained at the mid-plane to their design positions, circumferential temperature profiles were obtained for all seven tubes at an axial position 1-in. upstream of the spacer. Analyses of the data indicated that some cross-flow probably existed. Heat-transfer coefficients, estimated from an axial traverse of the surface temperature of a peripheral tube, varied from about 48 $Btu/hr \cdot ft^2 \cdot {}^\circ F$ at the inlet to 26 $Btu/hr \cdot ft^2 \cdot {}^\circ F$ at

the exit with a second maximum in the region immediately downstream of the spacer.

To determine whether the cross-flow indicated by the heat-transfer measurements was the result of channel inlet conditions, one of the peripheral tubes in the heat-transfer apparatus was replaced by a naphthalene-coated rod. For a position 1-in. upstream of the spacer, it was observed that the heat-transfer and mass-transfer data showed similar patterns. A subsidiary experiment using fiber tufts showed a rotational flow at the inlet which could be stopped or reversed in direction by inserting small obstructing strips into the inlet plenum. It was concluded that modification of the inlet configuration was needed to assure coaxial flow in the heat-transfer apparatus.

A preliminary measurement of the velocity distribution far downstream ($L/d_e = 50$) in a septafoil channel having a $\gamma = 2$ tube spacing was completed. For a Reynolds modulus of 52,000, the profiles were observed to be symmetrical with respect to the tube positions. The maximum velocity in the outer flow region was 30% above the mean velocity; in the inner flow region, the maximum-to-mean velocity ratio was 1.15. In the region of closest approach of the tube to the channel wall, the velocity ratio was less than 0.8. Similar measurements at $L/d_e = 20$ showed some skewness in the patterns.

Part 2. Materials Research and Testing

4. Metallurgy

Developmental work on the continuous process for conversion of UF_6 to UO_2 has continued, but the desired degree of reproducibility has not yet been attained. Certain batches of material from the process have been readily sinterable to a density of >96% of theoretical, and attempts are being made to duplicate these conditions.

Compression testing of high-density UO_2 has shown it to withstand loads of 5000 psi at 1500°C with only moderate deformation. All available

data related to the thermal conductivity of UO_2 have been compiled, and an apparatus is being constructed for measuring the conductivity at temperatures up to 1350°C.

Apparatus was designed and is being constructed for experimental measurements of the fission products released from irradiated UO_2 upon postirradiation heating to temperatures above 1000°C. The release rate data thus obtained may be used to predict the pressure buildup in fuel capsules under reactor conditions. Eight UO_2 pellets of various enrichments are being irradiated for use in these experiments.

Data were obtained from tube-burst tests of fuel capsule tubing at 1800°F which show that results previously reported must be corrected. The strength at 1800°F is considerably lower than expected. Burst tests of welded tubing at various temperatures show that failure always occurs in the weld zone, and that the time to rupture is considerably less than for seamless tubing. The collapsing behavior of welded tubing is, however, analagous to that of seamless tubing.

A series of modified tube-burst tests was conducted to complete the evaluation of the end-closure joints. The edge-fusion-welded joint gave very favorable results. Results from extensive thermal cycling of pressurized capsules confirmed that the capsules are thermally stable and have adequate strength up to 1400°F.

Results from strain cycling of capsule tubing indicate that temperature has no influence on the number of cycles to failure. Environmental effects on strain cycling are being studied.

Brazing studies on simulated spacers for the mid-plane of the fuel elements were initiated, and the optimum diametral gap between spacer and tube wall was determined. Collapsing tests on capsules with spacers and without internal support indicate that, under severe deformation, failure may occur at the braze joint. The metallurgical effects of the brazing cycle on all mechanical properties of the capsule tubing are being determined.

The reactions of stainless steel with low levels of contaminants in helium and argon are being studied. Creep tests of precarburized

stainless steel specimens and of other heats of stainless steel indicate that creep-rupture life in CO and CO_2 is greater than in argon, in contradiction to results previously reported. On this basis it may be concluded that carburization of the stainless steel will occur; however, the creep-rupture data from tests in argon give a conservative design basis and a conservative prediction of fuel element life.

Welding tests were conducted on cast fuel element hanger material, and the results indicate that mechanized welding of the joint should be possible. The specification for helium leak testing of completed fuel capsules is being given a final review.

Considerable developmental work is being performed on reference standard defects for eddy-current inspection of tubing. Notches produced by electrical-discharge machining are most reliable, but transverse filed notches are more easily prepared and are considered to be acceptable. The procedure specification for eddy-current inspection of tubing has been revised on the basis of this work. An additional large batch of tubing was evaluated that had been ordered with close dimensional tolerances but without specified inspection. Total rejection of the tubing was greater than 40%, principally because of mechanical defects.

The 4-in. thick plates obtained from Lukens and welded at Chicago Bridge and Iron are being sectioned for the preparation of samples for the determination of pre- and postirradiation properties. Inspection techniques for thick weldments are being developed using the pulse-echo ultrasonic method.

Diffusion bonding and brazing of beryllium are being studied. Diffusion bonds created by the pressure exerted from differential thermal expansion in a molybdenum jig show promise. Brazing with alloys which wet beryllium has not been successful because cracks occur in the joints as a result of differential contraction.

Evaluations of extruded tubing from England revealed considerable dimensional variation, as observed in tubing received previously. Radiographic inspection, which seems to be the most definitive technique for determining the quality of beryllium tubing, revealed numerous

inclusions and several deep pits and gouges. Batches of small-diameter tubing are being obtained from foreign and domestic sources for more complete evaluation.

A survey of available data on the reactions of beryllium with gases has been completed. Determinations are to be made of the reactions of beryllium with CO_2 at temperatures up to 750°C, at which temperature carburization of the beryllium is expected.

5. In-Pile Testing of Components and Materials

The irradiation of eight full-size (diameter only) single fuel rod specimens in the ORR has continued for about five months of the scheduled six-month period. Thermal cycles have been induced by changing the barrier gas, by using the cadmium shutters, and by reactor power fluctuations. Seven similar capsules are being irradiated in the ETR.

Initial operation of the GETR helium loop revealed the need for several design changes, including revision of the compressor housings and the addition of a large heater. When the changes had been made and numerous leaks had been repaired, the loop appeared to be ready for operation.

Thirteen miniature capsules have been irradiated in the LITR and six tests are now under way. Because of difficulties with platinum-platinum-rhodium thermocouples, rhenium-tungsten thermocouples have been installed in all recent LITR experimental assemblies. For higher temperature experiments, a new capsule has been designed which incorporates a hollow ceramic insulator around the UO_2 fuel.

The first instantaneous fission-gas release experiment was completed. It was concluded that at temperatures above 1300°F the fission gases were released from the ThO_2-UO_2 sample by a diffusion process and that recoil contributions were minor. A system of charcoal adsorbers has been installed for a new experiment so that xenon and krypton may be separated from the rest of the fission products in the sweep gas and then separated from each other.

The fission-product-release data obtained in postirradiation studies have been tabulated and are being analyzed. The wide range of results

at similar temperatures indicate that other experiments may be necessary to verify the data. Mass spectrometer analyses of the gas from four capsules have shown the ratio of total krypton to xenon to be approximately 1:7.

Postirradiation examinations of LITR capsules are under way at GEVAL. Efforts are being made to improve burnup determinations and to obtain better samples. The density-measuring equipment is being modified, and means for obtaining oxygen-to-uranium ratios are being studied. It is expected that an ORNL hot cell (modified cell 6) will be ready for postirradiation examinations in November 1959.

The closed-cycle-loop irradiation facility in the ORR was put into operation. Two coated graphite samples containing ThO_2-UO_2 fuel are being irradiated.

Further investigations of irradiation effects on platinum-platinum-rhodium thermocouples were carried out. It was found that the error in emf output of an irradiated thermocouple depends on the location of the thermal gradient with respect to rhodium transmutation and on the total neutron exposure.

Additional data were obtained in the study of radiation effects on structural materials. Further evidence was obtained which shows that the impact transition temperature increases and the ductile energy absorption decreases with increasing irradiation dose. Studies of the effect of high-temperature irradiation in the brittle fracture properties of steel have shown that irradiation at 575°F leads to less change than irradiation at lower temperatures and that a variation in the magnitude of the effect is found even in steels of similar types.

A study of the effects of irradiation on beryllium has been initiated in collaboration with General Nuclear Engineering Corporation.

6. Out-of-Pile Testing of Materials and Components

The program of out-of-pile tests of reactor materials compatibility and the structural integrity of fuel elements has continued. A summary of data obtained from analyses of gas samples from static pot tests

indicates that the temperature of the heated specimen has no appreciable effect on the gaseous impurity concentrations. Low-pressure thermal-convection loop tests were continued, and the first high-pressure thermal-convection loop test was completed. The EGCR fuel element mockup contained in the loop showed an adherent gray-green oxide on all surfaces.

The EGCR fuel element mockup tested in the initial forced-circulation loop test was also removed from the test system. It had a tightly adhering black oxide on all surfaces.

Additional data were collected on the evolution of gases from graphite at elevated temperatures. Characterization of the various types of graphite through ash content, porosity, surface area, and loss in weight by degassing has been initiated. Nine types of graphite have been studied.

Apparatus has been constructed for studying the process by which krypton and xenon diffuse "upstream" in helium flowing through a graphite sleeve under a diving force consisting of a differential pressure. The information obtained will be used to evaluate the possibility of removing the fission product krypton and xenon diffusing from unclad fuel elements by purging with a "sidestream" of the coolant helium through an annulus between the fuel element and a graphite sleeve.

In a study of methods for removing impurities from coolant gases, measurements are being made of the thermal conductivities of absorbents. Linde molecular sieves for the retention of krypton and xenon are being evaluated.

An extensive investigation of means for measuring high temperatures has been initiated. Studies are being made of the effect of the means of attachment on the measurement of surface temperatures in high-velocity cooling gas, the stability of rhenium-tungsten thermocouples in the temperature range 1500–2000°C, the Chromel-Alumel thermocouple drift problem, and the effects of transmutation under irradiation.

A system has been designed for automatic continuous analysis of helium. The system will be used initially on the low-pressure thermal-convection loop.

7. Development of Test Loops and Components

Design work was completed and fabrication was initiated on the gas-cooled loop for operation in the ORR that is designated GCR-ORR loop No. 1. Advanced clad fuel elements are to be tested in this loop. GCR-ORR loop No. 2 is being designed as a facility for testing unclad fuel elements.

Developmental work has continued on gas compressors and electric motors. A grease-lubricated centrifugal compressor is undergoing an endurance test at 400 psig with a suction temperature of 600°F. Preparations are being made for a high-temperature test of a regenerative compressor, and a test system is being assembled for testing compressors with gas-lubricated bearings. A compressor ordered from Bristol-Siddeley Engineers, Ltd., is to be tested at suction temperatures from 150 to 1000°F and pressures up to 400 psia.

Facilities are being developed for testing electric motors for high-temperature service. The characteristics of motors operating in high-temperature helium are to be determined.

PART 1. DESIGN INVESTIGATIONS

1. REACTOR PHYSICS

Power-Density Distribution in EGCR

Additional studies have been made of the power-density distribution in the EGCR with the aim of reducing the uncertainties in the results of previously reported calculations.[1] The previous calculations were two-dimensional reactor calculations in which the core was represented as a homogeneous medium and the control rods and the stainless steel experimental tubes were represented explicitly as heterogeneities in the homogeneized core material. The manner in which the core is homogeneized is, to some extent, arbitrary, since it is not always evident where to locate the boundary between a lattice irregularity and the homogeneized region. The different results obtained with two methods of treating the core in the vicinity of an experimental tube on the axis of the EGCR are illustrated in Fig. 1.1. In one case all the fuel and moderator are homogeneized into a material which extends to the surface of the tube. In the other case the core is homogeneized within a volume which excludes the core lattice cell containing the experimental tube. Since the tube is at a normal fuel element position, the moderator of one lattice cell is treated in this case as a region of pure graphite surrounding the tube. It is clear from Fig. 1.1 that a serious uncertainty is present in both the details of the power-density distribution near the tube and its effect on the over-all power-density distribution in the core. The results reported previously[1] were obtained using the first method described above.

In order to eliminate the uncertainty arising from the method of homogeneization for the specific case of the EGCR and to provide basic data with which to study the problem of lattice irregularities, a calculation was done in which all the heterogeneous characteristics of the EGCR core, including the eight experimental tubes, were included

---

[1] GCR Semiann. Prog. Rep. June 30, 1959, ORNL-2767, p 45.

explicitly. This was a four-group, two-dimensional, diffusion-theory calculation using the geometry shown in Fig. 1.2. Each of the 216 fuel elements in the core is represented by a fuel element of square cross section to bring the total number of space points required for the calculation to within the limits set by the available storage of the computer being used.[2] Although the analysis of the results is not yet complete enough to permit a general comment on the problem of lattice irregularities, several results can be given which are significant to the design of the EGCR.

Thermal-neutron flux distributions along three representative directions in one quadrant of the core are presented in Fig. 1.3. The cross sections in the fuel regions were adjusted in such a way that the ratio of the average moderator thermal-neutron flux to the average fuel thermal-neutron flux is in good agreement with P-3 calculations for the hot, clean reactor with 2.2% enrichment. The outside diameters of the experimental tubes are 8 in. and 4.5 in., with a radius-to-thickness ratio of 15, since these dimensions represent the current design.

The pronounced flattening effect of the four central tubes is apparent from the figures, as well as the tendency of the large tubes to hold down the power generation in channels near the core diagonal. The over-all peak-to-average power-density ratio is 1.286, which is slightly higher than the value of 1.26 reported previously.[1] It has not yet been determined how much of this difference is due to the smaller tube sizes in the present calculation and how much may be ascribed to the explicit treatment of all the heterogeneities. The average power of each channel in one quadrant of the core is given in Table 1.1. The normalization is to an average of unity.

Other results which are significant to the EGCR design are the following:

---

[2]This calculation was done on the IBM-704 computer at the Martin Company, Baltimore, Maryland, which is equipped with a 32K core-storage unit.

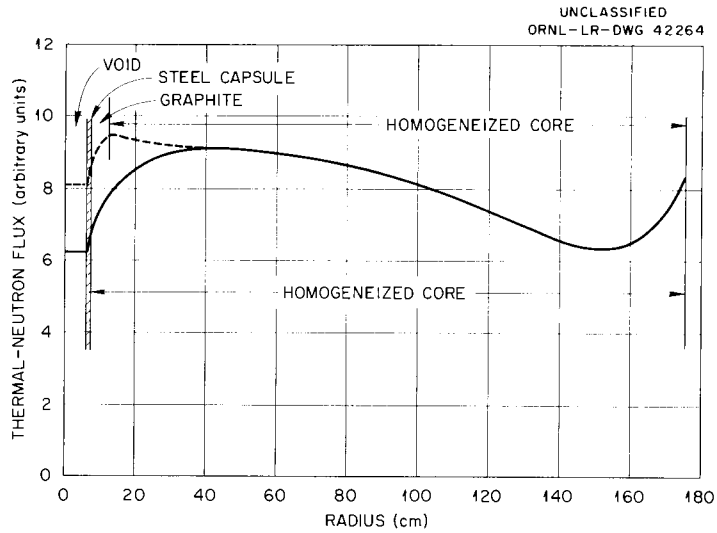

Fig. 1.1. Thermal-Neutron Flux Near an Empty Central Experimental Tube for Two Different Methods of Homogeneization.

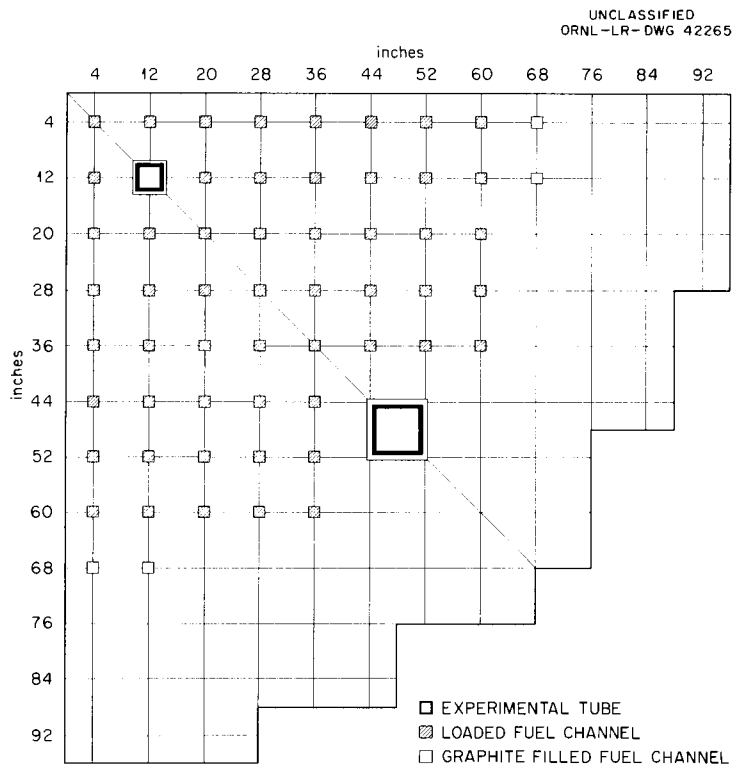

Fig. 1.2. Geometric Representation Used in Two-Dimensional Heterogeneous Reactor Calculation of EGCR Core and Reflector. Only one quadrant is shown.

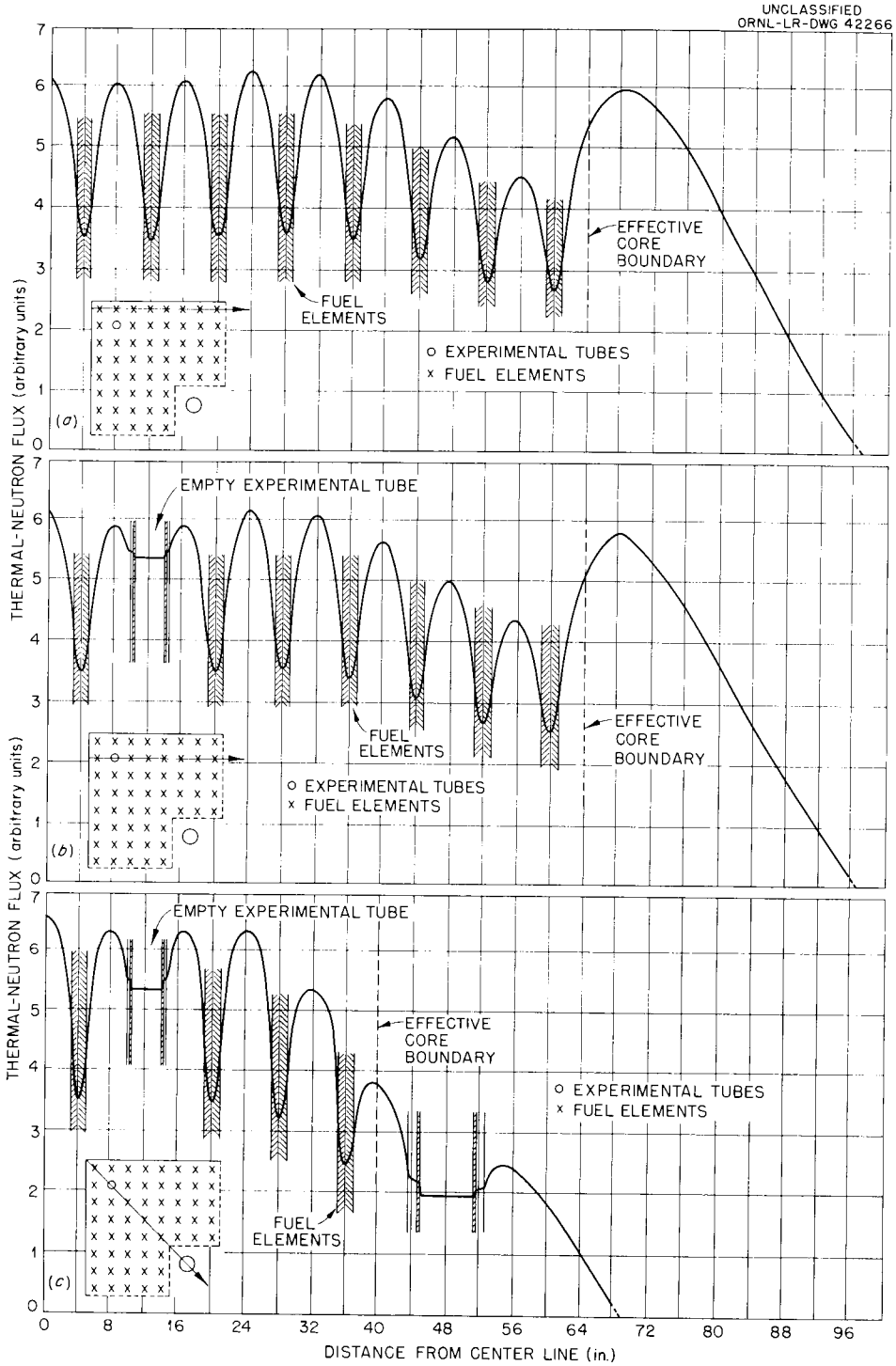

Fig. 1.3. Thermal-Neutron Flux Distributions Along Three Directions in the EGCR Core.

Table 1.1. Average Power of Each Channel in One Quadrant of the EGCR

y (in.)	Average Power (Normalized to Average of Unity) in Indicated Channel (x,y)							
	x = 4 in.	x = 12 in.	x = 20 in.	x = 28 in.	x = 36 in.	x = 44 in.	x = 52 in.	x = 60 in.
4	1.249	1.230	1.267	1.286	1.240	1.139	0.992	0.891
12	1.230		1.236	1.257	1.203	1.097	0.949	0.848
20	1.267	1.236	1.240	1.217	1.137	1.017	0.869	0.769
28	1.286	1.257	1.217	1.143	1.027	0.888	0.743	0.651
36	1.240	1.203	1.137	1.027	0.875	0.713	0.592	0.535
44	1.139	1.097	1.017	0.888	0.713			
52	0.992	0.949	0.869	0.743	0.592			
60	0.891	0.848	0.769	0.651	0.535			

1. Essentially no asymmetry in the power-density distribution occurs in channels adjacent to the four small experimental tubes.

2. Adjacent to the large experimental tubes the power-density distribution is unsymmetrical in the channels near the core boundary, with the maximum variation across a channel being approximately 6% of the average in the channel.

3. The upswing of the power-density distribution at the core-reflector boundary which is characteristic of the homogeneous core model does not occur, although the thermal-neutron flux does increase in the moderator beyond the last row of fuel elements.

In addition to the above calculation for the entire EGCR core, a series of supercell calculations has been done in which an experimental tube is placed at the center of a three-by-three array of fuel channels. The fluxes in this system have been found to be essentially identical to those in the same array around each of the small tubes of the entire core calculation described above.

The effect of an empty fuel channel on the power-density distribution in the EGCR has been estimated by calculating the fluxes in a nine-by-nine array of fuel channels with the central channel being void. The thermal-neutron flux for this case is shown in Fig. 1.4. The peak-to-average ratio of the power-density distribution in the array is 1.074. The ratio of the power in the hottest channel to that in the unperturbed channels is 1.082. A hot-channel factor of approximately this magnitude will be encountered during fuel unloading operations.

Power-Density Distribution in Seven-Rod Cluster Fuel Elements

In an effort to determine the accuracy of various models used to predict neutron flux distributions in seven-rod fuel clusters, a comparison was made, as reported previously,[3] between theoretical distributions and detailed experimental results obtained at Atomics

[3] GCR Semiann. Prog. Rep. June 30, 1959, ORNL-2767, p 54.

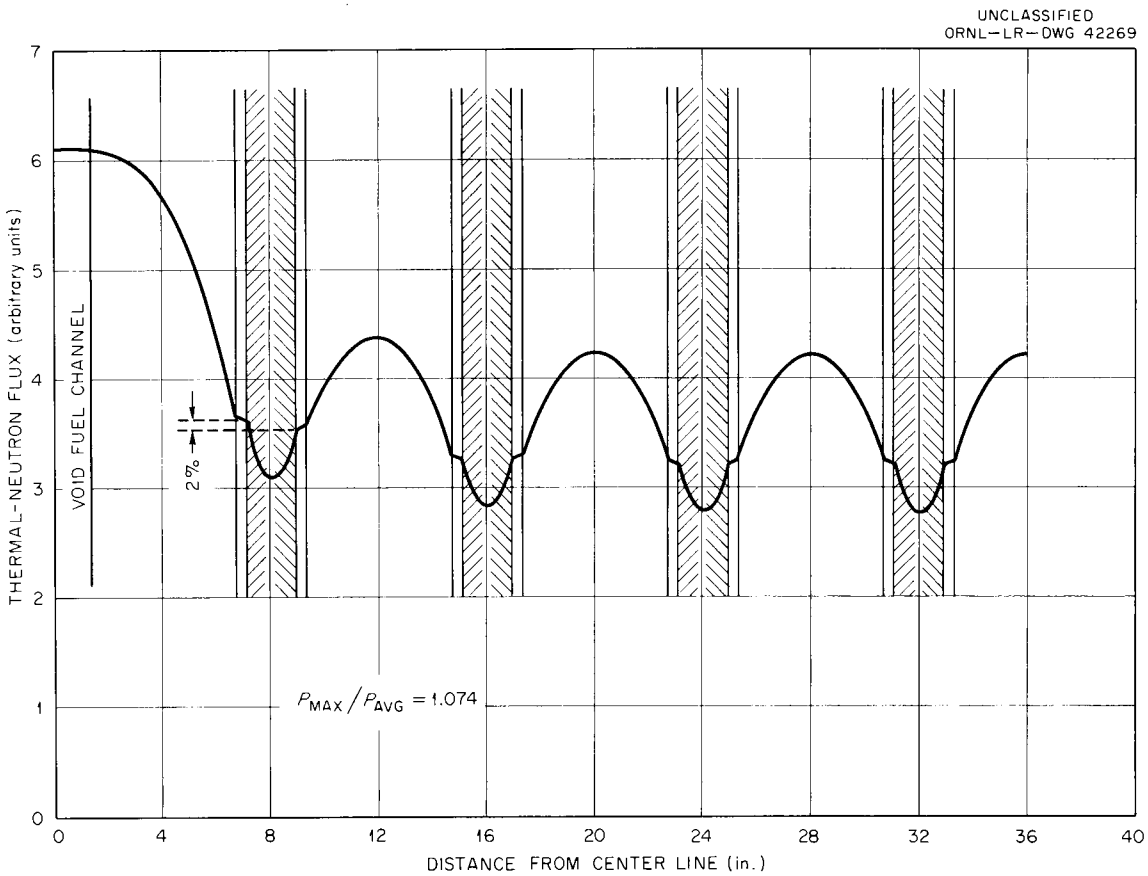

Fig. 1.4. Thermal-Neutron Flux Distribution in One Quadrant of a Nine-by-Nine Array of Fuel Channels with the Central Channel Void.

International.[4,5] In this study it was found that the fluxes obtained from an annular one-velocity, one-dimensional P-3 solution to the neutron-transport equation can be used to construct the power distribution in the individual rods of cluster fuel elements.

A comparison (Table 1.2) of calculated results with preliminary experimental results[6] recently obtained from EGCR experiments performed in the Physical Constants Test Reactor (PCTR) at Hanford provides further verification of the validity of the selected model. The calculations have now been extended to the EGCR fuel element.

Table 1.2. Comparison of PCTR and Calculated Neutron Flux Ratios for EGCR Model with a Fuel Enrichment of 1.8%

	Experimental	Calculation
Ratio of average flux in the fuel of the outer rod to the average flux in the fuel of the central rod	1.094	1.125
Ratio of average surface flux to average fuel flux		
For central rod	1.033	1.057
For outer rod	1.045	1.070
Ratio of maximum surface flux to minimum surface flux of outer rod	1.243	1.295

[4]W. W. Brown et al., Exponential Experiments with Graphite Lattices Containing Multirod Slightly Enriched Uranium Fuel Clusters, NAA-SR-3096 (Jan. 15, 1959).

[5]R. A. Laubenstein et al., Sodium Graphite Reactor Quar. Prog. Rep. Jan.-Mar. 1955, NAA-SR-1347, p 18 (Oct. 1, 1955) (classified).

[6]Personal Communication from E. R. Wagner (Allis-Chalmers) to C. A. Preskitt (Aug. 1959).

The model used for the P-3 calculations represented the six outer rods as a concentric annulus having a thickness equal to one fuel rod (unclad) diameter and an appropriately reduced uranium density (that is, the same total amount of uranium as in the actual six rods). The stainless steel cladding for the outer rods was represented by annuli adjacent to the outer fuel annulus and having thickness equal to that of the actual cladding. Effective neutron temperatures computed from the formula of Bate, Coveyou, and Osborne[7] with flux-weighted macroscopic cross sections were found to be 945 and 985°K, respectively, for the EGCR with 2.0% and 2.6% enriched fuel clusters during full power operation. These temperatures were employed in determining the Maxwell-Boltzmann averaged macroscopic cross sections for the P-3 calculations. The power distribution in the outer rods of the cluster was obtained from the P-3 flux calculation by using the method described in ref 8. A small empirical correction derived from detailed comparisons between P-3 calculations and the Atomics International measurements was applied. In effect, the deviation of the calculated distribution from the measured distribution at several points in the rod was correlated with the rod absorption cross section.

The flux traverse across an outer rod perpendicular to a diameter of the cluster was estimated by averaging the outer and inner fluxes at a given radius along a cluster diameter. An examination of the experimental data showed that the 90-deg flux trace can be estimated quite accurately by using this technique.

Flux distributions for both the 2.0 and 2.6% cases are shown in Figs. 1.5 and 1.6. Ratios of the average flux in the moderator to the average flux in the fuel, the central rod fuel surface flux to the

---

[7]R. R. Coveyou, R. R. Bate and R. K. Osborne, Effect of Moderator Temperature Upon Neutron Flux in Infinite, Capturing Medium, ORNL-1958 (Sept. 29, 1955).

[8]T. K. DeBoer, Calculation of Radial Neutron-Flux Distribution in EGCR Lattice Cell, ORNL CF 59-8-140 (Aug. 31, 1959).

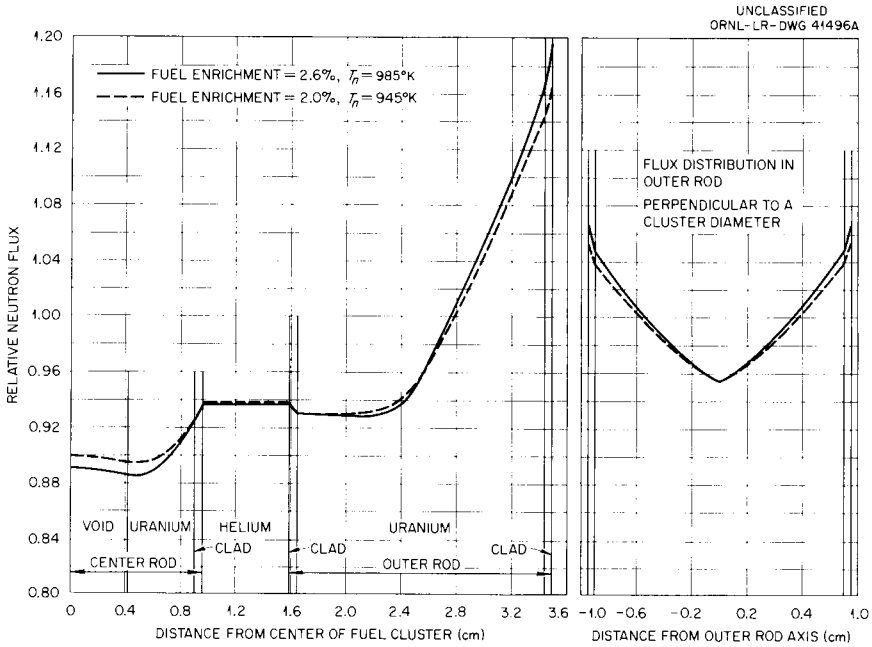

Fig. 1.5. Neutron Flux Distribution in EGCR Fuel Cluster Normalized to an Average Neutron Flux in the Fuel of 1.0.

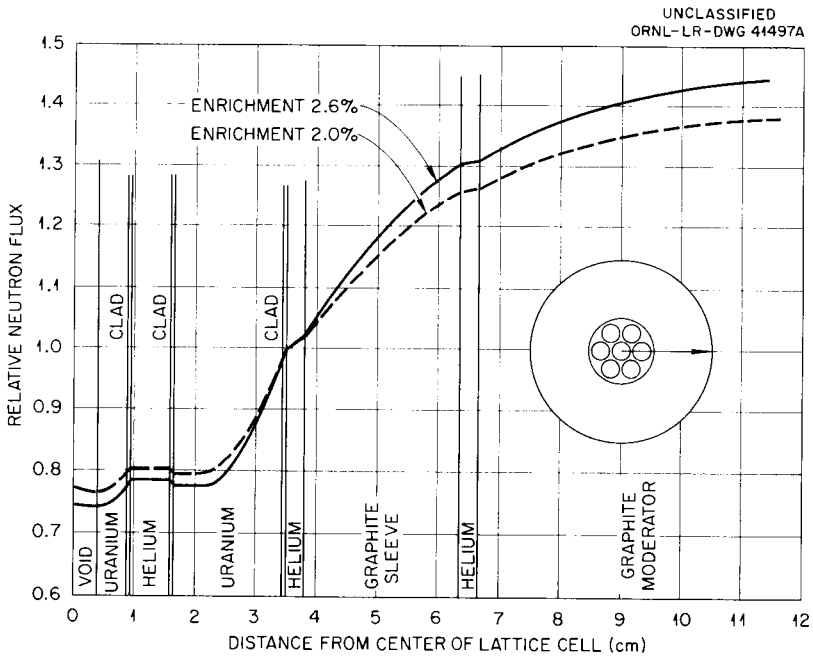

Fig. 1.6. Neutron Flux Distribution in EGCR Lattice Cell.

average flux in the central rod fuel, and the average flux in the outer rod to the average flux in the central rod for these cases are given in Table 1.3.

Table 1.3. Neutron Flux Ratios in the EGCR Lattice Cell

	Ratios for Fuel Enrichment of 2.0%	Ratios for Fuel Enrichment of 2.6%
Ratio of fuel surface flux to average flux in central rod	1.022	1.028
Ratio of average flux in outer rod to average flux in central rod	1.11	1.13
Ratio of average flux in moderator to average flux in fuel	1.52	1.61

Power-Density Achievable in Gas-Cooled Reactors with Ceramic Fuel Elements

The cost of power from a gas-cooled reactor is strongly dependent on the capital cost per kilowatt, which is, in turn, dependent on the power density or heat generation rate divided by the total core volume. Therefore in order to evaluate gas-cooled reactors that would operate with a ceramic material as both fuel and moderator, a study was made of the factors that determine the maximum power densities.[9] In such a reactor the power density may be limited by the ability of the ceramic to withstand the thermal stress imposed upon it, by the ability of the gas to carry away the heat produced, by the rate of gas temperature

[9]R. S. Carlsmith, Power Density in Ceramic-Fuel-Element Gas-Cooled Reactors, ORNL CF 59-8-87 (Aug. 14, 1959).

rise in the direction of flow, or by all three factors. For simplicity in making the calculations, the power density was assumed to be uniform throughout the core, and criticality limitations were disregarded. It was assumed that the ceramic structure could be made self-supporting and would be unclad.

The results of the study indicate that power densities of 100 to 200 w/cm^3 are attainable with uranium-bearing graphite and that power densities of 50 to 100 w/cm^3 are attainable with uranium-bearing beryllium oxide. Still higher power densities may be possible, particularly with beryllium oxide, if a way can be found to use very thin ceramic sections or if a ceramic of superior high-temperature thermal stress resistance is developed. It should be kept in mind, of course, that the use of unclad fuel elements implies a degree of fission-product retention which has not as yet been completely demonstrated.

In a fuel element in which heat is being generated at a uniform rate per unit volume, the maximum heat generation rate, Q, limited by the thermal stress within the element, can be written,

$$Q = RS , \tag{1}$$

where R depends on the physical properties of the material at the temperature in question,

$$R = \frac{k(1 - \nu)\sigma}{E\alpha} , \tag{2}$$

where

k = thermal conductivity,

ν = Poisson's ratio,

σ = tensile strength,

E = Young's modulus,

α = coefficient of thermal expansion,

and S is a shape factor which depends on the geometry of the element

and the temperature distribution. In this study it was assumed that fuel-bearing beryllium oxide could safely be subjected to an R of 250 Btu/hr·ft at 2000°F and that fuel-bearing graphite could withstand an R of 2690 Btu/hr·ft at 1800°F. (A thermal stress of 8000 psi in the beryllium oxide and 800 psi in the graphite is implied.) It is believed that these values are conservative, although there is a great deal of scatter in the available data.

For flat plates of thickness X_1, subject to uniform internal heating, it can be shown that

$$S = \frac{12}{X_1^2} \quad . \tag{3}$$

From this relation the value of Q, the allowable heat generation per unit volume of fuel element, can be calculated as a function of fuel element thickness. Similarly, the power density (the heat generation per unit core volume) can be expressed as a function of the fuel element thickness and the spacing between elements. The power densities, expressed in this fashion, that are attainable with parallel plates of graphite, are shown in Fig. 1.7. Similar information for beryllium oxide is presented in Fig. 1.8.

A second consideration which may limit the power density of the reactor is the ability of the gas to transfer heat from the fuel element surface and to remove the heat. Neglecting compressibility effects, the heat transfer and fluid flow correlations can be expressed as

$$Q' = h \, \Delta T \quad , \tag{4}$$

$$\frac{hD_e}{k} = 0.023 \left(\frac{D_e G}{\mu}\right)^{0.8} \left(\frac{C_p \mu}{k}\right)^{0.4} \quad , \tag{5}$$

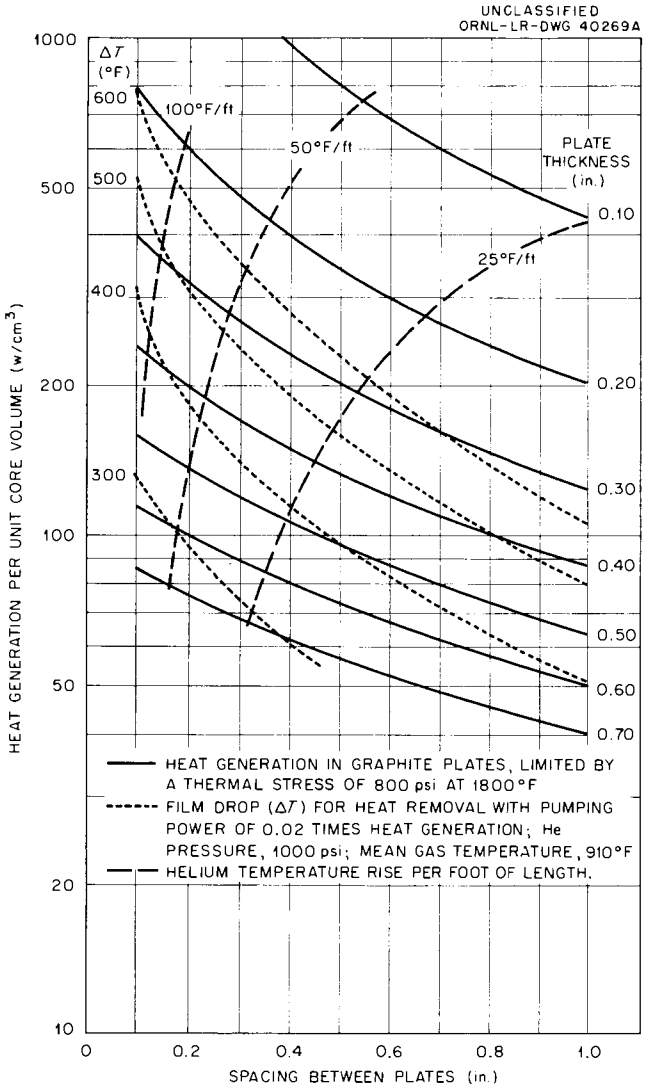

Fig. 1.7. Heat Removal from Graphite Plates Cooled by Helium Gas.

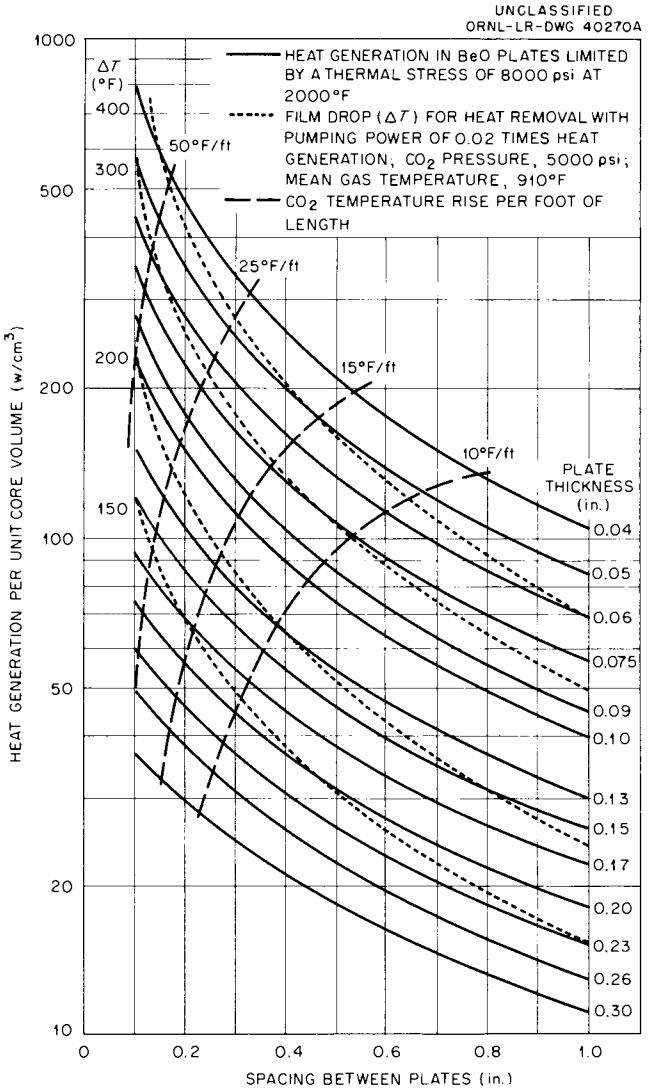

Fig. 1.8. Heat Removal from Beryllium Oxide Plates Cooled with CO_2.

$$\Delta p = \frac{G^2 f L}{\rho\, g_c \frac{D_e}{2}} , \tag{6}$$

$$q_p = \frac{W' \Delta p}{\rho J Q' L} \tag{7}$$

$$f = 0.046 \left(\frac{D_e G}{\mu}\right)^{-0.2} \tag{8}$$

where the symbols have the meanings:

Q' = heat transfer per unit of surface area (heat flux),

h = heat transfer coefficient,

ΔT = temperature drop from solid surface to bulk gas condition,

D_e = equivalent diameter, $D_e = 2X_2$,

X_2 = spacing between plates,

k = thermal conductivity,

C_p = specific heat,

G = mass flow per unit cross-sectional area,

μ = viscosity,

Δp = pressure drop,

f = friction factor,

L = length of passage,

g_c = conversion factor in Newton's law of motion,

q_p = pumping power required per unit of heat extracted,

W' = mass flow of gas,

ρ = gas density,

J = mechanical equivalent of heat.

Since $C_p\mu/k$ does not vary widely for gases, a value of 0.78 can be substituted in Eq. 5, yielding the simplified relationship

$$h = 0.027 \frac{C_p G^{0.8} \mu^{0.2}}{D_e^{0.2}} . \tag{9}$$

The combination of Eqs. 4, 6, 7, 8, and 9 yields the equation

$$Q' = \frac{742\ \mu^{0.2}\ C_p^{1.4}\ \Delta T^{1.4}\ q_p^{0.4}\ \rho^{0.8}}{X_2^{0.2}}\ , \qquad (10)$$

and since the power density is equal to $2Q'/(X_1 + X_2)$, the power density, as limited by heat removal considerations, can be expressed as a function of plate thickness and plate spacing for given values of the physical properties of the gas, the gas film temperature drop, and the pumping power ratio. Since the heat removal must be equal to the heat generation, these values can be plotted on the same graphs as were used previously. This has been done for beryllium oxide plates cooled with CO_2 on Fig. 1.8 and for graphite plates cooled by helium gas on Fig. 1.7.

A third consideration which can limit the core design is the rate at which the gas temperature rises as a function of length in the direction of flow. Each of the heat removal rates referred to previously implies a rate of temperature rise given by

$$\frac{\partial T}{\partial L} = \frac{Q'}{W' C_p}\ .$$

Since the over-all temperature rise is limited to the neighborhood of 1000°F, a particular rate of temperature rise fixes the approximate length of the core. It must not be too short due to nuclear considerations and must not be too long due to mechanical considerations. Values for the rate of temperature rise are also plotted on Figs. 1.7 and 1.8.

In using the graphs from this study as a basis for design it is apparent that the maximum power densities are achieved with fuel element sections as thin as possible and cooling passages as small as possible. The degree to which the thickness of the fuel element can be reduced depends partly on the details of the mechanical design and

partly on the ceramic fabrication process to be used. It appears that beryllium oxide sections less than 0.100 in. or graphite sections less than 0.250 in. will lack the necessary rigidity and strength. It may be that the economics of fuel element production would necessitate a choice of a considerably thicker fuel element and a consequent reduction in power density. Cooling passage widths of 0.200 in. should be possible, although the problems of assembly tolerances and warping become severe with small passages.

Physics of Fuel Element Clusters

An investigation has been made of the reactor physics aspects of different fuel element clusters. Extensive studies were conducted to determine how the multiplication factor, k, varies with number of rods (7, 19, 37, 49, 61), cladding thickness, cladding material, interrod spacing, lattice pitch, solid and cored rods, fuel enrichment, and fuel-to-moderator ratio. Uranium oxide was the fuel considered, and type 304 stainless steel and beryllium were the two cladding materials used. Batch loading, uniform exposure, 3% leakage, and a xenon and samarium poisoning loss of $\delta k = 0.032$ were assumed for the lifetime calculations. The lifetimes for continuous fueling would be approximately twice those given here.

Temperature-corrected cross sections were used in all calculations. The method of correcting flux-weighted cross sections was that given by Coveyou *et al.*[10] and by Campbell and Freemantle.[11] Factors appropriate to these methods were taken, for convenience, from an ACF Job Report.[12]

---

[10] R. R. Coveyou, R. R. Bate, and R. K. Osborn, J. Nucl. Eng. 2, 153 (1956).

[11] C. G. Campbell and R. G. Freemantle, Effective Cross Section Data for Thermal Reactor Calculations, AERE-RP/R-2031 (1956).

[12] Effective Neutron Cross Sections, ACF Job Report No. 3-135-1.0 (Oct. 29, 1958).

A new formula for calculation of the fast effect was used.[13] The basic differences between this formulation and previous ones are the choice of the fission threshold energy and the inclusion of subthreshold captures. In connection with the fast effect, the neutron collision probability for clusters has not been accurately determined; in this study, the cluster in each case was approximated by a single homogeneous rod having the same amount of material as the cluster and equal in cross-sectional area to the surface enclosed by a membrane stretched around the cluster. The effects of (n,2n) and (n,α) reactions, of elastic scattering in beryllium cladding, and of inelastic scattering in type 304 stainless steel cladding were simulated by adjustment of the uranium oxide cross sections. A formula for resonance-escape probability of the same form as found in ORNL-2500[14] was used in the calculations. Values for the resonance integrals of the elements in type 304 stainless steel were taken from a table by Macklin and Pomerance,[15] while the moderating effect of beryllium cladding was accounted for by a "rubber band" surface term correction.[16]

Thermal utilization factors were computed by the method used in ORNL-2500,[14] with the disadvantage factors calculated by the P-3 spherical harmonics method using the IBM-704. The model employed in the P-3 calculations was the same as that described above for the study of power-density distribution in seven-rod cluster fuel elements.

The basic results of the study are shown in Figs. 1.9 through 1.13. The results show, as one would expect, that greater subdivision of the fuel requires higher enrichment for a given fuel lifetime, in the case of stainless steel cladding. In the case of 0.040-in.-thick beryllium

---

[13]G. R. Hoke, The Fast Fission Factor, ORNL CF 59-9-61 (to be issued).

[14]The ORNL Gas-Cooled Reactor, ORNL-2500, Part 2, p 2.13 (April 1, 1958).

[15]R. L. Macklin and H. S. Pomerance, Resonance Capture Integrals, International Conference on the Peaceful Uses of Atomic Energy, Vol. 5 P/833, p 896 (1955).

[16]E. Hellstrand, J. of Appl. Phys. 28, No. 12, p 1493 (July 1957).

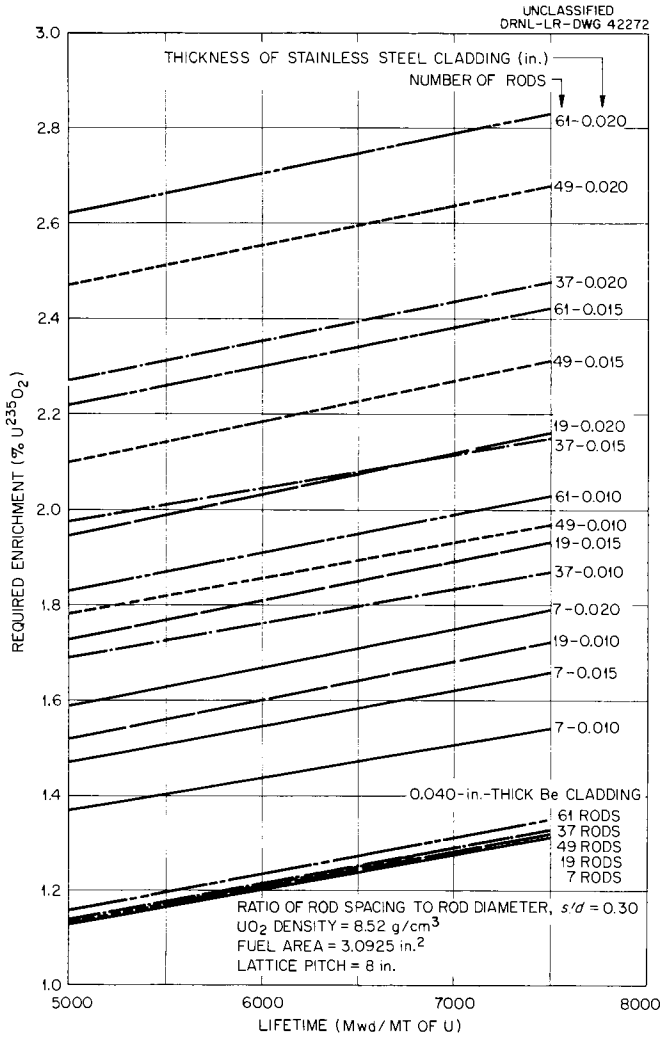

Fig. 1.9. Enrichment vs Lifetime for Stainless-Steel- and Beryllium-Clad Fuel Rods as a Function of Number of Rods in Fuel Element Cluster at a Lattice Pitch of 8 in.

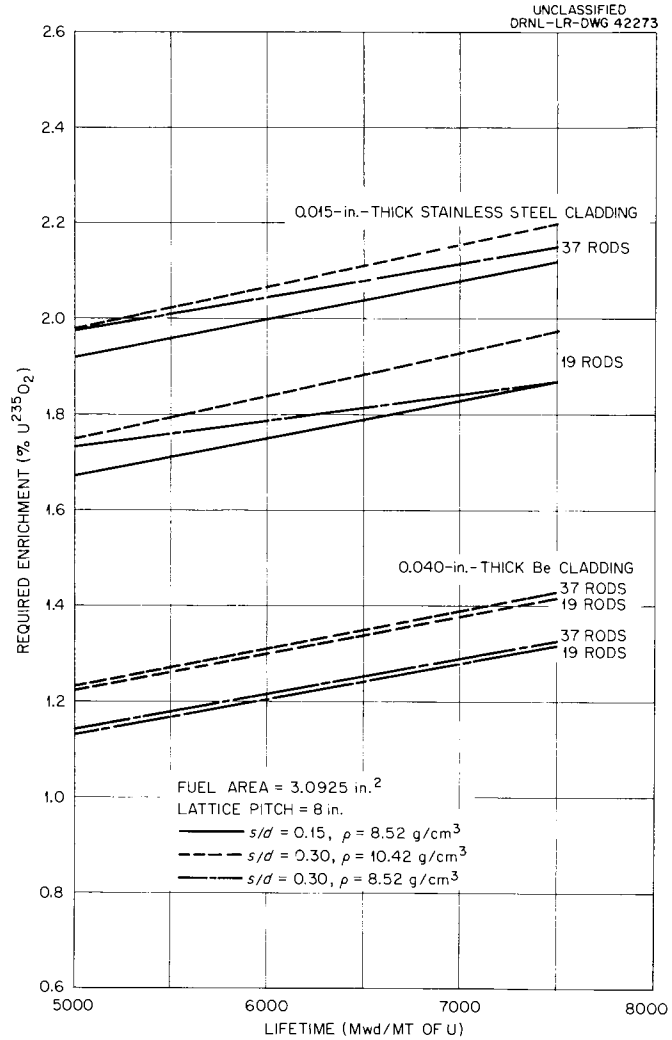

Fig. 1.10. Enrichment vs Lifetime for Stainless-Steel- and Beryllium-Clad Fuel Rods as a Function of Number of Rods, UO_2 Density, and Ratio of Rod Spacing to Rod Diameter.

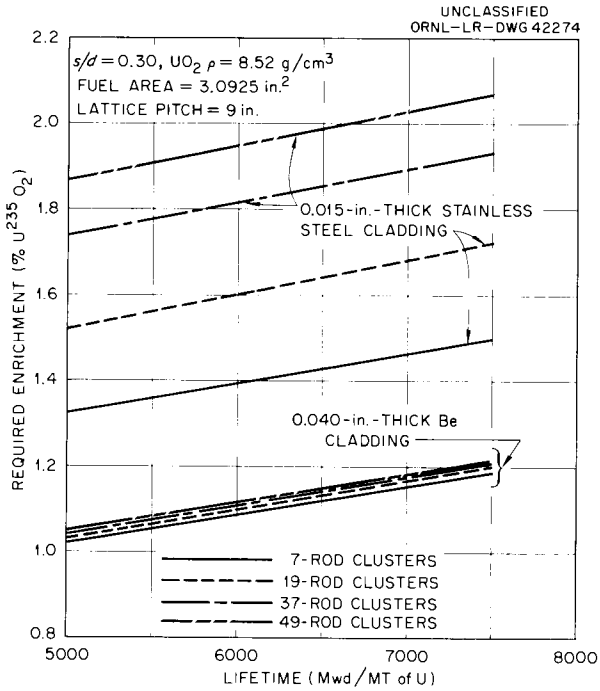

Fig. 1.11. Enrichment vs Lifetime for Stainless-Steel- and Beryllium-Clad Fuel Rods as a Function of the Number of Rods at a Lattice Pitch of 9 in. and a Fuel Area of 3.0925 in.^{2}.

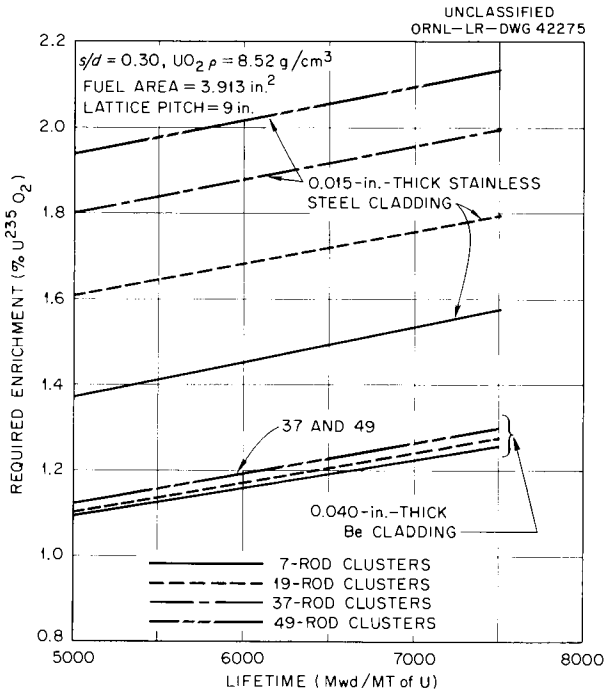

Fig. 1.12. Enrichment vs Lifetime for Stainless-Steel- and Beryllium-Clad Fuel Rods as a Function of the Number of Rods at a Lattice Pitch of 9 in. and a Fuel Area of 3.913 in.^{2}.

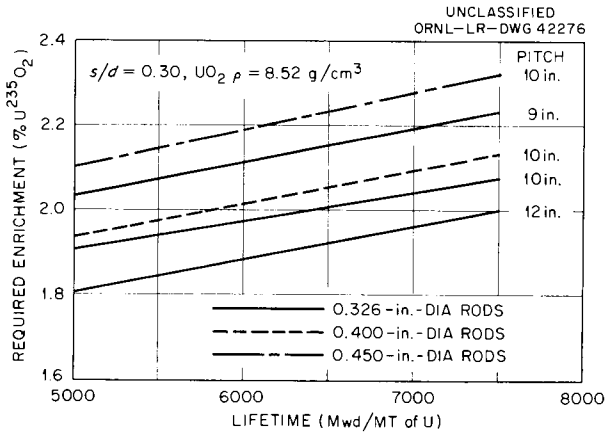

Fig. 1.13. Enrichment vs Lifetime for Rods Clad with 0.020 in. of Type 304 Stainless Steel in 37-Rod Clusters as a Function of Lattice Pitch and Rod Diameter.

cladding, however, a very small increase in enrichment is necessary when the number of rods in the cluster is increased from 7 to 61. Slight increases in the values of ϵ and p over those for stainless steel cladding are part of the effect of beryllium cladding.

Fast-Neutron Reactions in BeO

The probability of (n,2n) and (n,α) reactions in beryllium has been calculated by Häfele[17] using an essentially exact calculation of the neutron flux as a function of energy. The same technique has been applied, with Häfele's help, to the case of BeO. Results, given in Table 1.4, were based on upper and lower limit estimates of the (n,2n) cross section.

Table 1.4. Fast Reactions in Be and BeO

	Be	BeO
(n,2n) max	0.11845	0.07943
(n,2n) min	0.09397	0.06034
(n,α) beryllium	0.04235	0.02915
(n,α) oxygen		0.00444
Net fast effect		
max	1.076	1.046
min	1.051	1.027

[17] W. Häfele, The Fast-Neutron Multiplication Effect of Beryllium in Reactors, ORNL-2779 (Sept. 8, 1959).

2. REACTOR DESIGN STUDIES

Structural Investigations

Study of Fuel Cladding Behavior Under Arbitrary Temperature Distributions

The theoretical study of the deflections (bowing) and stresses in fuel element cladding[1] has been extended to include temperature functions of the following form:

$$t = \sum_m \sum_n D_{mn} \cos n\theta \sin \frac{m\pi x}{L} + \sum_k \sum_j D_{kj} \sin k\theta \sin \frac{j\pi x}{L} ,$$

where L is the length of the shell, θ and x are the angular and axial coordinates, respectively, and the coefficients, D_{mn} and D_{kj}, are predetermined functions of the summation indices m, n, k, and j. A function of this form is applicable to cases where the temperature distribution is not symmetrical about a diameter; hence, shells for which the locus of minimum temperature forms a spiral along the tube can be analyzed. The attempt to use the series to represent a concentrated force, as suggested previously,[1] was unsuccessful because too many terms in the series were required.

During the initial studies, the temperature was assumed to vary linearly along the diameter and to be independent of the length. Four shells with both length-to-radius (L/a) and radius-to-thickness (a/h) ratios within the range from 10 to 100 were investigated. It was found that the dimensionless deflection parameter, $w/(\alpha \Delta t\ a)$, for these shells was independent of the a/h ratio but varied directly with the quantity $(L/a)^2$. Here, w is the lateral deflection, α is the coefficient of thermal expansion, and Δt is the maximum diametral temperature differences.

---

[1] GCR Semiann. Prog. Rep. June 30, 1959, ORNL-2767, p 26.

In order to compare the results obtained by the series method with those given by beam theory, the curvature of a beam, as defined in the elementary theory, was expressed as

$$\frac{d^2w}{dy^2} = \frac{-\alpha\ \Delta t\ L^2}{a} f(y) = (\text{constant})\ f(y) \quad , \tag{1}$$

where y is the dimensionless axial coordinate x/L and f(y) is an unspecified function of y.

If f(y) = 1, Eq. 1 applies to a beam with simply supported ends and a constant temperature along the length; therefore, the deflection becomes

$$w = \frac{\alpha\ \Delta t\ L^2}{4a}\ y(1 - y) \quad , \tag{2}$$

and the center, or maximum, deflection is

$$w = \frac{\alpha\ \Delta t\ L^2}{16a} \quad .$$

The deflections calculated by using the series solution agreed with those from Eq. 2 to within ±1 in the third significant figure, which is within the accuracy obtained when the constant along the length [f(y) = 1 in Eq. 1] is represented by a sine series.

The following function was used in the examination of cases where the temperature varied linearly along the circumference from 0 to ±180 degrees:

$$t = t_0\left(0.5 + \frac{\theta}{\pi}\right) \quad . \tag{3}$$

On the basis of the results for five shells (a/h = 10 and 20, and 10 $\leq$ L/a $\leq$ 100), it was again concluded that the deflection parameter,

defined earlier, was independent of the a/h ratio but varied directly with $(L/a)^2$. The initial circular cross section became slightly "pear shaped" (except near the ends), but both the 0–180 and the 90–270 degree diameters increased by the same amount, namely, $2.0\ \alpha t_0 a$, for each shell considered. The line of symmetry was the 0–180 degree diameter.

The maximum deflection when the temperature is linear with circumference is approximately 27% below that given by the elementary linear theory, as shown in Fig. 2.1. It was reported previously[2] that experimental results gave maximum deflections approximately 12% below those calculated using linear theory. This discrepancy may be partially attributed to the fact that the experimental model did not have zero radial displacement at the ends as did the theoretical model, inaccuracy in the coefficient of thermal expansion used in comparing the experimental and theoretical results, deviations from a circumferentially linear temperature profile, and experimental error.

On the basis of profiles obtained from heat transfer experiments, the temperature profile around the circumference of a fuel element can be represented by a function of the following general form:

$$t = b \cos \theta + c \sin \theta + d \sin 2\theta \quad . \tag{4}$$

This representation appears to offer sufficient latitude for use in conjunction with thermal analysis work. More terms will be added, if necessary, when actual temperature profile becomes better known.

Although further work will include the investigation of several sets of values for the constants in Eq. 4, thus far only the set of values given below has been used:

$$t = 0.0632 \cos \theta - 0.4969 \sin \theta + 0.1629 \sin 2\theta \quad . \tag{5}$$

---

[2] Ibid., p 77.

The temperature profile given by this equation is shown in Fig. 2.2, where it is compared with one that is linear along a diameter and is represented by the following equation:

$$t = -0.5 \cos (\theta - 97.25) \quad . \tag{6}$$

In both Eqs. 5 and 6, the maximum diametral temperature difference is one degree along the 97.25–277.25 degree diameter.

A set of shells in which a/h was taken equal to 10 and 20 and L/a was taken equal to 10, 50, and 75 was considered for each of two groups of investigations. The circumferential temperature profile was represented by Eq. 5 for all units. In the first group, the temperature was assumed to be constant over the length, while in the second group it was assumed to vary linearly with length (right side of Eq. 5 was multiplied by y). Here, again, the dimensionless deflection parameter was found to be a linear function of $(L/a)^2$, when $L/a > 10$. Also, in each group, the bowing of the cylinder appeared to be in the plane containing the diameter over which the maximum Δt occurred.

The deflections obtained for the first group are shown graphically in Fig. 2.3, where they are compared with those calculated from linear theory (Eq. 2). The linear theory yields deflections which are approximately 2% below the series solution for $L/a = 10$, but the two methods yield identical values for L/a equal to 50 and 75.

In order to compare the deflection of the second group with the deflections obtained from linear theory, the f(y) function in Eq. 1 was taken equal to y. This yielded the following expression for the deflection along the length of a beam with simply supported ends:

$$w = \frac{\alpha \, \Delta t \, L^2}{12a} \, y(1 - y^2) \quad . \tag{7}$$

In Fig. 2.4 the deflections for the second group, which were obtained from the series solution, are compared graphically with those

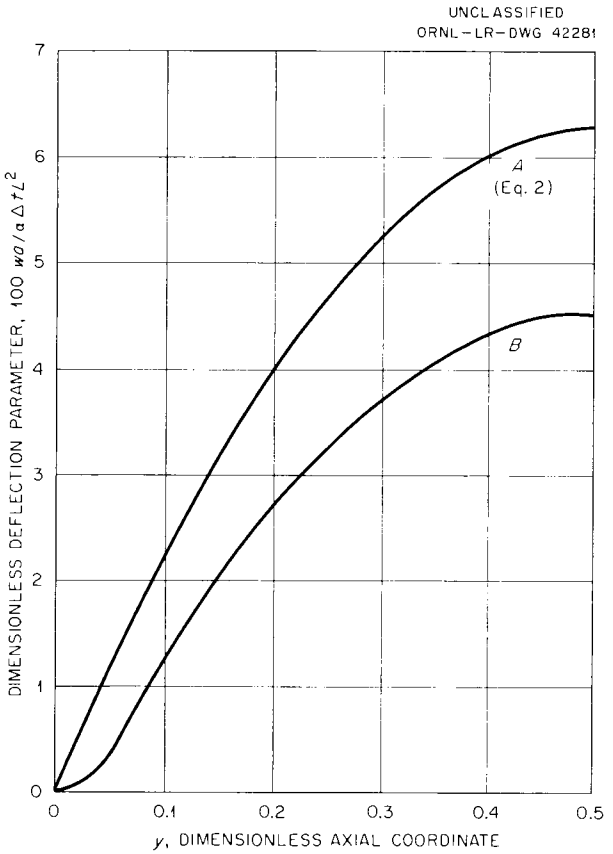

Fig. 2.1. Lateral Deflection Along Length of Shells When Temperature is Linear Along Diameter (Curve A) and When It Is Linear Along Circumference (Curve B).

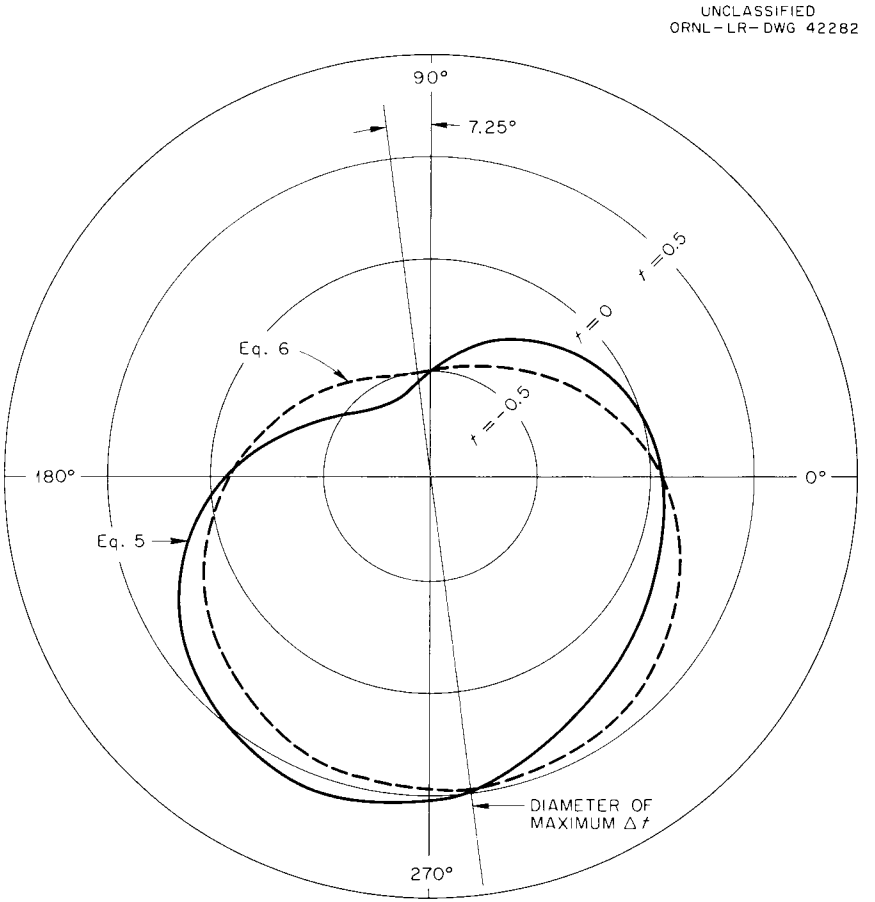

Fig. 2.2. The Temperature Profiles Represented by Eqs. 5 and 6.

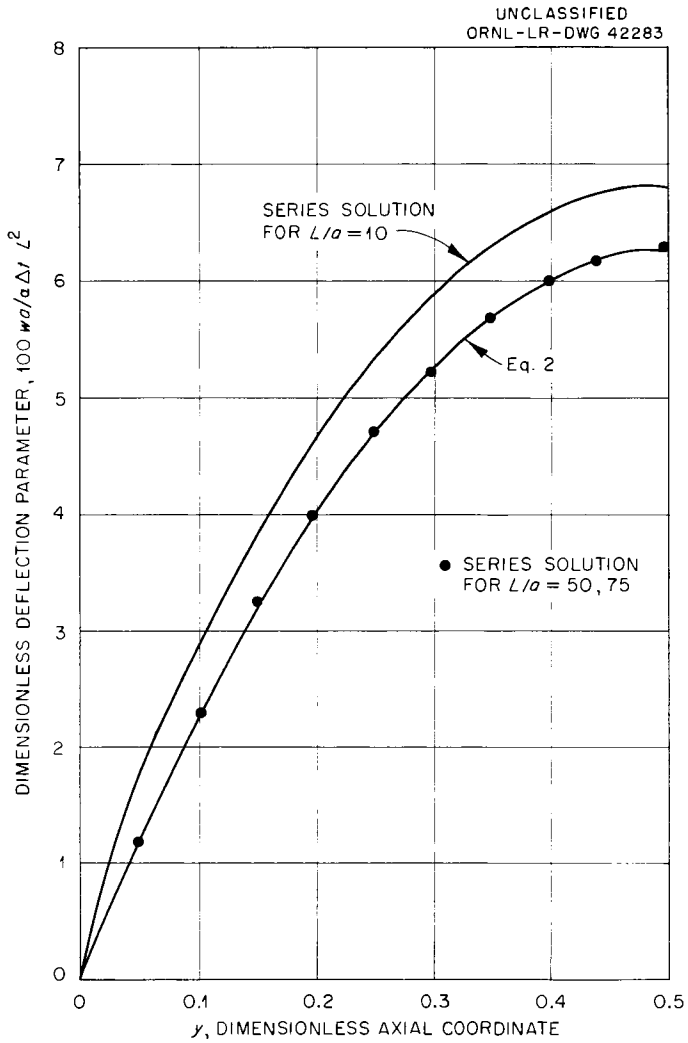

Fig. 2.3. Lateral Deflection of Shells Along the Length in the Plane Containing the 97.25–277.25 Degree Diameter for the Temperature Profile Represented by Eq. 5.

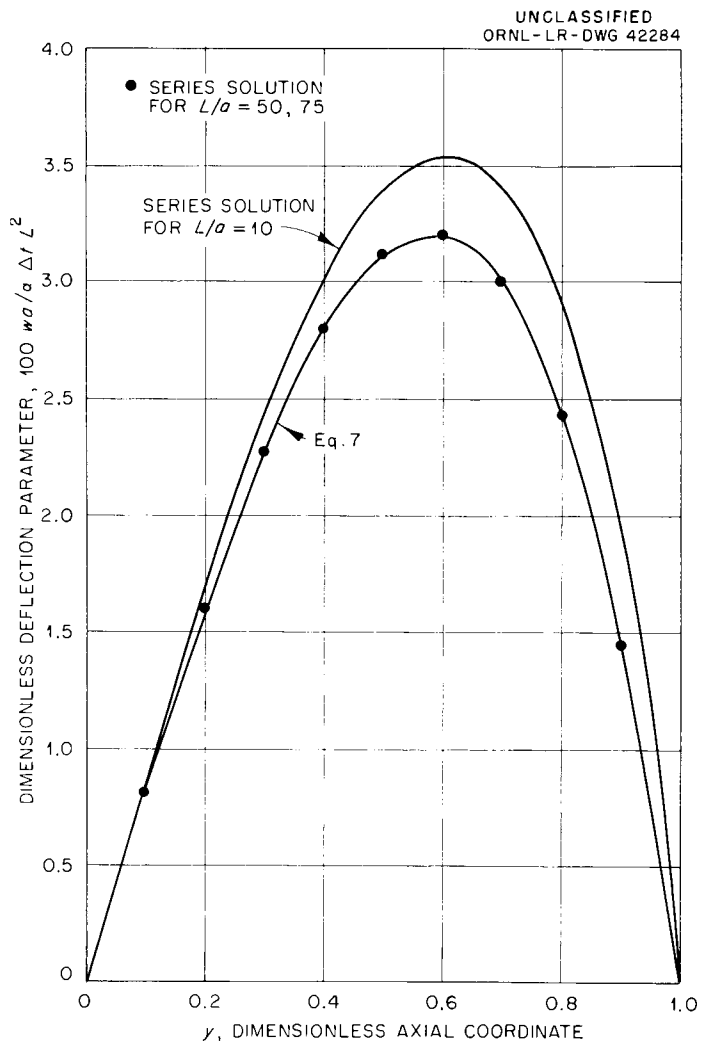

Fig. 2.4. Lateral Deflection Along Length of Shells in the Plane Containing the 97.25–277.25 Degree Diameter for the Temperature Profile Represented by y Times the Right Side of Eq. 5.

given by Eq. 7. As may be seen, the linear theory gives deflections approximately 1% below those from the series solution for L/a = 10, but the results are identical for L/a equal to 50 and 75.

A report describing the entire analysis will be published when the studies applicable to the EGCR fuel element have been completed.

Creep Behavior of Fuel Element Cladding

The deflection or bowing of the EGCR fuel element cladding as a result of temperature differences across a rod can be predicted using elastic theory. However, elastic analyses are not applicable for elements in the higher temperature regions of the reactor; therefore, an analytical study is also being made to determine the magnitude of bowing as dictated by the creep characteristics of the material. Throughout this study the temperature has been taken as a linear function of the diameter.

The analytical model is based on the assumption that the temperature differential is suddenly applied and an initially elastic system exists. The restrained bowing of the element puts a force on the central spacer and produces stresses in the element walls. However, subsequent creep of the material results in thermal relief of the initial forces. The creep relationship chosen for the analysis is one which agrees closely with experimental data for type 304 stainless steel, and it is given by

$$\dot{\epsilon} = \left(\frac{\sigma}{A}\right)^n ,$$

where ϵ is the strain rate, σ is the stress, and A and n are constants.

As a first step in calculating the displacements, the time decay of the force on the central spacer has been computed for mean temperatures of 1300, 1400, 1500, and 1600°F. The temperature differences across the rod were taken as 30, 40, and 50°F. The force vs time curves for each mean temperature value are shown in Figs. 2.5 through 2.8. The

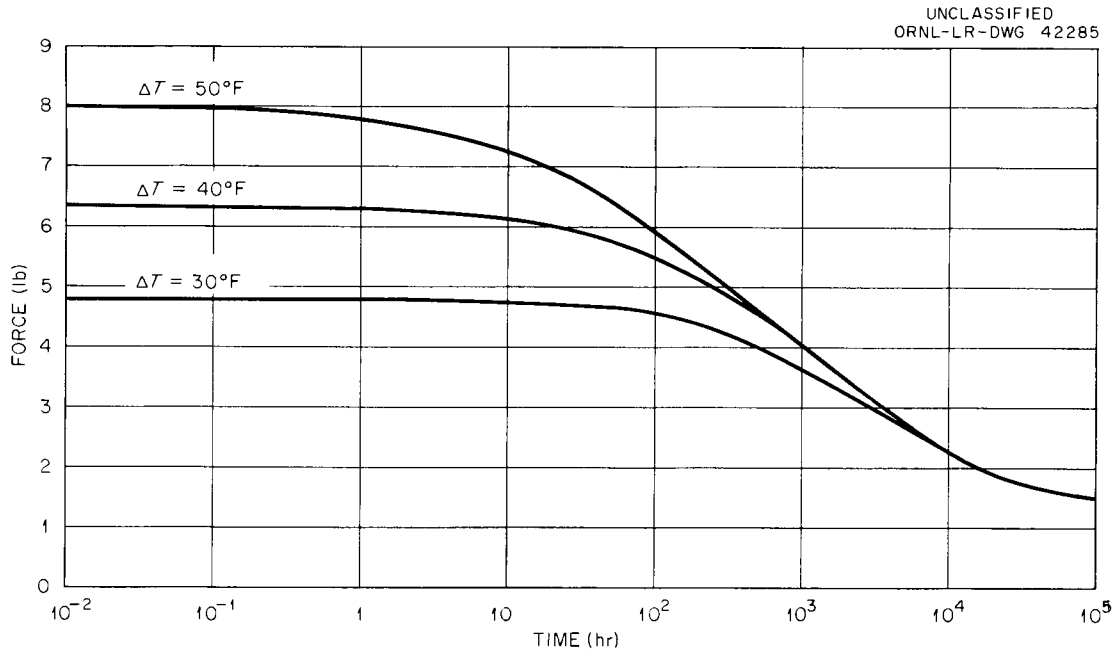

Fig. 2.5. Time Decay of Force on Central Spacer of EGCR Fuel Element for Various Temperature Differences Across a Rod at a Mean Temperature of 1300°F.

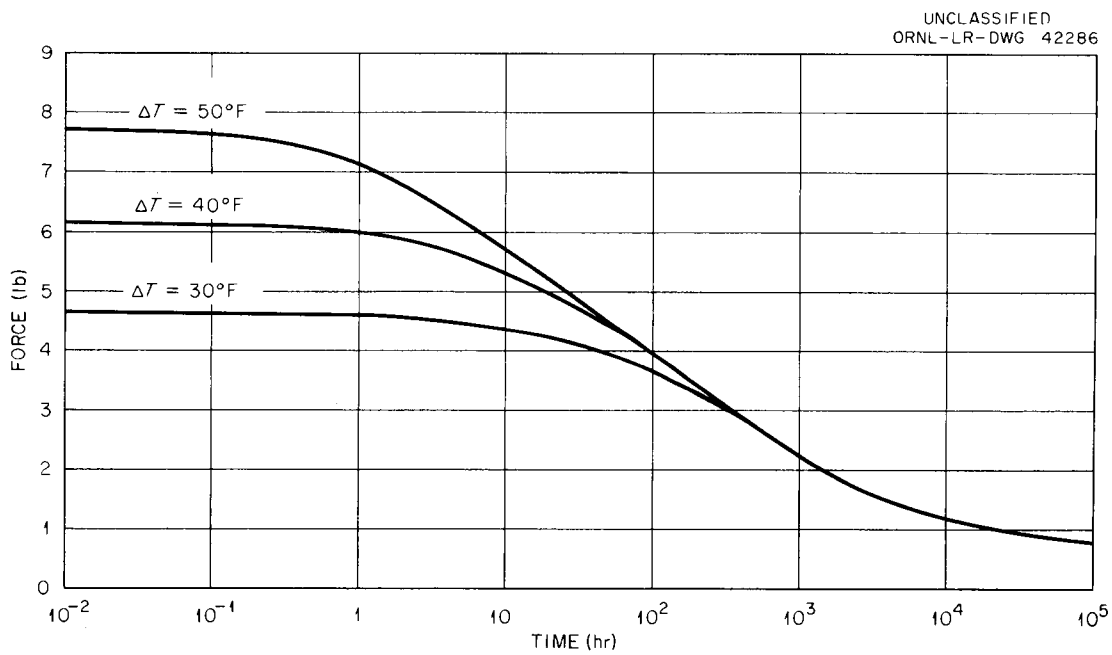

Fig. 2.6. Time Decay of Force on Central Spacer of EGCR Fuel Element for Various Temperature Differences Across a Rod at a Mean Temperature of 1400°F.

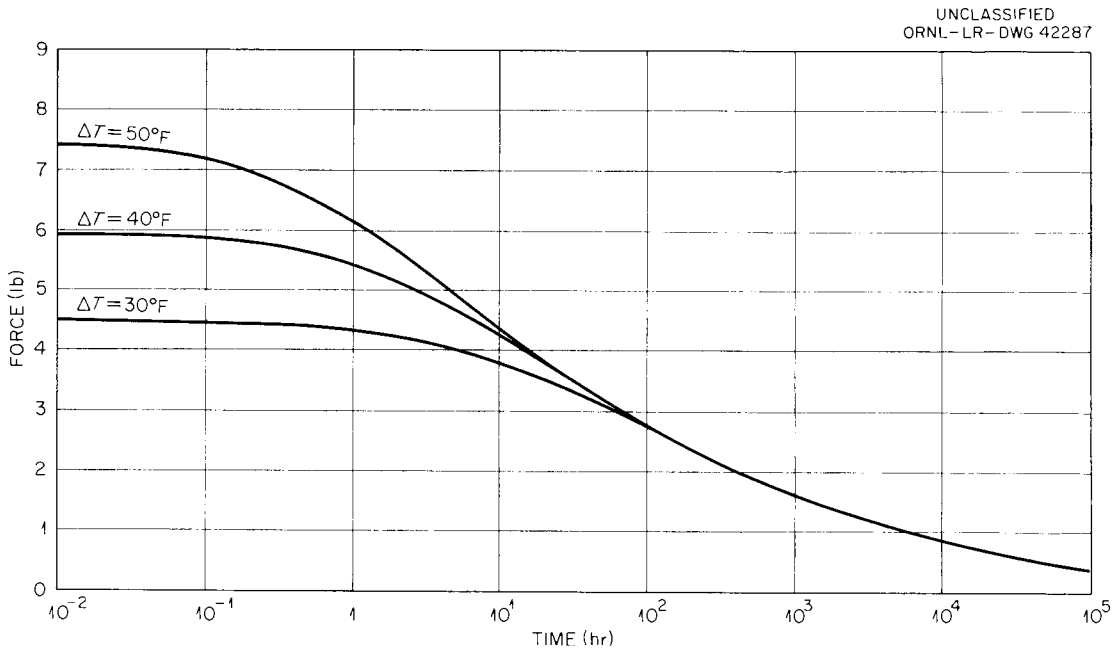

Fig. 2.7. Time Decay of Force on Central Spacer of EGCR Fuel Element for Various Temperature Differences Across a Rod at a Mean Temperature of 1500°F.

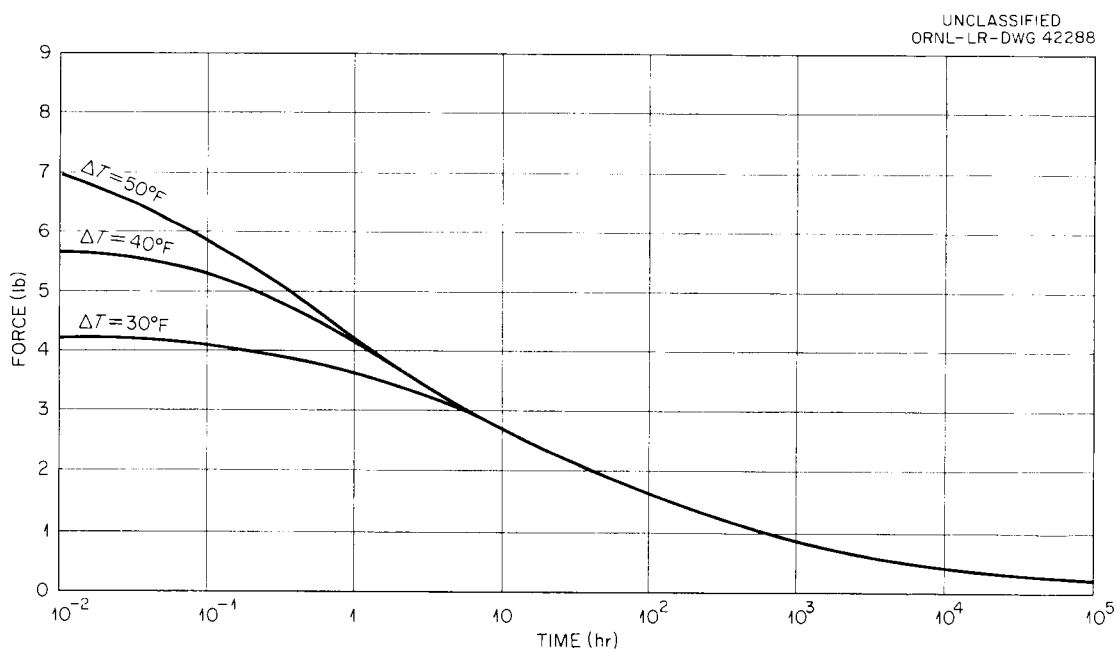

Fig. 2.8. Time Decay of Force on Central Spacer of EGCR Fuel Element for Various Temperature Differences Across a Rod at a Mean Temperature of 1600°F.

initial force is directly proportional to the mean temperature, and the figures show that after a given time, corresponding to each temperature, the force is independent of the temperature difference.

The stress state of a general cross section is such that the creep deformation will tend to decrease the initial thermal curvature along a tube. However, the configuration is dependent upon the integrated effect over the length of the element. The profile of the axial center line as a function of time is being calculated for each case using a creep analysis similar to that employed to obtain the constraint force vs time histories.

Tests of Threaded-Pin-Type Graphite Column Joints

It has been proposed that the graphite core for the EGCR be made of individual square columns, 16 in. on a side and 232 in. long.[3] Each column is composed of five blocks, stacked vertically, and fastened together by threaded graphite pins. Male and female joints between mating blocks are also used for resisting horizontal shear forces on the columns.

In order to determine the load-carrying ability of the proposed column design, tests were run on single joints. The test joints, made of AGOT graphite, are shown in Fig. 2.9. All the units are one-fourth scale, and each block has four holes corresponding to the fuel channels. The central hole in each block is tapped to receive the threaded pin. The boss on the end of the block on the left (Fig. 2.9) fits into a recess in the mating block.

The pin is 4 in. long, and it has left- and right-hand threads, 1 5/8 in. long, on opposite ends. The threads are 1-in.-dia, 8 threads per inch, Whitworth-type, with class 2 fit. There is a 1/8-in.-wide groove for thread relief between the left- and right-hand threads; at

---

[3] Experimental Gas-Cooled Reactor Preliminary Hazards Summary Report, ORO-196, p 3.7 (May 1959).

that point the diameter is 13/16 in., that is, approximately 0.040 in. less than the root diameter of the threads.

A unit prepared for testing is shown in Fig. 2.10. In the tests, pure moment loadings were applied to the blocks and deflections were measured at the joint by means of two dial indicators, one at each edge of the block. The load was applied through a Baldwin SR-4 load cell. The bottom support pins were placed 20 in. apart and the top pins were separated by a distance of 16 in. so that the magnitude of the bending moment was equal to the magnitude of the applied load.

Two pin specimens were tested; in each case the pre-torque on the pin was 60 in.-lb. Fracture occurred at the groove in the pin when the bending moment reached 1200 in.-lb in one case and 1250 in.-lb for the other. A typical pin fracture is shown in Fig. 2.11. If it is assumed that the pins were in pure tension, the stress at failure was approximately 1200 psi in both cases.

The deflection at the joint was linear with load and it reached a maximum of 0.020 in. at failure. The load was applied in 20 in.-lb increments and an attempt was made to measure the amount of permanent deformation after each incremental load increase. However, no permanent deformation was detected up to the load at failure.

A third test was run with no preload on the pin and a 1/16-in. gap between the graphite blocks. In this case the element was subjected to a pure bending load, and it failed when the applied moment reached 160 in.-lb. Again, fracture occurred at the groove in the pin. The data obtained gave the flexural strength as approximately 2900 psi.

Since the region of failure was always in the groove between the left- and right-hand threads and the stress concentration factor for Whitworth threads is approximately twice that of the fillet in the 1/8-in. groove, the graphite pins did not appear to be notch sensitive. A brittle type of failure always occurred, and the elongation at rupture was negligible.

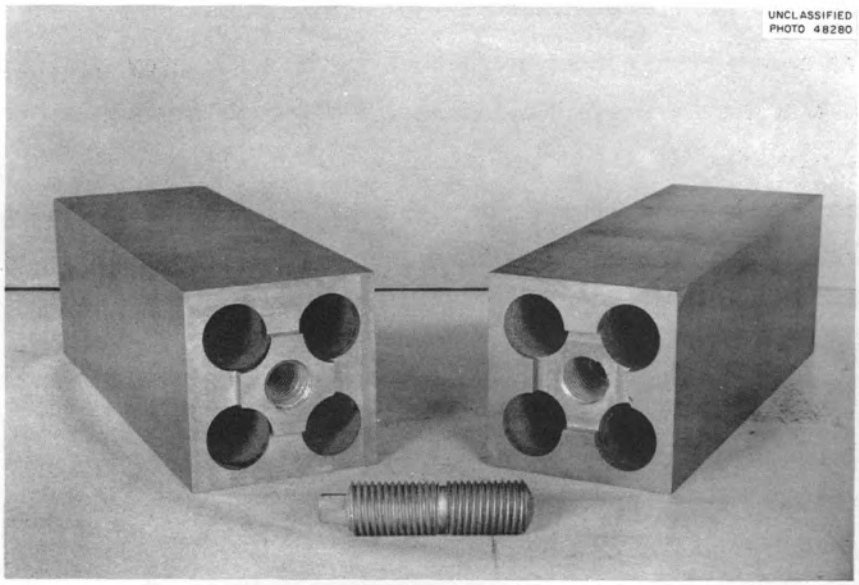

Fig. 2.9. One-Fourth Scale Graphite Column Blocks and Threaded Pin.

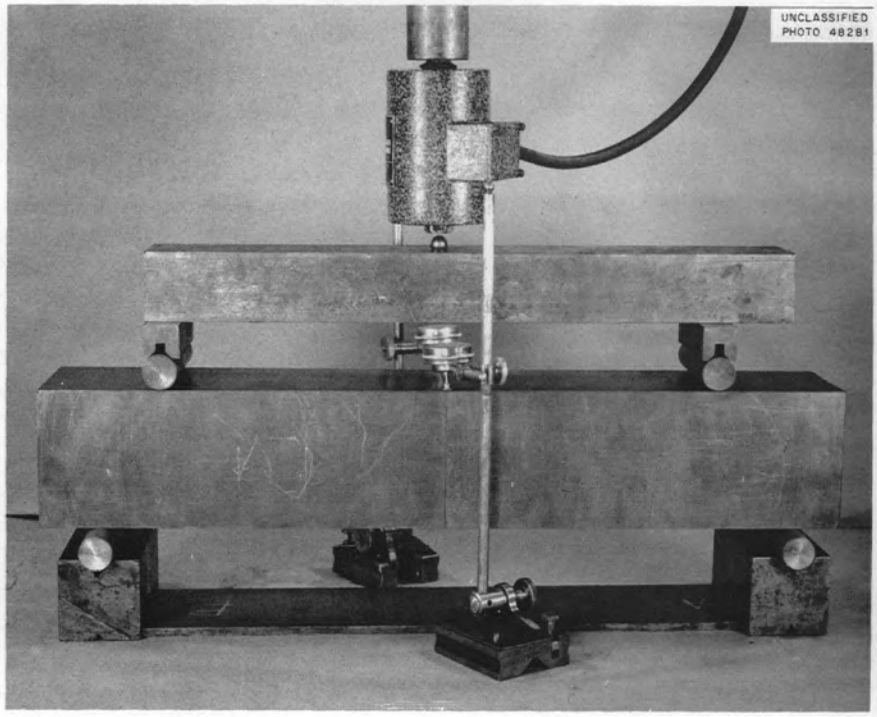

Fig. 2.10. Graphite Column Joint Specimen Set Up for Testing.

Tests of Metal-Clad Graphite Bodies

Since metal-clad graphite fuel elements have many desirable features from both the heat transfer and nuclear standpoints, a test program has been initiated for studying behavior of the cladding. The cladding materials considered thus far tend to expand away from the graphite when the temperature of the element is increased; therefore, the first objective is to study the mode of collapse of the cladding when it is forced to conform to the outside of the graphite structure. In addition, the number of thermal cycles required to cause failure of a given element will be determined. Once the mode of collapse has been established, means for minimizing peak strains and controlling the collapse pattern will be investigated.

Fabrication of the first metal-clad graphite body has been completed. The encapsulated portion is made up of two 3.96-in.-OD solid cylinders of grade CS-312 graphite (see Fig. 2.12) which were screwed together to form a single 68-in.-long cylinder. Preforming of the metal cladding was suggested as a means for controlling its collapse characteristics, and therefore helical grooves were machined into the graphite cylinders, as shown in Fig. 2.12, to serve both for preforming the metal tube and to provide voids into which the metal can deform in accommodating the differential thermal expansion. The grooves are of semicircular cross section with a 1/16-in. radius and a helix angle of 45°.

Prior to assembly of the test unit, the graphite cylinders were degassed at 900°C in a vacuum of 10 μ Hg. Following this, helium was bled into the furnace to restore it to atmospheric pressure, and the cylinders were sealed into helium-filled containers until the final assembly of the element was made.

The metal envelope is a type 321 stainless steel welded tube which has a 4-in. OD and a 0.016-in. wall. This tube was welded to end caps that were threaded onto the graphite cylinder. A tube was mounted in one end cap to provide communication with the inside of the envelope. The container was evacuated to 10^{-5} μ Hg, and a pressure gage was attached to the small tube so that leaks in the cladding could be detected.

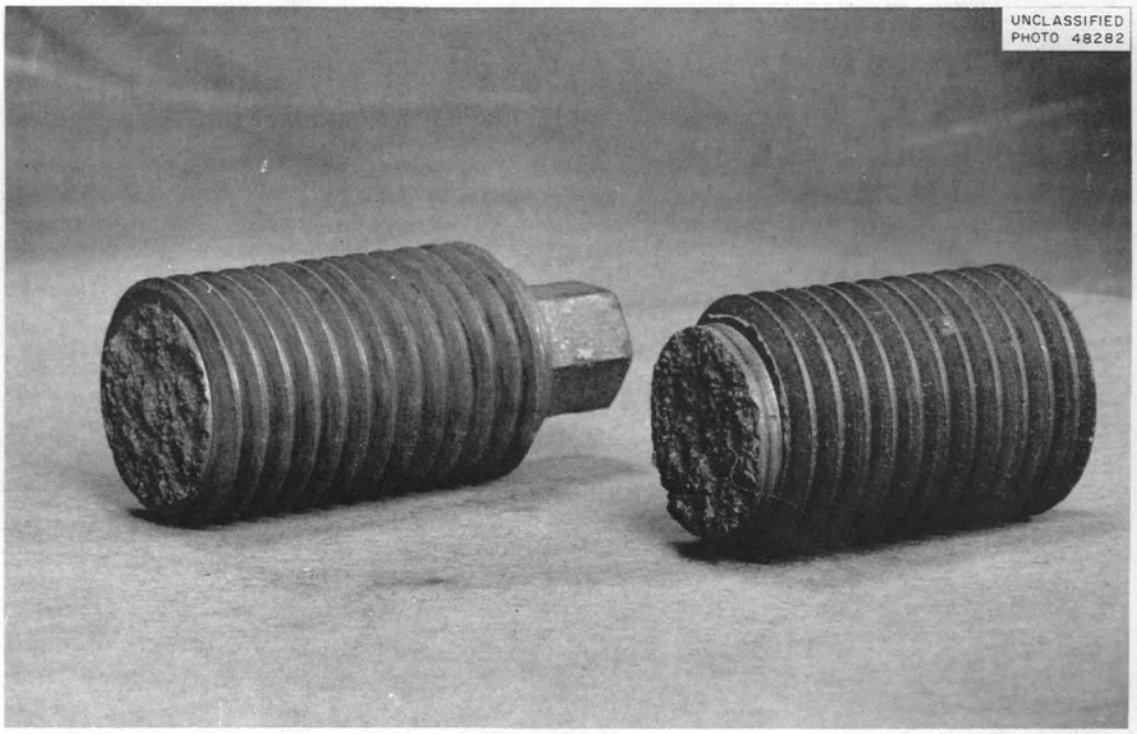

Fig. 2.11. Threaded Graphite Pin After Fracture.

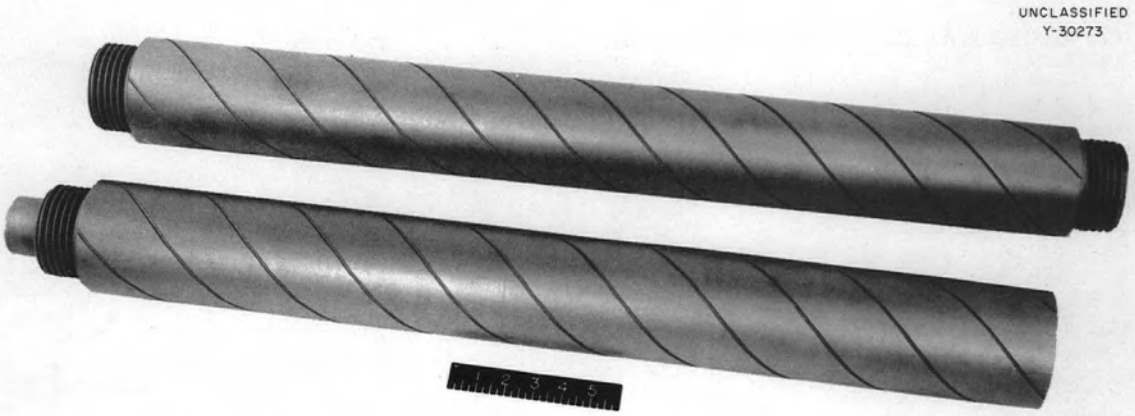

Fig. 2.12. Solid Graphite Cylinders.

The metal-clad element was then placed in a pressure chamber and exposed to an external pressure of 2500 psi in order to collapse the cladding into the grooves. During this process, two external wrinkles were formed in the cladding; one was a longitudinal wrinkle approximately 1/16 in. in height along the complete length of the graphite, and the other was a circumferential wrinkle at the joint between the graphite and the end cap. Pictures of the grooves and wrinkles in the cladding are shown in Figs. 2.13 through 2.16. Figure 2.13 shows the grooves at the mid-point where the two graphite rods are joined. It may be noted in Fig. 2.14 that along the longitudinal weld in the tube the cladding did not completely deform into the groove. The longitudinal wrinkle may be seen in Fig. 2.15, and Fig. 2.16 shows the circumferential wrinkle at the end of the element.

The furnace to be used in the testing program and the first test element partially lowered into the furnace are shown in Fig. 2.17. The element will be tested in an atmosphere of helium. The external pressure will be 300 psi, and the temperature along the element will be varied from approximately 600°F at the bottom to approximately 1300°F at the top. The temperatures will be cycled from room temperature to the above maxima until rupture of the cladding occurs.

Thermal Performance of Fuel Elements

Thermal Analysis

In any analytical model for investigating the temperature structure and thermal stability of a seven-rod fuel element cluster, a determination must eventually be made of the effect of heat conduction around the circumference of the element on the actual temperature and the effect of this temperature variation on the displacement or bow of the element. Even for a design such as that proposed for the EGCR fuel elements with central spacers to limit the movement of the rods, a knowledge of the effects mentioned above is needed for estimating the magnitude of the hot spot or hot streak along the tube. This estimate may be especially

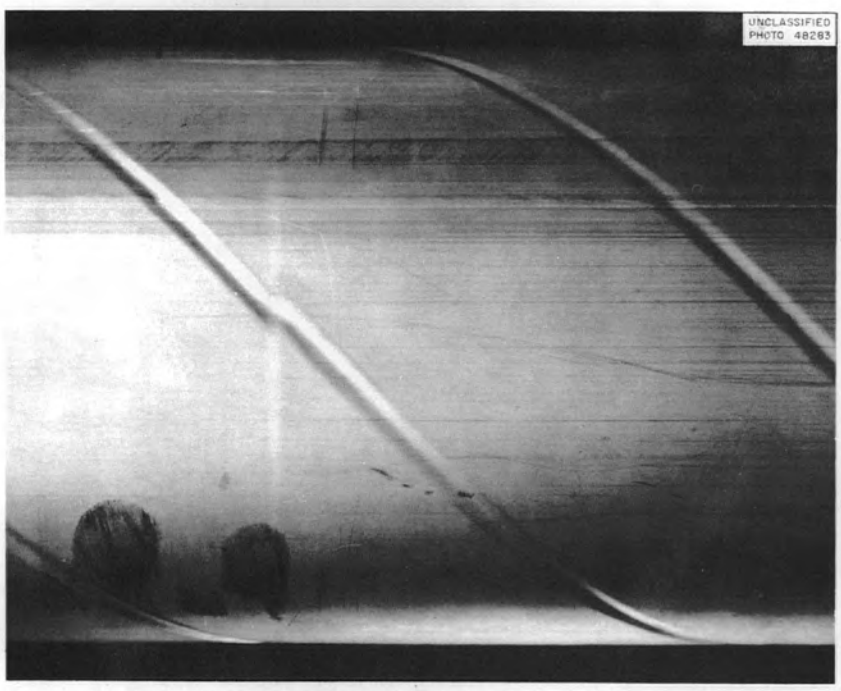

Fig. 2.13. Central Region of Test Unit After Collapse of Cladding onto Helically Grooved Graphite Cylinders.

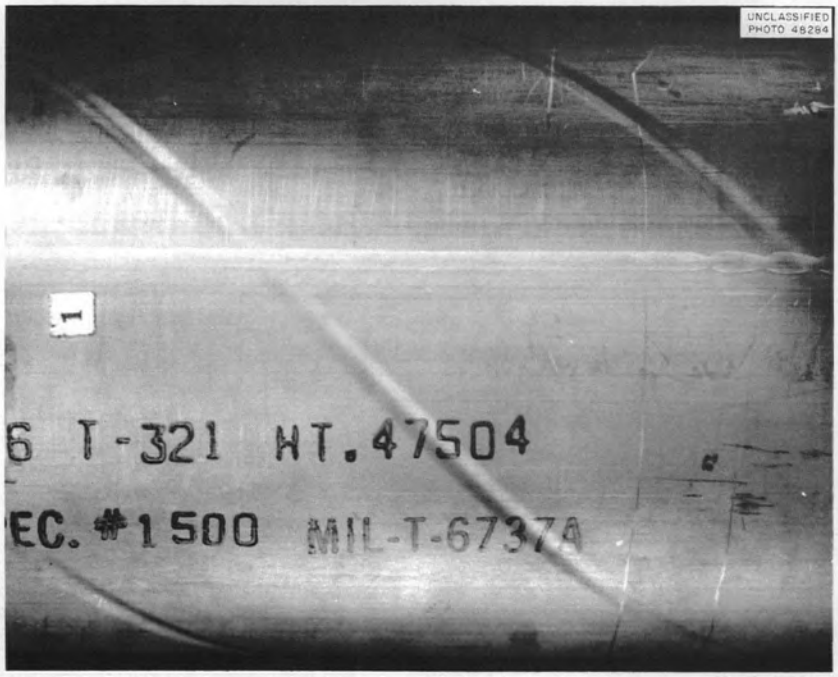

Fig. 2.14. Test Unit Showing Collapse of Cladding into Groove in Region of Seam Weld of the Cladding Tube.

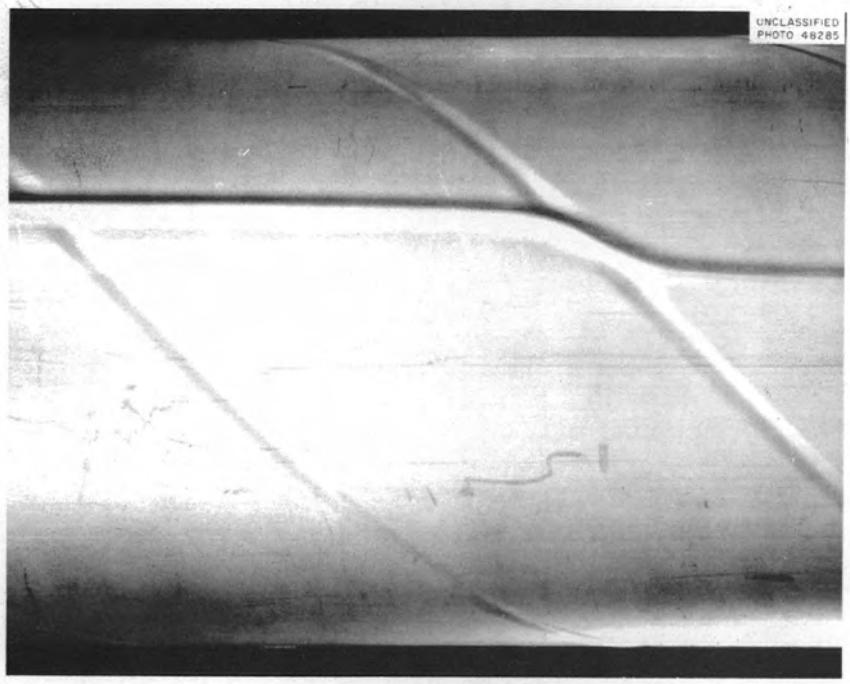

Fig. 2.15. Test Unit Showing Longitudinal Wrinkle in Cladding.

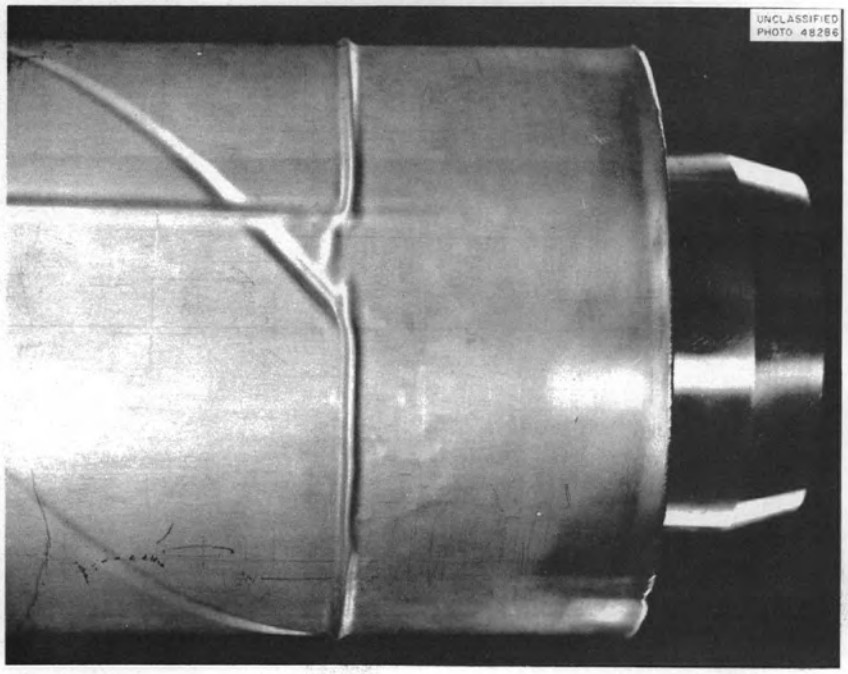

Fig. 2.16. Test Unit Showing Circumferential Wrinkle in Cladding at the Joint Between the Graphite and the End Cap.

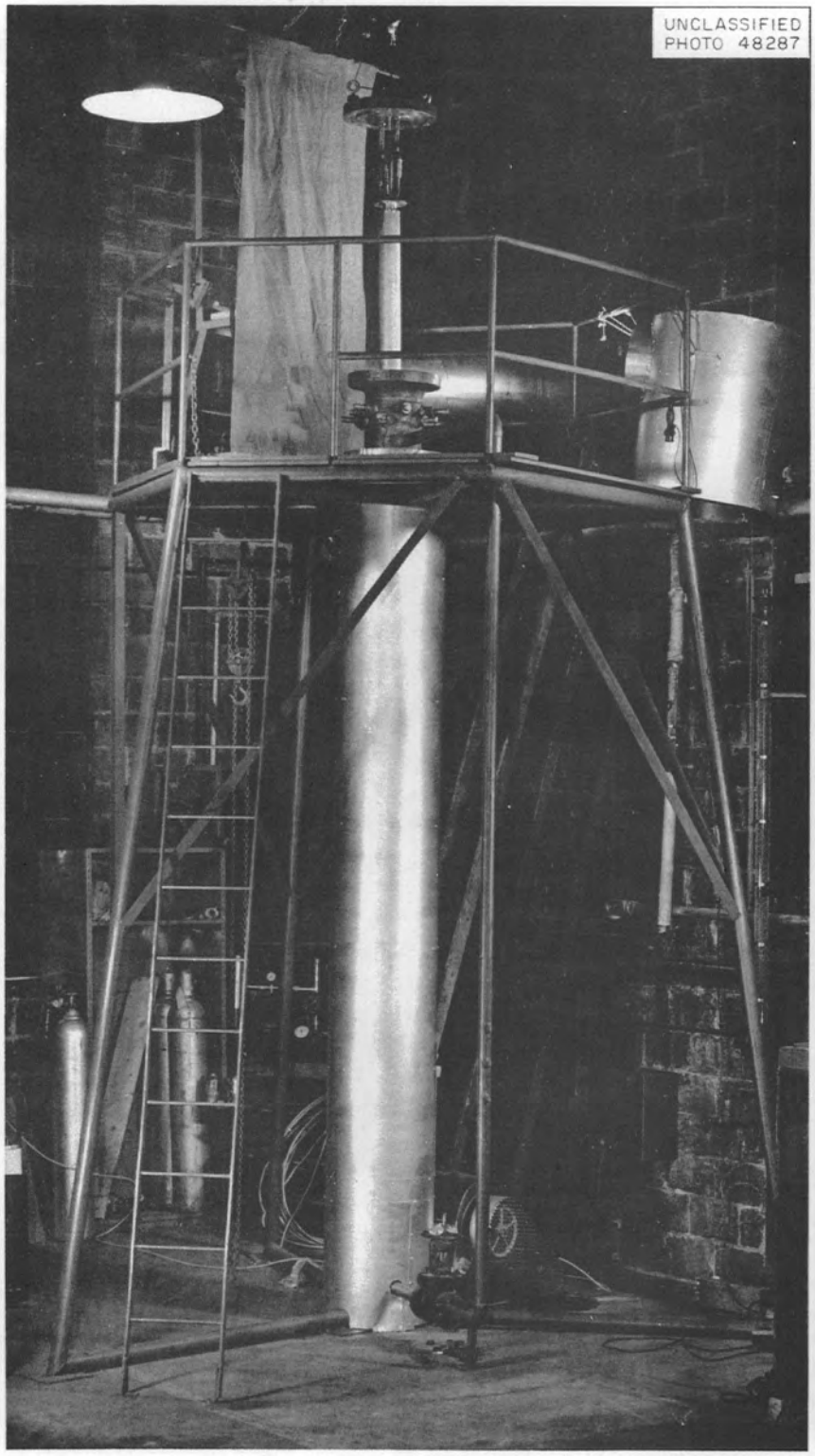

Fig. 2.17. Furnace With Metal-Clad Graphite Unit Partially Lowered Into Test Position.

important for a design with an appreciable flux gradient across the outer rods of the assembly.

The temperature distribution in the thin, cylindrical shell which contains the fissionable material was determined analytically by assuming that the temperature profiles around the shell were similar at various axial locations along the rod. This assumption was justified by the experimental results of the resistance-heated-tube heat transfer experiments.[4] The determination of the heat transfer between the fuel elements and the coolant gas was based on the assumption that the coolant gas flowing along the rods could be considered to be flowing in six parallel channels around each rod. The solution to this exterior heat transfer problem gives the bulk fluid temperature and heat transfer coefficient in six separate segments around the rod. The temperature distribution in the shell is then obtained as the solution to the conduction problem of a piecewise constant heat input on the inner surface of the shell with a corresponding piecewise constant heat transfer coefficient and bulk fluid temperature on the outer surface of the shell.

This method of calculating the temperature in the cladding of the fuel rods has been used with success in calculating the temperature profile about the simulated fuel rods of the experimental system mentioned above.[4] The effect of the temperature profile on the displacement of the elements is described in the preceding section of this chapter on "Structural Investigations."

EGCR Fuel Element Vibrations

In the design of a fuel element one of the many factors which must be investigated is the aerodynamic stability of the element. In the case of the EGCR seven-rod fuel cluster, calculations have been made for the natural frequencies and amplitude of vibrations. A study has also been completed for determining the possibility of an element tending to "wrap-up" or twist about the central rod of the cluster.

---

[4] GCR Semiann. Prog. Rep. Dec. 31, 1958, ORNL-2676, p 36.

The natural frequencies investigated were the torsional frequencies for one end of the element fixed and for both ends fixed and also the flexural frequencies. The results are presented in Table 2.1. The

Table 2.1. Natural Frequencies of EGCR Fuel Rods

Torsional Frequencies (cycles/sec)		Flexural Frequencies (cycles/sec)
Both Ends Fixed	One End Fixed	
553	309	26
1130	936	105
1739	1583	235
2370	2260	419
3050	2910	654
3700	3700	942
4400	4300	1282

amplitude of the flexural vibration was calculated from the results of Burgreen[5] and found to be approximately 0.006 in.

In the study for determining the tendency of an assembly of suspended elements to twist about the central element, the approach was to determine a lower limit of the velocity which could "wrap-up" an assembly. This minimum velocity approach was very conservative, and thus the actual velocity required would be considerably greater. For the EGCR design the minimum critical velocity was about 450 ft/sec or about 1.5 times the highest velocity in the elements.

Parametric Study

A set of charts has been prepared to facilitate the evaluation of the thermal performance of a helium-cooled reactor.[6] The system

[5]D. Burgreen, "Vibration of Rods in Parallel Flow," Nucleonics, August 1959.

[6]L. G. Epel, A Parametric Study of a Gas-Cooled Reactor, ORNL CF 59-7-88 (July 24, 1959).

considered was fueled with UO_2 with the fuel assemblies consisting of clusters of long cylindrical elements, each covered by a stainless steel jacket. The axial power distribution was assumed to be a "chopped cosine" having an axial peak-to-average ratio of 1.32. The evaluation of such a system normally involves a number of iterative calculations. The purpose of the study was to prepare charts to eliminate the need for tedious calculations and to point out regions which appear attractive for a more concentrated exploration. The charts do not determine an optimum operating point.

The three dependent variables which can be evaluated from the graphs are (1) diameter of the coolant channel, (2) pressure drop across the core, and (3) pumping power. The values of these parameters can be determined only after a number of independent variables are fixed. The independent variables are (1) gas inlet temperature, (2) gas outlet temperature, (3) maximum fuel rod surface temperature, (4) fuel rod diameter, (5) number of fuel rods per cluster, (6) heat output per foot of rod at the center of the reactor, (7) coolant gas pressure, and (8) length of coolant channel. These eight quantities uniquely determine the three parameters sought once the coolant physical properties are assumed. The number of variables involved requires the use of several intermediate parameters, and the results can be obtained only from a series of charts. The charts facilitate a rapid evaluation of the dependent variables.

Helium Purification System for the EGCR

In order to limit graphite burnup and carbon mass transfer in the EGCR, it has been specified[7] that the normal, steady-state level of helium coolant impurities must not exceed the following values:

Component	Limit (ppm by wt)
CO_2	18,000
H_2	1,000
N_2	1,000

Once graphite degassing is complete, it is expected that in-leakage of water will be the major source of coolant impurities. Water vapor in the coolant will react with the hot graphite to produce CO, CO_2, and H_2, as well as some CH_4 (and possibly smaller amounts of other hydrocarbons). Therefore, to insure the proper control of the impurity levels, specific provision must be made for the steady or intermittent removal of H_2O, CO_2, CO, H_2, and hydrocarbons from the coolant system.

A detailed analysis[8] of the helium purification problem has led to the recommendation of a purification system which incorporates the following units and operations.

1. Catalytic Converter. A bypass stream of helium at 1050°F would be withdrawn from the coolant system at the rate of 130 lb/hr, passed through a filter (possibly optional), mixed with slightly less than the stoichiometric amount of oxygen required for the oxidation of the CO, H_2, and hydrocarbon impurities, and then sent to a catalytic converter containing Girdler G-43 platinum catalyst operating at a temperature of approximately 1100°F.

2. Cooler-Condenser. The "oxidized" bypass gas from the catalytic converter would join a stream of buffer helium (up to 800 lb/hr at 360°F and 305 psia) from the helium blower and compressor water seals and then enter a cooler-condenser. Here the gas would be cooled to 90°F or less and the bulk of its water vapor would be removed by condensation.

3. Silica-Gel Adsorber. The cool, partly-dried gas from the cooler-condenser would then pass through a bed of silica gel, where virtually all the remaining water would be removed.

4. Linde Molecular-Sieve Adsorber. The dry gas from the silica-gel adsorber would then enter a bed of molecular-sieve adsorbent which would remove practically all the CO_2.

---

[7] Appendix to Gas-Cooled Reactor Preliminary Design, p F-62, IDO-24027 (March 1959).

[8] F. A. Anderson, Proposed Helium Purification System for the Experimental Gas-Cooled Reactor (EGCR), ORNL-2819 (Oct. 2, 1959).

5. Filter and Compressor. The effluent gas from the molecular-sieve adsorber would be dry and free of CO_2, but it would still contain the CO, H_2, and hydrocarbons that entered the purification system in the unoxidized stream of buffer helium. It would be filtered, compressed to 318 psia, and discharged to the reactor vessel coolant system. The primary purpose of the filter would be to remove particulate matter that entered the purification system or that was produced within the system (as a result of adsorbent-bed attrition, for instance) so that this material would not injure the compressor or be returned to the coolant system.

The proposed purification system does not include provisions for the planned removal of radioactive impurities, such as krypton or xenon, or for the removal of minor impurities, such as nitrogen and argon.

EGCR Hazards Evaluation

As previously noted[9] the EGCR Hazards Report[10] was submitted for review by the Hazards Evaluation Branch and the Advisory Committee on Reactor Safeguards in May. Subsequent discussions with members of the Hazards Evaluation Branch revealed their concern on several points which were not covered in sufficient detail in the original report. In order to resolve these issues in time for the formal ACRS hearing on July 24, 1959, a supplemental report was prepared by Kaiser Engineers, Allis-Chalmers Manufacturing Company, and Oak Ridge National Laboratory.[11] The points in question included (1) reduction of the gaseous contamination within the containment vessel following the maximum credible accident, (2) total exposure as a function of distance from the containment shell following the maximum credible accident (including justification of the self-shielding in the calculation of direct exposure from the

---

[9] GCR Semiann. Prog. Rep. June 30, 1959, ORNL-2767, p 94.

[10] Experimental Gas-Cooled Reactor Preliminary Hazards Summary Report, ORO-196 (May 1959).

[11] Supplement to ORO-196 (July 17, 1959).

activity released to the containment shell), (3) sources of water within the containment shell, and (4) discharge of activity from relief valves.

Closely related to the question of the level of gaseous contamination within the vessel is the question of the specified containment vessel leakage rate. There is a tendency to apply the tightest attainable leakage specification to the reactor containment vessel regardless of the possible reactor activity release. However, there did not appear to be any basis for accepting the complications and added costs attendant to an arbitrarily established leak rate other than that shown to be necessary by a conservative analysis.

In the original hazards analysis, it was assumed that 90% of all activity released to the containment vessel, except the noble gases, would be deposited within the containment vessel and thus not be available to leak out. Although the existence of the deposition process is generally admitted, the lack of experimental data has prevented designers from taking credit for any such process in hazards analyses. Furthermore, although some data on "plating out" are now available which indicate that the process is important, the EGCR can attain the necessary factor of 10 reduction in the 8-hr inhalation exposure by recycle filtering of the gaseous contamination in the containment vessel, even without taking credit for other removal processes. Thus the reduction of the contamination by deposition, settling, decontamination factor of the shell leak, etc., will be in addition to that allowed, and is expected to be significant.

The total exposure following the maximum credible accident was recalculated. Inasmuch as the design criterion for the plant is that the maximum credible accident shall not result in an off-site exposure in excess of 25 r within 8 hr after the accident, the containment vessel leakage rate was set accordingly and resulted in a specification of 2.2%/day.

In the analyses, an exposure of 50 r to the thyroid and 25 r to the bone was assumed to be equivalent to 25 r total body. Since the

calculation had shown that the exposure to the bone was less than one-half that to the thyroid, the thyroid exposure of 50 r determined the allowable leakage rate. This dose has three components: (1) inhalation exposure from the radioactive cloud formed by activity leaking out of the containment vessel into the atmosphere, (2) direct external exposure from the radioactive cloud, and (3) direct external exposure from the activity within the containment shell. The determination of the exposure from the first two sources involves the calculation of atmospheric dispersion of the activity and, for the third source, the calculation of the distribution of the activity within the containment vessel. The direct exposure from activity within the containment shell was calculated by assuming that all activity released from the fuel element was uniformly distributed throughout the containment vessel volume, and an allowance was made for the attenuation of the radiation flux by the building structure. Thus at the point of highest off-site exposure, which occurred at a distance of ~2400 ft, the 8-hr contribution of each of the three sources was the following:

Source	Equivalent Total Body Exposure (r)
Inhalation	24
Submersion	0.9
Direct from container	0.1
Total	25

Computations of the reactivity values for the EGCR show that if the core is flooded with water when the reactor is clean and cold and all the control rods are inserted, the k_{eff} would be approximately 1.13. For this reason it is important to assure that the reactor core cannot become flooded. There are two possible modes by which water might enter the reactor vessel. These are (1) failure of a pipe or vessel wall which separates the reactor coolant system from a water-cooling circuit and (2) flooding of the EGCR containment shell while some portion of the primary circuit is open. While it is extremely unlikely that either

of these circumstances could occur, the design has been arranged to prevent such entry of water from flooding the core.

There are two major constraints under which the relief system must be designed. First, the relief valves must always be capable of protecting the system on which they are installed, and, second, gas cannot be released outside the containment shell if its activity level is above the specified maximum. Thus, since the primary system can contain activity, it is possible that the system might relieve itself at such a time when the activity was too high to be safely released to the atmosphere. In this event it would be relieved to the containment vessel, although the exact point of discharge has not yet been determined.

Design Study of Advanced Steam Generators

The once-through boiler with its tube axes parallel to the axis of the pressure vessel, as described in the previous report,[12] shows promise of being a low-cost steam generator. The preliminary design study indicated that it would give a compact heat transfer matrix with good utilization of the pressure vessel volume but that the arrangement tends to give units 100 to 200 ft tall. Since a variety of considerations makes it desirable to minimize the over-all vessel height, the effects of tube diameter and fin height on tube length were investigated. The calculations were extended to evaluate the cost and weight of both the tube matrix and the pressure vessel.

Most approaches to the design of heat exchangers make use of trial-and-error techniques which depend very heavily on the judgment of the designer. There are, however, so many possible combinations and permutations of variables for the case at hand that this approach seems unsatisfactory. An analysis disclosed that the many different parameters could be related in such a fashion that the problem could be reduced to two simultaneous equations which could be readily solved graphically. In the analysis, the pumping power loss for the gas flowing through the

[12] GCR Semiann. Prog. Rep. June 30, 1959, ORNL-2767, p 6.

steam generator was taken as equal to 1% of the heat transferred, since experience has shown that this will give a system close to the optimum. The water velocity was chosen to be 30 ft/sec where the fluid leaves the region in which boiling takes place. This value was chosen because boiler experience has shown that difficulty with water flow instability is likely at low loads if the full-power velocity is below this value. A higher boiler outlet velocity would require an increased tube length. Three tube diameters were chosen; namely, 1/2, 3/4, and 1 in. OD. The tube wall thicknesses were made equal to 10% of the outer diameter to provide adequate strength. Bare tubes and finned tubes having fin heights of both 1/8 and 3/8 in. were considered. For the finned tubes, two fin thicknesses were chosen, 0.035 and 0.0625 in., with six fins per inch of circumference. The thermal conductivity of the fin material was taken to be that of a low chrome-moly steel, that is, 18 Btu/hr·ft^2 (°F/ft). If stainless steel were used in the fins, the fin thickness would have to be increased approximately 25% to obtain the same performance. The bulk of the calculations were made with CO_2 at 1000 psi as the reactor coolant.

The analysis was carried out first for a single tube. The effects of fin height and tube diameter on the pressure vessel were then evaluated by considering a reactor output of 1320 Mw. It was further assumed that 65% of the cross section of this vessel would be used for the heat transfer tube matrix, and that the balance would be required for a central duct, thermal insulation, etc. (The cost or weight of the pressure vessel in dollars or pounds per kilowatt of heat transferred is quite insensitive to either of these two assumptions.)

The results of the calculations are shown in Figs. 2.18 and 2.19. From Fig. 2.18 it is apparent that, for the minimum over-all vessel height, the fin height should be about 1/8 in. Bare tubes give nearly as small a vessel height. The effects of the fin height on the over-all weight of both the fin matrix and the cylindrical length of pressure vessel required are given in Fig. 2.19, together with the cost of the tubing and the cost of the tubing plus that of the pressure vessel. No

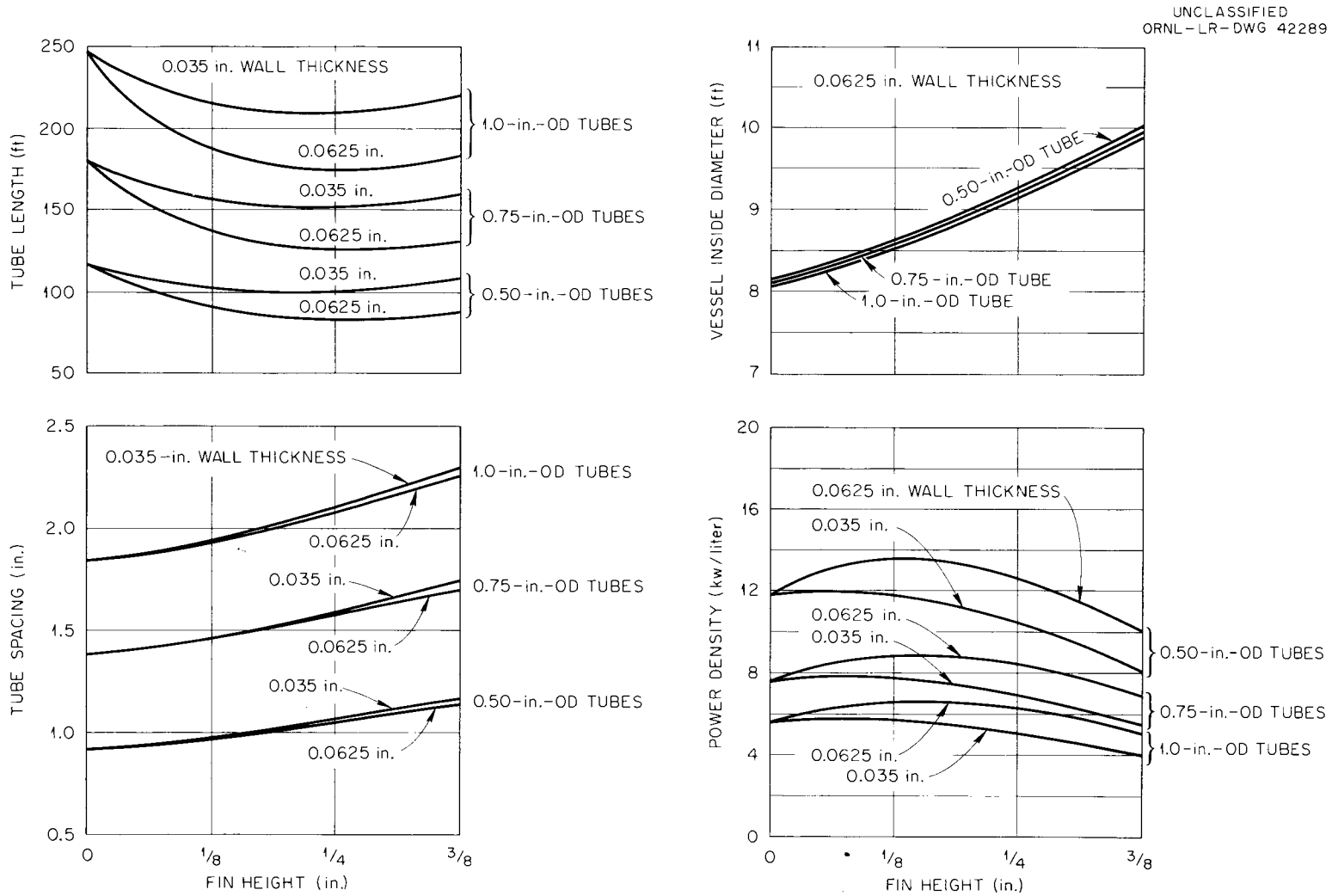

Fig. 2.18. Effects of Steam Generator Fin Height, Fin Thickness, and Tube Diameter on Tube Length, Tube Spacing, Vessel Diameter, and Average Power Density in the Pressure Vessel.

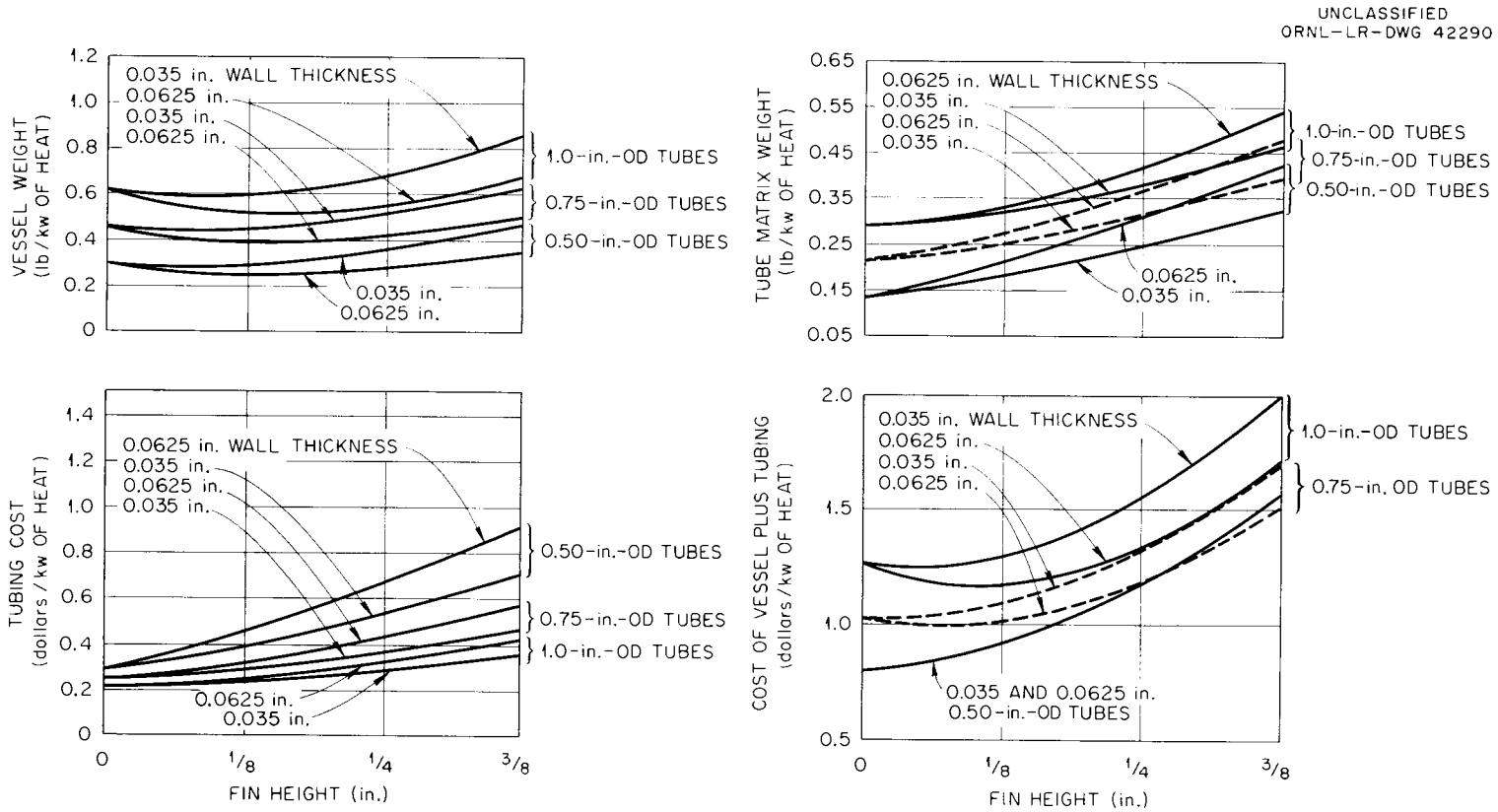

Fig. 2.19. Effects of Steam Generator Fin Height, Fin Thickness, and Tube Diameter on the Weight and Cost of the Tubing and the Cylindrical Section of the Pressure Vessel.

allowance was made for the vessel hemispherical heads, and no attempt was made to include the cost of fabricating the manifolds and installing the tube bundles which would make up the heat exchanger matrix, partly because the data available left much to be desired and partly because it appears that these costs will be approximately proportional to the cost of the tubing. The cost of finned tubing per pound was taken to be the same as that for the bare tubing of the same size, a fair approximation judging from the limited cost data available on finned tubes. The cost of the cylindrical pressure vessel (without heads) was estimated from data given in ORNL-2500.[13] As may be noted, the vessel diameters fell in a narrow range for all the cases considered, and hence the vessel cost in dollars per pound is practically constant. It may also be seen that there would be little tube matrix support structure in this type of steam generator, and therefore its cost would not be important.

In reviewing the curves it appears that there is little advantage to be gained from the use of fins and that the lowest cost and lightest weight unit can be obtained with bare tubes. It is also apparent that there is a major advantage to be gained through the use of the smallest diameter tubing considered, namely, 1/2-in.-OD tubing. While this tubing is small for a conventional coal-fired boiler, it is tubing of the size which is practically standard for the steam generators being used with pressurized-water and boiling-water reactors and should be entirely satisfactory for this application.

It is surprising at first to find that the vessel height actually increases as the fin height is increased beyond 1/8 in. This comes about because the fin efficiency drops to around 40% with 3/8-in. fins and the high heat loadings associated with the 1000-psi gas. A higher thermal conductivity fin, that is, aluminum or copper, or a greater fin thickness would improve the performance of the 3/8-in. fins. This can be deduced by comparing the performance of 0.035-in. and 0.0625-in. steel fins.

---

[13] The ORNL Gas-Cooled Reactor, Fig. 11.1, p 11.3, Vol. 4, ORNL-2500 (April 1, 1958).

3. EXPERIMENTAL INVESTIGATIONS OF HEAT TRANSFER AND FLUID FLOW

Resistance-Heated-Tube Heat-Transfer Experiment

The investigation of heat transfer in the septafoil geometry, as mentioned previously,[1] is now primarily oriented toward establishing criteria for the thermomechanical stability of the tubes in a seven-tube cluster when a nonuniform circumferential surface temperature distribution exists. The model 3 heat-transfer apparatus[1] designed for this study incorporates an adjustable spacer at the axial mid-plane of the cluster so that the tubes can be maintained at fixed and known positions. In the initial experiments, the tubes were restrained at the mid-plane to their design positions in order to provide a base for future comparisons. For this condition, circumferential temperature distributions have been obtained for all seven tubes at a position about 1-in. upstream of the spacer ($L/d_e = 17.9$) and for a single peripheral tube at 18 axial positions ranging from the inlet to the outlet.

The preliminary results of this study are presented in Table 3.1 for the transverse distribution of all seven tubes and in Table 3.2 and Fig. 3.1 for the axial profile of the peripheral tube in the No. 2 position. The peripheral tubes were numbered arbitrarily in a clockwise direction around the channel (for reference, the air flow into the upper plenum can be represented by a vector drawn between outer tubes 3 and 4 and pointed toward central tube 7). This scheme of tube numbering, while not in agreement with that used in reporting interim model 3 heat-transfer results, is consistent with the tube designations in the other reports in this series.[1,2] The data have been adjusted to a

---

[1] GCR Semiann. Prog. Rep. June 30, 1959, ORNL-2767, p 75.

[2] GCR Semiann. Prog. Rep. Dec. 31, 1958, ORNL-2676, p 36.

Table 3.1. Circumferential Temperature Profiles at $L/d_e = 17.9$

Angular Position[a] (deg)	Temperature[b] (°F)						Central Tube, No. 7
	Peripheral Tube No.						
	1	2	3	4	5	6	
0	8.6	5.5	7.4	5.2	1.0	8.4	0.5
20	12.2	11.2	12.4	10.1	4.3	13.9	1.0
40	16.1	15.6	18.2	15.1	8.6	19.0	1.1
60	19.0	20.7	20.9	18.6	10.3	21.7	1.8
80	21.5	21.5	23.6	19.7	10.4	22.9	2.4
100	23.7	25.8	27.4	24.2	13.0	25.6	2.1
120	27.6	29.6	31.7	26.1	17.7	25.0	2.4
140	30.0	31.3	34.3	24.9	25.0	22.1	2.1
160	28.1	29.7	30.4	20.2	22.8	16.2	2.2
180	24.2	23.8	22.3	14.6	16.4	11.7	1.6
200	20.6	18.1	15.7	9.0	11.3	7.3	1.0
220	14.9	15.1	10.3	5.3	8.1	4.1	1.3
240	11.9	11.8	8.3	3.4	5.5	1.7	1.2
260	10.3	7.5	5.9	3.1	4.0	0.8	1.7
280	4.8	5.0	2.8	1.4	4.0	0.3	0.7
300	0.8	1.8	0.9	0.7	2.4	0.3	0.4
320	0	0	0	0	1.4	0	0
340	3.0	1.2	2.2	1.5	0	1.8	0.9
$t_{surf,\ min}$	353	359	355	353	358	359	360
$t_{surf,\ mean}$	371	375	375	364	368	371	361

[a]The angular position on the tube surface was chosen such that the 0-deg point on a peripheral tube was on the side adjacent to the central tube (corresponding to the points of closest approach of the tubes to each other) and was measured in a clockwise direction facing downstream, i.e., in the direction of flow. The 0-deg location on the central tube was matched to the 0-deg position for tube 5.

[b]Listed in °F above the minimum surface temperature for the tube.

Table 3.2. Axial Variation in Mean Surface Temperature of Tube 2

L/d_e	Mean Surface Temperature (°F)	L/d_e	Mean Surface Temperature (°F)
0	248	20.0	302
5.0	322	21.0	313
6.5	330	24.0	370
7.5	339	26.5	397
10.0	354	27.5	402
12.0	367	30.0	418
16.0	385	35.0	441
17.9	381	37.0	446
19.0	337	38.0	446

common base (that is, corresponding air inlet temperatures, flows, and surface heat fluxes) using the relation:

$$t_{s,x} = t_{a,i} + \Delta t_{axial} + \Delta t_{radial} \quad .$$

The axial and radial temperature differences can be expressed in terms of the heat flux and the air flow rate. The over-all mean heat flux for this series of runs was 6500 Btu/hr·ft^2 with a flow rate of 2060 lb/hr (N_{Re} = 68,000), an air inlet temperature of 108°F, and an average axial temperature rise of 68.7°F.

From a polar plot of the data of Table 3.1, it may be seen that there exists a skewness and asymmetry in the circumferential temperature profiles for the peripheral tubes which is similar to that observed in earlier[3] heat-transfer experiments. Thus, of the minima which could be expected to occur in the vicinity of 120 deg and 240 deg, the first does not appear and the second is displaced to about 320 deg. Further, the primary maximum, which in this tube spacing arrangement (γ = 4) is anticipated at 180 deg, is found in the region of 120 to 140 deg. In addition, the observed maximum and minimum locations are nearly diametrically opposed. This pattern, in all major details, describes the

[3]GCR Semiann. Prog. Rep. Dec. 31, 1958, ORNL-2676, p 40.

results for the six peripheral tubes and indicates that the flow is not completely coaxial with the tubes. The possibility that this cross flow is associated with the entrance to the channel is discussed in detail in the following section on mass transfer studies in the model 3 heat transfer apparatus.

The axial variation of the mean surface temperature along peripheral tube 2 is shown in Fig. 3.1. For this axial traverse, the over-all heat flux was maintained at 6700 Btu/hr·ft^2 with N_{Re} = 67,600 (an air flow of 2055 lb/hr). The inlet air temperature was 118°F, and the average air temperature rise was 69°F. The mean temperature was obtained by graphical integration of the circumferential temperature profile at each position. The sharp break at the mid-plane (L/d_e = 19) results from the increased turbulence existing in the wake of the spacer. Since the three set screws[4] which contact each tube act as extended surface, lower tube surface temperatures will occur in the regions of the contacts. Thus, through conduction in the tube wall, the effect of the spacer is also detected upstream of the spacer location.

The curves of Fig. 3.1 suggest that established thermal conditions may not exist anywhere within the cluster. To check this, local heat-transfer coefficients were calculated and plotted as a function of distance along the cluster (see Fig. 3.2). In this determination, the local flux was evaluated from the electrical measurements, the electric current was taken as the average of the values observed during the 18 runs, and the resistance was calculated by integrating the expression for the electrical resistivity of type 304 stainless steel as a function of temperature[5] along the curve of Fig. 3.1. The air temperature was assumed to vary linearly with distance along the tube. From the curves of Fig. 3.2, the heat-transfer coefficient seems to be approaching an asymptotic value of 26 Btu/hr·ft^2·°F, with this limit

---

[4]GCR Semiann. Prog. Rep. June 30, 1959, ORNL-2767, p 76.

[5]H. L. Dickenson and C. P. Welch, Heat Transfer to Supercritical Water, ASME Paper No. 57-HT-7.

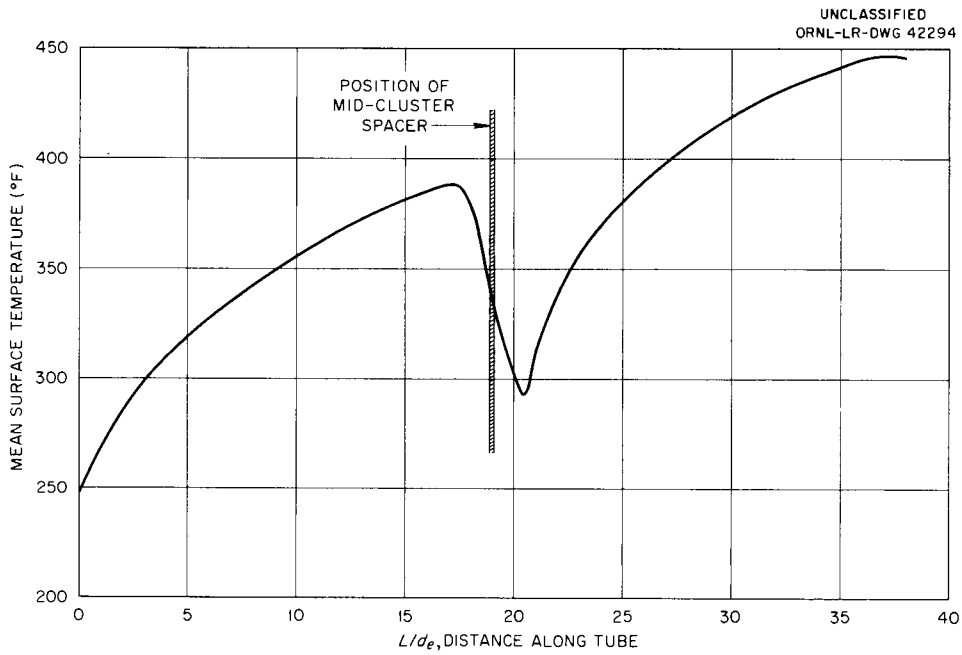

Fig. 3.1. Axial Variation of the Mean Surface Temperature for Peripheral Tube 2.

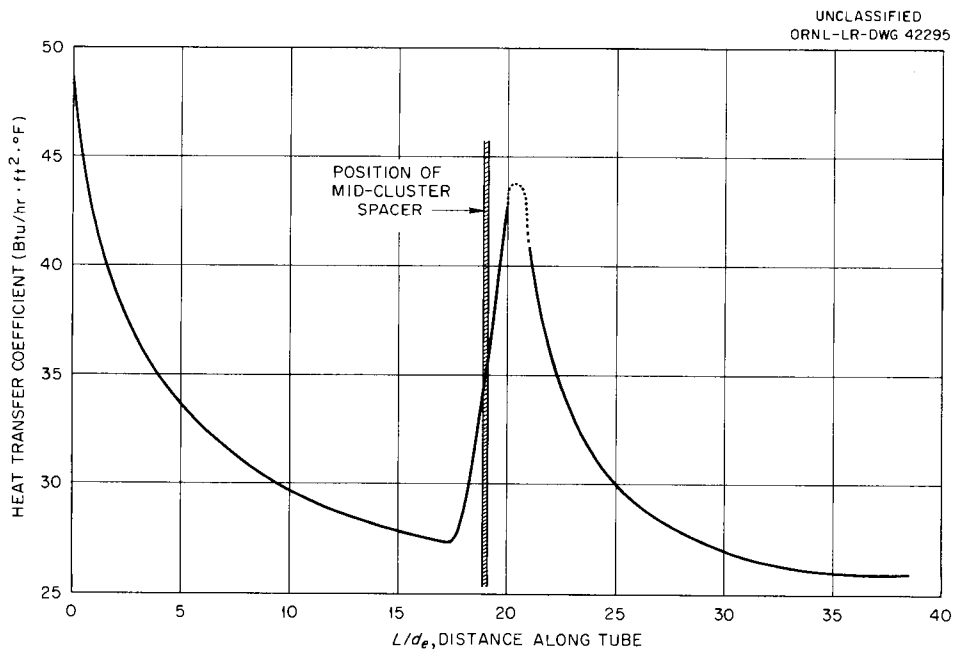

Fig. 3.2. Axial Variation of the Heat-Transfer Coefficient for Peripheral Tube 2.

being reached only at the exit end of the cluster. The combined thermal and hydrodynamic length of between 15 and 30 L/d_e (based on the final and initial portions of the test cluster, respectively) is not inconsistent with entrance-region data for air in circular tubes. For example, Boelter, Young, and Iversen[6] found an entrance length of 17 or greater for a uniform wall temperature system with various hydrodynamic entrance conditions; and Humble, Lowdermilk, and Grele[7] reported an entrance length greater than 50 for a uniform wall heat flux situation with a bellmouth hydrodynamic entrance.

Mass-Transfer Measurements

As discussed briefly in the preceding section on heat transfer in the model 3 apparatus, the over-all pattern of the circumferential temperature profiles at the mid-plane position indicated that the observed skewness may result from geometrical factors associated with either the channel entrance or the cluster itself. The alternative is, of course, that such temperature distributions are inherent to gaseous heat transfer in septafoil channels and that they arise from sources such as the variation in the thermal properties (primarily density and viscosity) of the coolant with temperature. To test this, the heated tube in the No. 2 position in the model-3 apparatus was replaced by a naphthalene-coated rod, and a series of isothermal runs were made The assembled cluster is shown in Fig. 3.3.

The data obtained by using the techniques previously described[8] are shown in Fig. 3.4. Since it was not possible to insert and remove

---

[6]L. M. K. Boelter, G. Young, and H. W. Iversen, An Investigation of Aircraft Heaters XXVII: Distribution of Heat-Transfer Rate in the Entrance Section of a Circular Tube, NACA Technical Note No. 1451 (July 1948).

[7]L. V. Humble, W. H. Lowdermilk, and M. Grele, Heat Transfer from High Temperature Sources to Fluids. I – Preliminary Investigation with Air in Inconel Tube with Rounded Entrance, Inside Diameter of 0.4 Inch and Length of 24 Inches, NACA Research Memorandum E7L31 (May 1948).

[8]GCR Semiann. Prog. Rep. June 30, 1959, ORNL-2767, p 80.

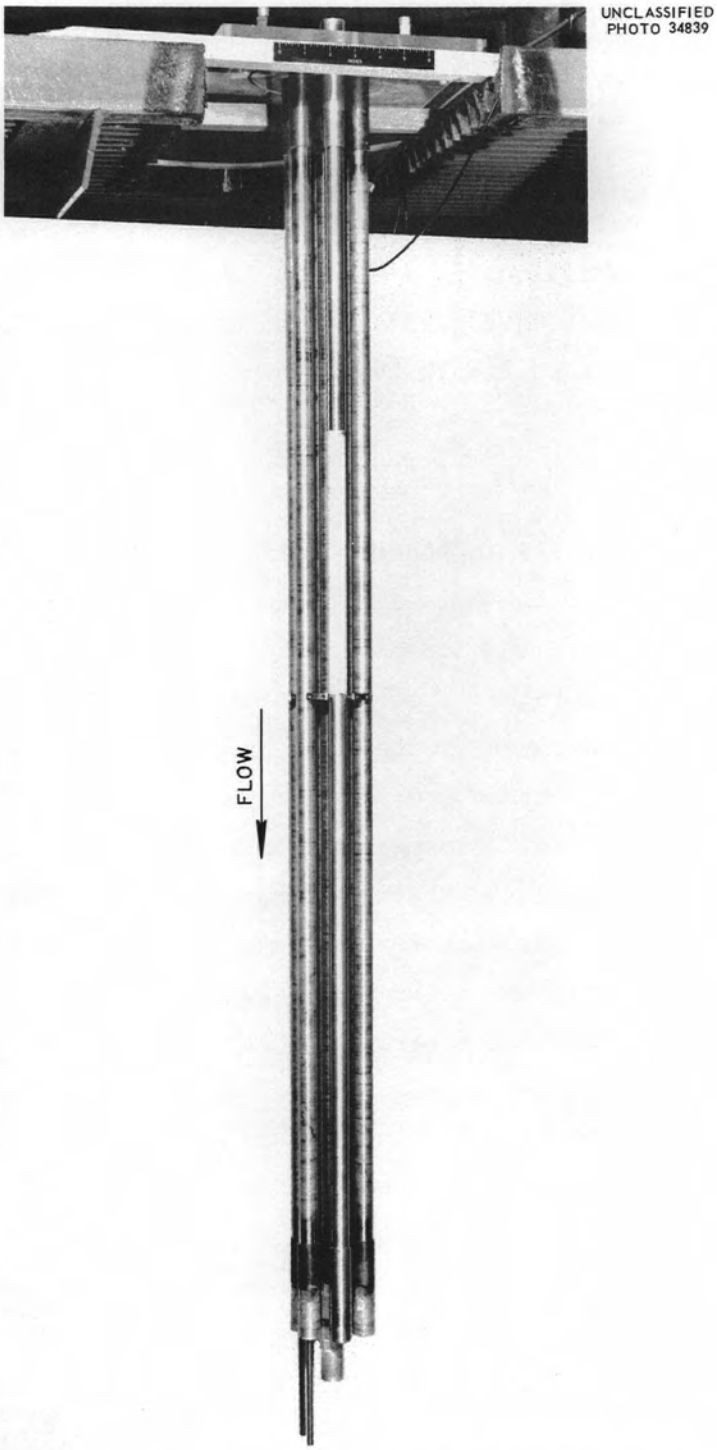

Fig. 3.3. Mass-Transfer Rod in Position 2 in the Model 3 Heat-Transfer Apparatus Tube Cluster.

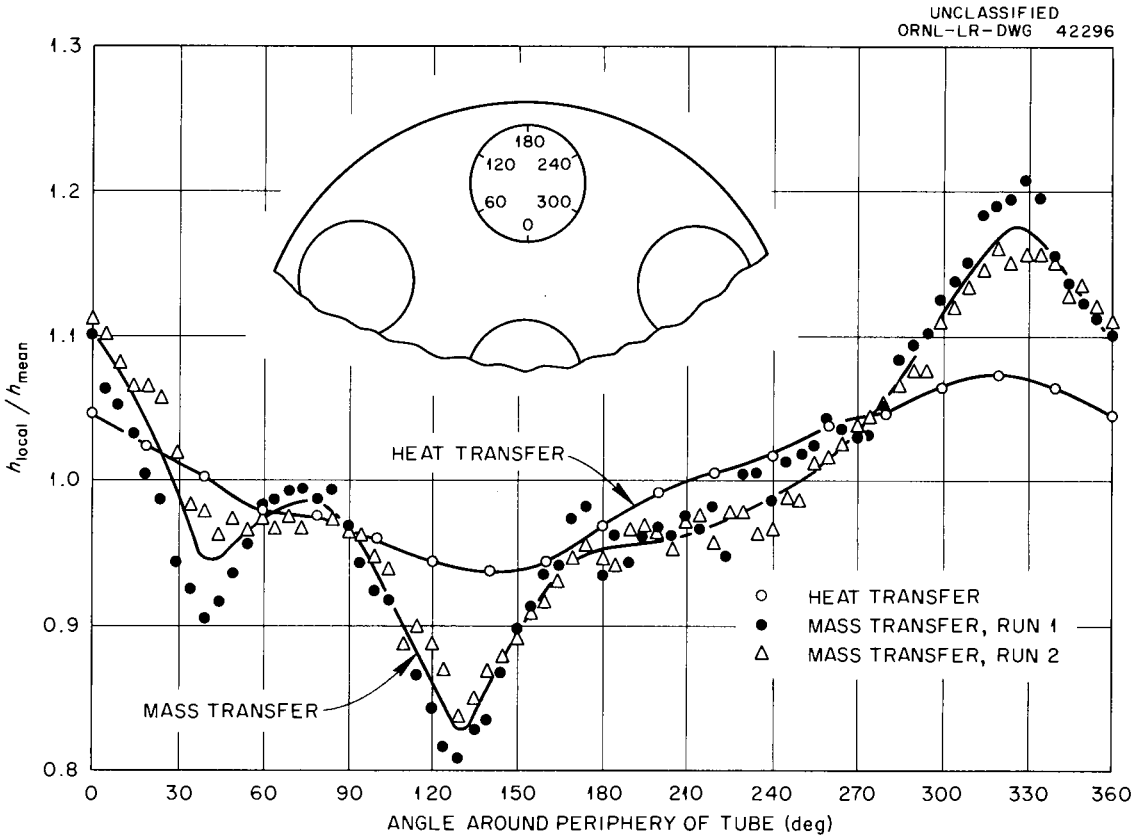

Fig. 3.4. Preliminary Comparison of Heat-Transfer and Mass-Transfer Data from the Model 3 Heat-Transfer Apparatus; Tube No. 2, $L/d_e = 17.9$, $N_{Re} = 68{,}000$.

the naphthalene-coated rod rapidly, the data should be taken as giving only a qualitative picture of the situation existing within the cluster during operation. With this restriction, then, the circumferential variation in the ratio of the local-to-mean heat-transfer coefficients as estimated from the mass-transfer data is compared in Fig. 3.4 with the similar ratio from the heat-transfer measurements (assuming a uniform gas temperature in the vicinity of the tube). The data were evaluated at a position 1 in. upstream of the mid-plane spacer (L/d_e = 17.9); the Reynolds modulus was approximately 68,000. Duplicate mass-transfer runs were made.

Both the heat-transfer and mass-transfer data show similar patterns, with a primary minimum at about 135 deg and a primary maximum at 330 deg. Since previous mass-transfer studies[8] did not show such skewed distributions, it would appear that the explanation for the observed temperature profiles lies in the nature of the flow rather than in thermal phenomena. The strong maximum at 330 deg results from the impingement of a cross flow on the tube in this region; the minimum at 135 deg then lies in the wake of the rod. The secondary maxima at 75 deg and perhaps in the vicinity of 190 deg are probably in the regions of flow separation.

While it is not certain that this effect is associated entirely with the channel entrance, an experiment in which cotton fibers were used to visualize the air flow within the inlet did indicate a rotational velocity component. This rotating flow seemed to be somewhat unstable (accounting perhaps for the variation noted between the two mass-transfer runs) and could be stopped or even reversed in direction by inserting small obstructing strips in the inlet plenum chamber. This would indicate that some modification is required in the geometry of the diffuser joining the inlet plenum to the air supply and in the location of two 90-deg bends immediately upstream of the diffuser.

It is evident from Fig. 3.4 that the mass-transfer technique predicts heat-transfer coefficients which, at the extremes, are as much as 15% greater than those measured directly in the heated-tube

experiment. This can be understood in that the temperature profiles determined in the model 3 experiment are smoothed by two mechanisms: (1) circumferential conduction within the tube wall and (2) the local increase in the electrical resistivity of the tube wall material with increasing temperature. For the latter factor, as the local tube wall temperature increases, the electrical resistance of the region increases. This in turn causes a decrease in the heat generation in that region; and hence a lower temperature. In a nuclear reactor, this effect is not present. Further, from the heat-transfer data (see Table 3.1), the circumferential heat flux is about 1/3 the radial (or normal) flux. For a reactor, in which the outward heat flux is perhaps ten times greater than in the model 3 heat transfer experiment, the circumferential heat flow will be a smaller percentage of the total; and the smearing effect of wall conduction will be lessened. Thus the mass-transfer experiments, although still on the high side, more closely predict the magnitude of the heat transfer coefficient in the reactor than is indicated by the comparison of Fig. 3.4.

Velocity Distribution in Septafoil Channels

The prediction of the heat transfer associated with the flow of air through a septafoil channel requires a knowledge of the velocity distribution in the gas stream. In analyzing the heat transfer in a system of similar geometry (axial turbulent flow through banks of rods or tubes), Deissler and Taylor[9] calculated the velocity profiles based on an assumed distribution of the eddy diffusivity of momentum. However, the Deissler-Taylor analysis, when applied to the central tube in the seven-rod cluster, estimated the maximum-to-average temperature difference to be only 1/3 that found experimentally. As a result, it was decided that a direct measurement of the velocity profiles was needed.

---

[9]R. G. Deissler and M. F. Taylor, Analysis of Axial Turbulent Flow and Heat Transfer Through Banks of Rods or Tubes, TID-7529 (Pt. 1), Book 2, November 1957.

The apparatus consisted of seven 45-in.-long, 1-in.-dia rods suspended within a 4-in.-ID Plexiglas channel, as shown in Fig. 3.5. One of the seven rods was constructed of a section of brass tubing (see Fig. 3.6) so that a short length of brass rod, instrumented with static and dynamic pressure probes, could be inserted at any of six axial positions. The probe section was rotated to survey a full 360-deg sector in the vicinity of the test tube; a succession of probes (as illustrated in the lower portion of Fig. 3.6) were used to determine the velocities at various distances from the tube surface. The instrumented tube could be located in any of the seven positions of the cluster, and adjustable top and bottom support structures allowed several rod center-to-center spacings to be studied. Air at essentially atmospheric pressure was used as the test medium. The entire unit was connected to the previously described air supply system.[10]

Water-filled U-tube manometers were used to measure the total and static heads; the impact head was then calculated from these readings. A direct measurement of the total static pressure difference gave results which, in general, agreed to within 5% with the calculated differences. The air temperature was measured by a copper-constantan thermocouple located at the inlet just below the bottom alignment spider, and the air mass flow rate was determined by an ASME sharp-edged orifice in the inlet line. An 8-in.-dia protractor secured to the top support spider (visible at the left end of the rod cluster in Fig. 3.7) was used to establish the angular position of the probe. Since the initial alignment of the pointer attached to the upper end of the instrumented tube with the Pitot tube was done visually, a possible 5-deg error exists in the angular readings. The effect of this misalignment was found to be significant only in the region of steep velocity gradients near the tube surface.

The results of a preliminary velocity survey are shown in Fig. 3.8. The profiles were obtained far downstream from the entrance

---

[10] GCR Semiann. Prog. Rep. Dec. 31, 1958, ORNL-2676, p 26.

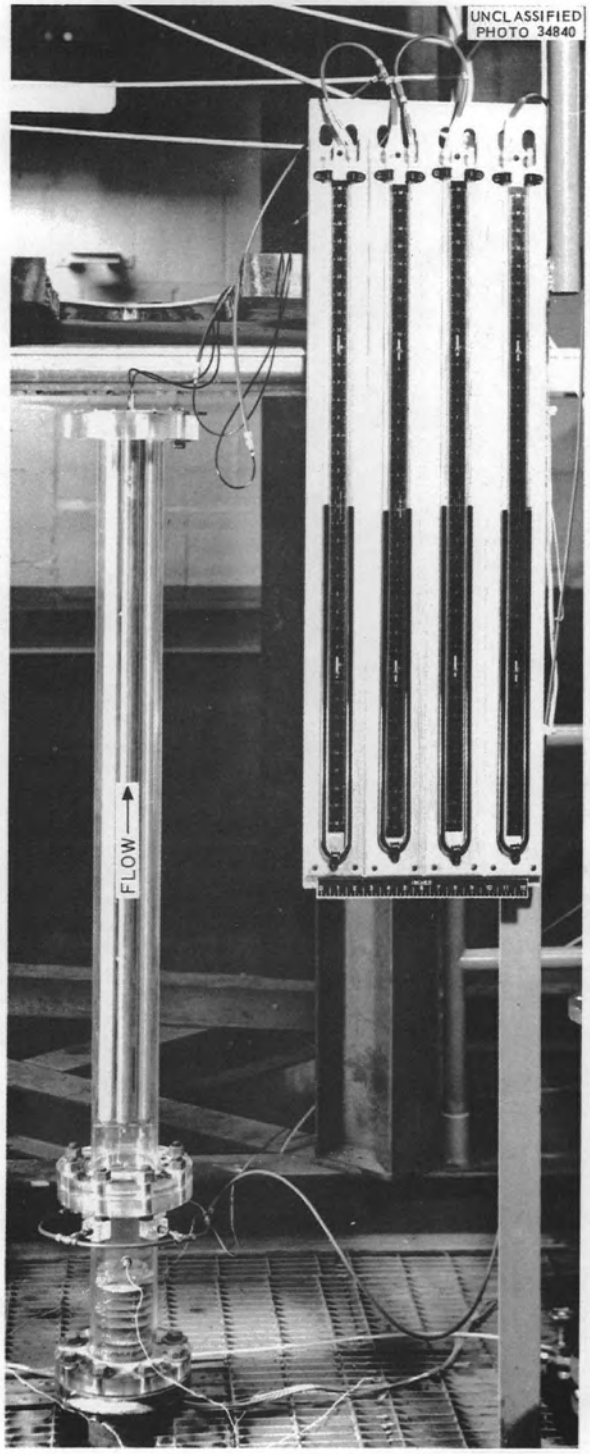

Fig. 3.5. Apparatus for Determining Velocity Distributions in Septafoil Channels.

UNCLASSIFIED
PHOTO 34837

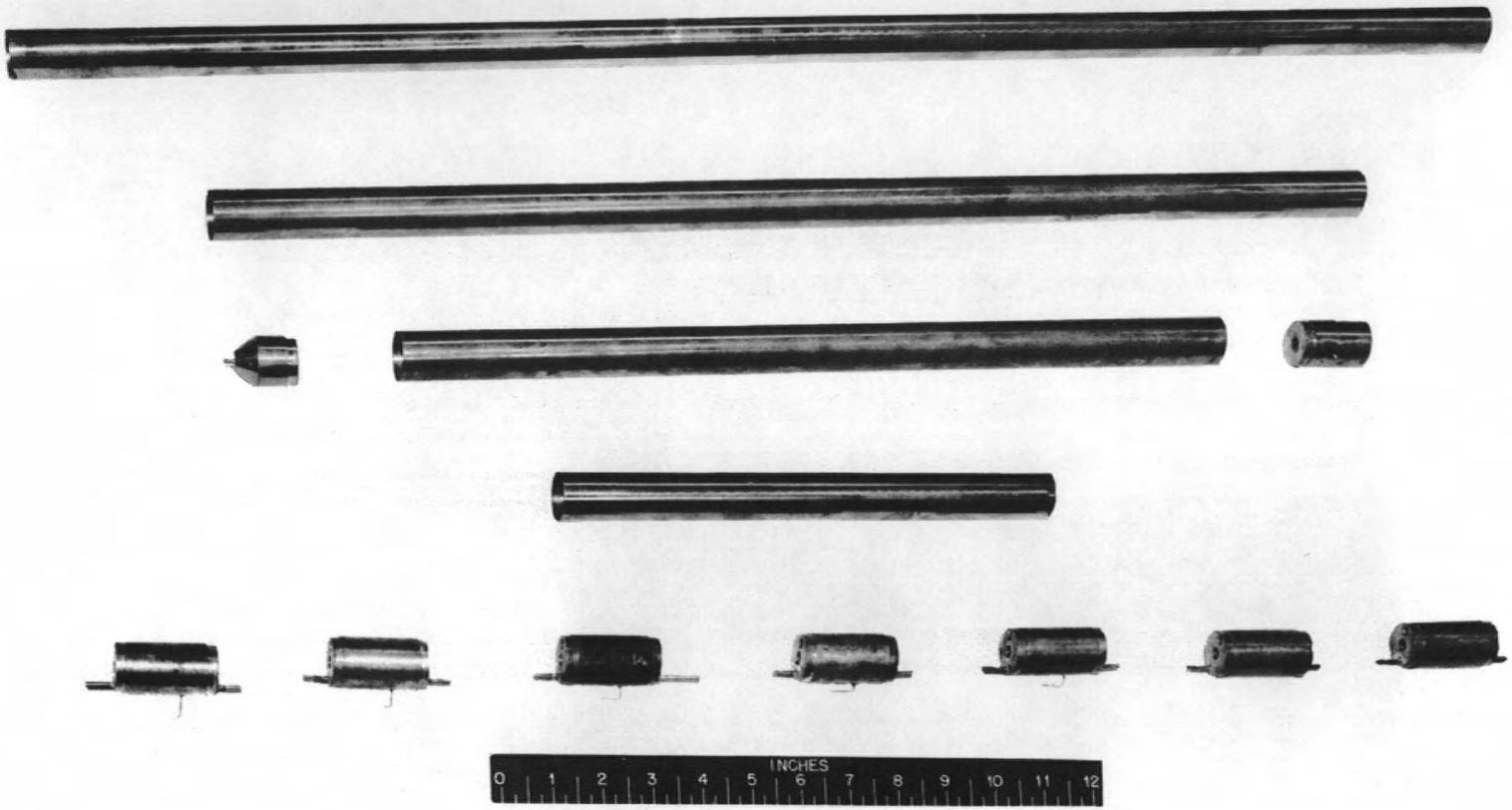

Fig. 3.6. Disassembled View of Instrumented Tube Showing Probe Sections.

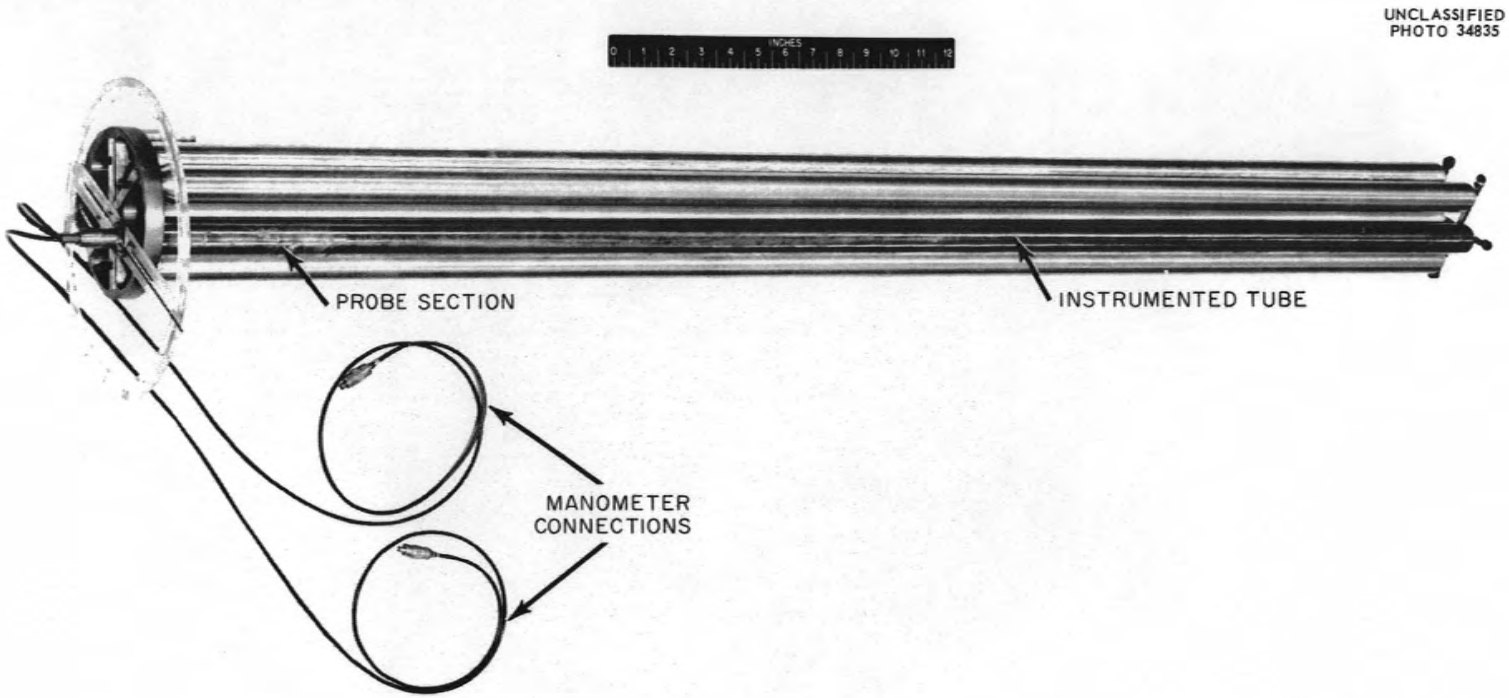

Fig. 3.7. Assembled Seven-Rod Cluster for Velocity Distribution Apparatus.

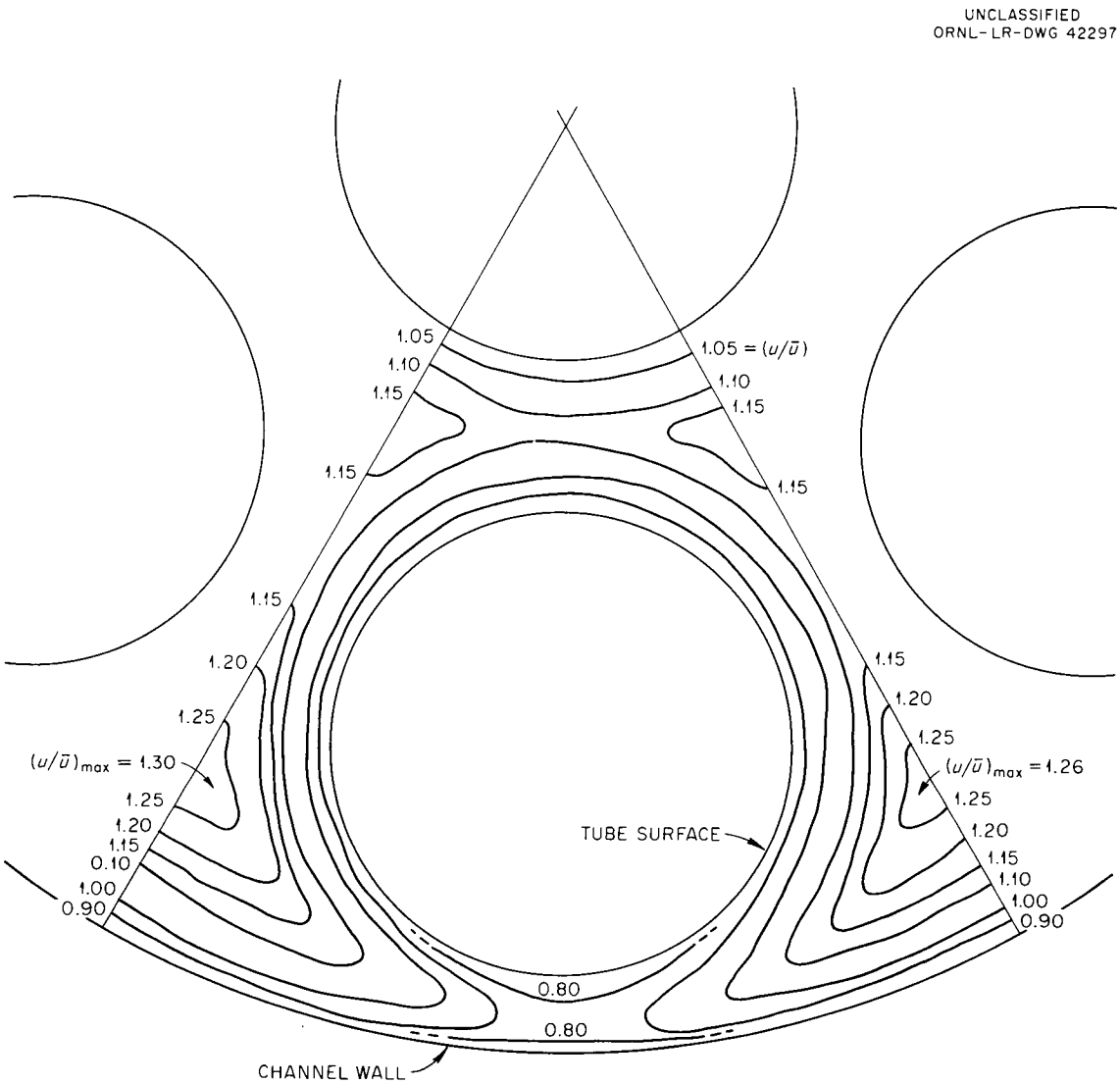

Fig. 3.8. Measured Velocity Distribution Between Tubes in a Septafoil Channel. $L/d_e = 50$; $N_{Re} \cong 52{,}000$; $\gamma = 2$.

(L/d_e = 50) for a Reynolds modulus of approximately 52,000. The tubes were located on 1.333-in. centers, corresponding to a 2:1 inner-to-outer ligament ratio. In calculating the velocity ratios plotted in Fig. 3.8, the local velocity was calculated from the expression

$$u = \left(2\, g_c\, R\, T_i\, \frac{\Delta P}{P_t} \right)^{1/2}$$

where R is the gas constant (53.3 ft/°R for air), T_i is the inlet air temperature (°R), ΔP is the measured total static pressure difference (lb/ft^2 absolute), and g_c is the conversion factor ($32.2\ lb_m \cdot ft/lb_f \cdot sec^2$). The mean velocity was determined from the air mass flow as measured at the orifice. Except for several points near the tube wall, three separate determinations of the velocity patterns gave results which were consistent to within 6%.

Fig. 3.8 shows the velocity profiles at the L/d_e = 50 position to be fairly symmetrical with respect to the tube centers. In the outer flow region to the left of the tube, a maximum velocity ratio of 1.30 was observed, while the maximum in the region to the right of the tube was only 1.26. For the inner flow regions, the maximum velocity ratio appeared to be 1.15. Initial measurements at L/d_e = 20 indicate roughly similar patterns. However, the difference in the velocity ratio maxima for the two outer regions was somewhat greater (1.25 on the left and 1.19 on the right) and a slight skewness was noted (a counterclockwise rotation of the pattern by about 5 deg).

PART 2. MATERIALS RESEARCH AND TESTING

4. METALLURGY

Fuel Materials Development

Fabrication of UO_2

The UO_2 powder currently being processed by the continuous double-calcination process is not yet as reproducible as is needed. Certain steps in the process, namely the filtration and drying of the ADU precipitate and the passivation or reoxidation of the calcined UO_2, have not been reduced to continuous reproducible operation. Small batches of powder of several different enrichments are currently being produced for the fabrication of irradiation-test specimens. When production of these batches has been completed, larger batches will be prepared with which to attain better control of the process on a continuous basis.

On the basis of surface-area measurements of UO_2 pellets of varying density, it can be predicted that the fission-gas release from pellets having densities above 96% of theoretical will be very low. During the past year, certain batches of oxide have been received which were readily sinterable to bulk densities as high as 97% of theoretical or even higher. The characteristics and processing history of these oxides are being studied in an attempt to obtain such densities reproducibly.

High-Temperature Compression Testing of UO_2

Compression testing of UO_2 bodies has been continued.[1] Specimens of hollow fuel pellets were tested at 1500 and 1800°C under a pressure of 5000 psi for 1 hr and 3 min, respectively. Two specimens tested at 1500°C for 1 hr were compressed 0.6 and 1.7% in length. A specimen tested at 1800°C would not support the test load, and indications were that the sample cracked during loading.

---

[1]GCR Semiann. Prog. Rep. June 30, 1959, ORNL-2767, p 102.

Thermal Conductivity of UO_2

A survey of the literature on thermal conductivity is nearing completion, and an extensive reference file on the measurement of physical properties of UO_2 and other refractory fuel materials is being established.

An apparatus for measuring the thermal conductivity of UO_2 is being constructed. The apparatus is based on the principle of radial heat flow under steady-state conditions, as originally developed by Powell.[2] The equipment is being designed to measure conductivity at temperatures up to 1350°C, using special molybdenum heaters, and it will operate in a containment vessel in a vacuum or a hydrogen atmosphere.

Fission-Product-Release Studies

An experimental program has been initiated for obtaining data with the method developed by Eichenberg *et al.*[3] on the rate of fission-product release from samples of the UO_2 proposed for use in the EGCR. Pellets which have been irradiated for short times at low temperatures are to be heated out-of-pile to temperatures above 1000°C, and the rate of Kr^{85} release is to be measured. The release-rate data obtained may be used to predict the pressure buildup in fuel capsules under reactor conditions by the method outlined by Booth.[4] Although the applicability of the release rates measured by this method may be criticized because of the low burnups and the absence of a thermal neutron flux, data for preliminary design calculations may be obtained most quickly by this technique and the relative release rates of different batches of UO_2 may be evaluated.

---

[2] R. W. Powell, *Proc. Phys. Soc.* **51**, 407 (1939).

[3] J. D. Eichenberg *et al.*, *Effects of Irradiation on Bulk Uranium Dioxide*, WAPD-183 (Oct. 1957).

[4] A. H. Booth, *A Method of Calculating Fission-Gas Diffusion From UO_2 Fuel and Its Application to the X-2-F Loop Test*, CRDC-721 (Sept. 1957).

Two types of apparatus have been designed and are being constructed. In one of these, the irradiated sample will be induction heated under vacuum and the released Kr^{85} will be collected in activated charcoal traps at -196°C. In the second apparatus, the sample will be dissolved in nitric acid and the Kr^{85} remaining in the sample will be collected.

At present, eight pellets of UO_2 of enrichments varying from 3.5 to 4.5 wt % U^{235} are being irradiated at a flux of approximately 7×10^{11} neutrons/cm^2·sec. The pellets have densities ranging from 94 to 95% of theoretical and are representative of the UO_2 being used in the helium-cooled loops at the GETR. Elementary calculations indicate that after a decay time of 1 to 2 months, activity levels will be sufficiently low to effect direct handling of the samples.

Mechanical Properties of Fuel Capsule Material

Investigations of the properties of type 304 stainless steel as a container material for UO_2 fuel pellets have continued. The experimental program has included tube-burst testing, strain-cycling studies, and investigation of the collapsing behavior of the capsule under an external pressure.

Tube-Burst Tests

The investigation of the time-to-rupture of seamless, 0.020-in.-wall, type 304 stainless steel capsules in terms of pressure and temperature is proceeding. The additional data obtained have indicated that revisions are necessary in the plot of time-to-rupture versus tangential stress presented previously.[5] The revised curves for seamless tubing tested in stagnant air at 1600, 1700, and 1800°F are shown in Fig. 4.1.

[5]GCR Semiann. Prog. Rep. June 30, 1959, ORNL-2767, p 105.

The 1600°F values are in good agreement with the tension stress-rupture values reported in the literature,[6] but the 1800°F values are considerably lower.

Burst tests of welded and redrawn tubing (Trentweld heat No. 880010, 0.750 in. OD, 0.020 in. wall thickness) have also been conducted, and the results are compared with corresponding values for seamless tubing in Table 4.1. Failure of the tube wall occurred in the weld area

Table 4.1. Comparison of Tube-Burst Test Data for Type 304 Stainless Steel Welded and Redrawn Tubing (Trentweld, Heat No. 880010) and Seamless Tubing

Temperature (°F)	Internal Pressure (psi)	Time to Rupture (hr)		Average Tangential Strain (%)		Maximum Tangential Strain (%)	
		Welded Tubing	Seamless Tubing	Welded Tubing	Seamless Tubing	Welded Tubing	Seamless Tubing
1300	700	153	300	10.8	1.86	15.4	3.2
1500	300	175	500	3.6	2.8	5.4	6.2
1700	50	147		5.4		6.5	
1800	50	65	152	4.1	3.6	6.1	3.9

of all specimens; a typical specimen tested at 1500°F with an internal pressure of 300 psi is shown in Fig. 4.2. As may be seen, the grain size in the weld area is considerably smaller than that of the remainder of the tube. In addition, the thickness of the wall in the weld area is approximately 0.002 in. less than the over-all thickness. Since this difference did not exist in the specimen before test, it must be concluded that the fine-grained metal deformed more readily.

Modified Tube-Burst Tests

A modified tube-burst test specimen was designed in order to evaluate end-closure joints under severe conditions of deformation. The

[6] Digest of Steels for High Temperature Service, The Timken Roller Bearing Company, Sixth Edition, p 58, 1957.

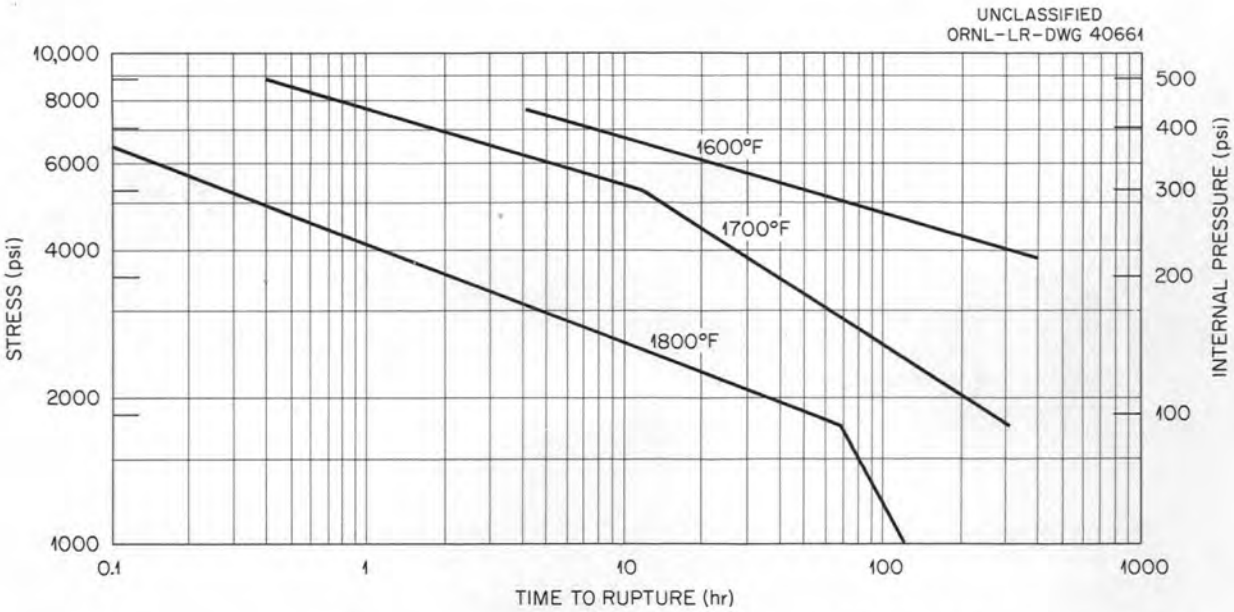

Fig. 4.1. Results of Burst Tests of 0.020-in.-Wall, 0.750-in.-OD, Type 304 Stainless Steel Seamless Tubing Tested in Stagnant Air at the Indicated Temperatures.

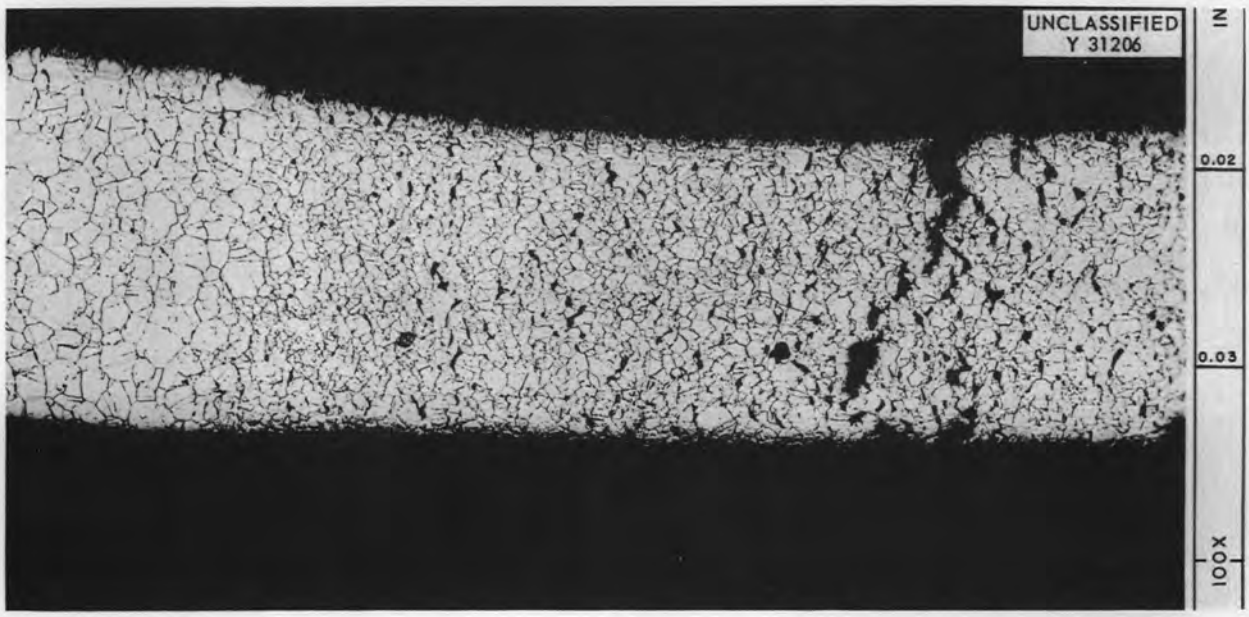

Fig. 4.2. Cross Section of Wall of Type 304 Stainless Steel Welded and Redrawn Tubing Tested at 1500°F with an Internal Pressure of 300 psi; Time to Rupture, 175 hr. Electrolytic etch. 100X.

specimen tube was machined from 1/2-in., sched-40, type 304 stainless steel pipe, as shown in Fig. 4.3, in order to minimize the tubing

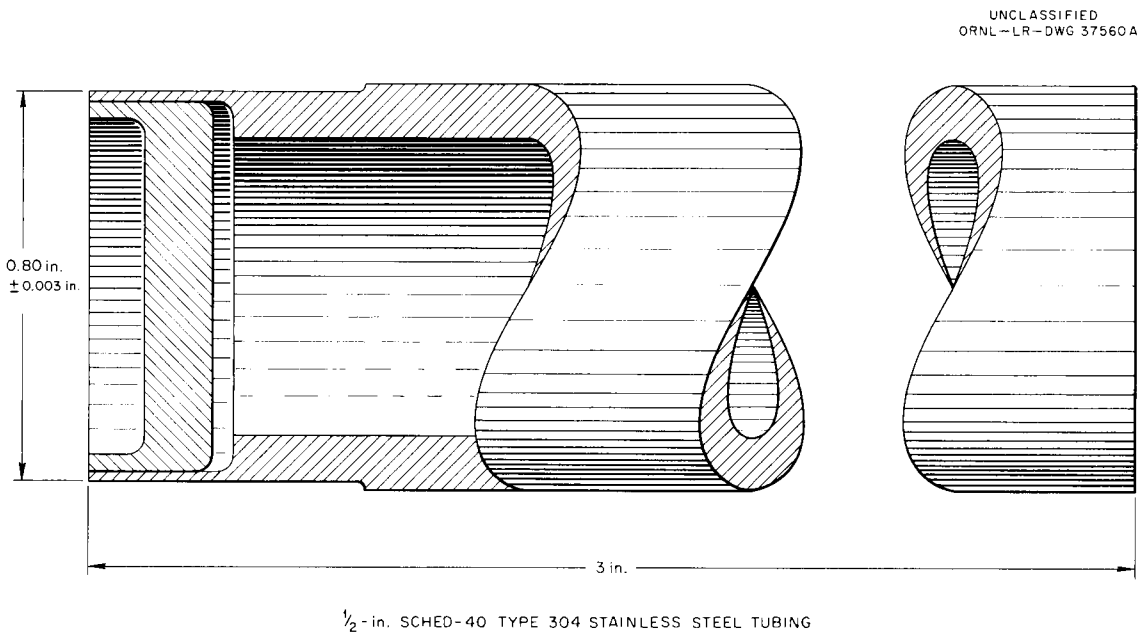

Fig. 4.3. Modified Tube-Burst Test Specimen Design for Evaluation of End-Closure Joints.

length-to-diameter ratio and promote rupture in the weld joint rather than in the tube. Specimens were prepared with the types of end closure to be evaluated and were tested at 1500°F. The results, presented in Table 4.2, indicate that the edge-fusion joint, when tested under these conditions, is superior to the plug weld because it deforms to a greater extent than the plug weld before failure. Photomicrographs of edge weld and plug weld specimens after testing are shown in Figs. 4.4 and 4.5. It may be seen that the fusion line of the edge-fusion joint has rotated approximately 30 deg from the horizontal, whereas the plug weld specimen ruptured through the weld with relatively slight deformation. The geometry used in the modified tube-burst test was selected to evaluate the merits of the welds under severe deformation

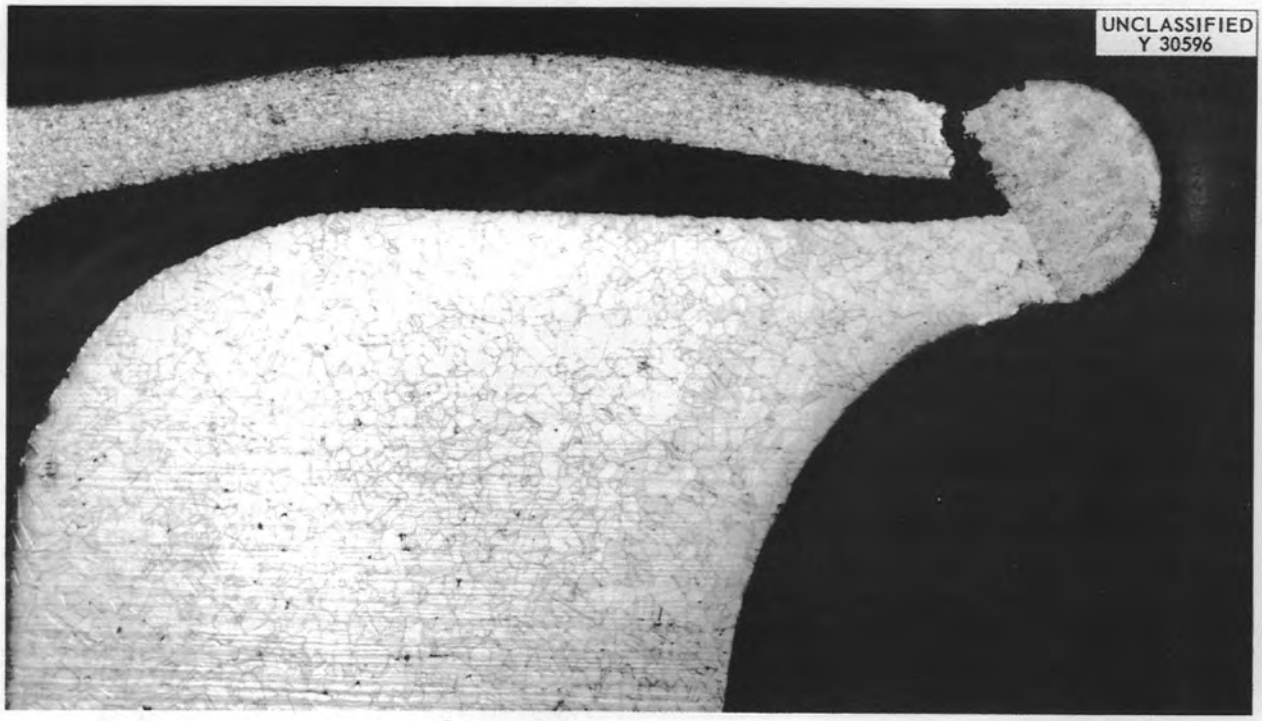

Fig. 4.4. Modified Edge-Weld Specimen After Tube-Burst Test. Etchant: 10% oxalic acid. 40X.

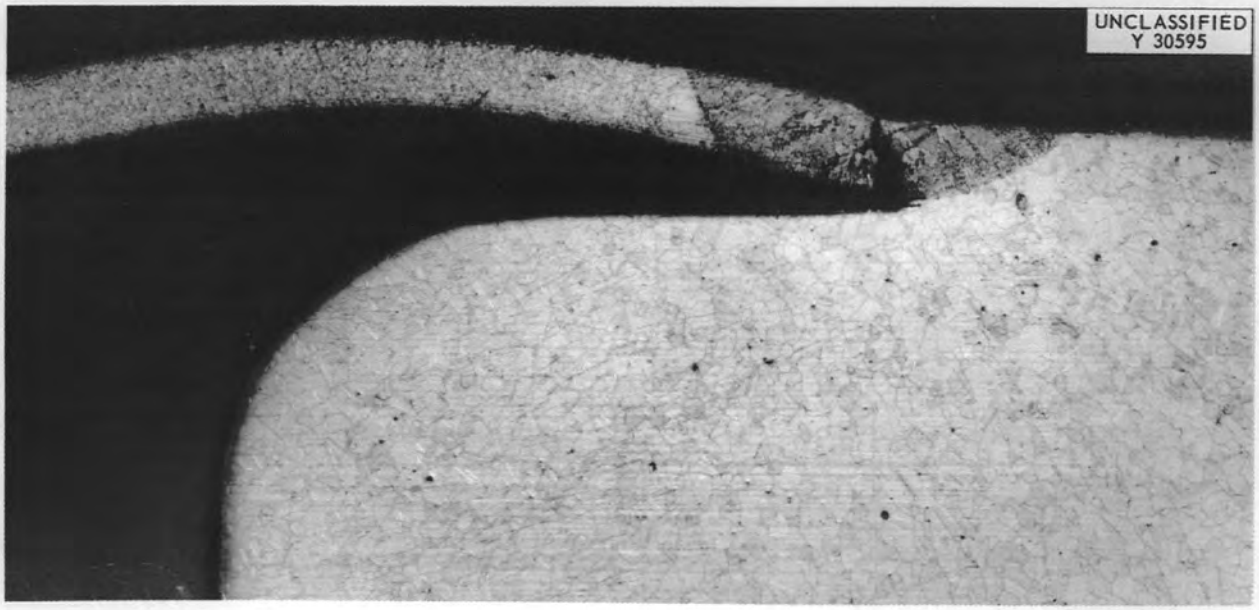

Fig. 4.5. Modified Plug-Weld Specimen After Tube-Burst Test. Etchant: 10% oxalic acid. 40X.

Table 4.2. Results of Tests at 1500°F of Modified Tube-Burst Specimens for Evaluation of End Closures

Internal Pressure (psi)	Type of End Closure	Time to Rupture (hr)	Tangential Strain (%)
485	Edge Fusion	32.8	3.7
	Plug Joint	1.8	1.2
420	Edge Fusion	63.8	3.6
	Plug Joint	4.2	1.6
330	Edge Fusion	112	4.0
	Plug Joint	3	1.4
235	Edge Fusion	479	5.4
	Plug Joint	107	2.5

and does not reflect on the rupture characteristics of fuel capsules. The probability of this amount of deformation ever occurring in a fuel element is small.

Strain-Cycling Tests

The investigation of the isothermal strain-cycling characteristics of type 304 stainless steel is continuing. Tests of 0.060-in.-wall specimens in an argon atmosphere at a strain-cycling frequency of 0.5 cycles/min have been completed at 1600°F. The results of these tests, which are summarized in Table 4.3, indicate, when compared with previously reported data obtained at 1300 and 1500°F,[7] that temperature has no major influence on the number of cycles to fracture in the range 1300 to 1600°F. Additional strain-cycle tests are in progress to determine the environmental effects of air, CO, CO_2, and hydrogen.

Collapsing Behavior

Studies of the creep-buckling behavior of the fuel capsules are

[7]GCR Semiann. Prog. Rep. June 30, 1959, ORNL-2767, p 105.

Table 4.3. Results of Strain-Cycling Tests of Type 304 Stainless Steel at 1600°F in Argon

Plastic Strain per Cycle (%)	Time in Test (hr)	Number of Cycles to Rupture
21.5	0.4	13
10.66	1.0	29
4.22	2.9	88

continuing. The ability to uniformly collapse capsules fabricated from seamless tubing and having a diametral clearance of 0.010 in. was demonstrated previously.[8] Capsules fabricated from Trentweld tubing and containing pellets to give a 0.010-in. diametral clearance also collapsed in a uniform manner when subjected to an external pressure of 500 psi at 1700°F for 12 hr.

A collapsing test was conducted on a tubular specimen (0.800 in. OD, 0.020 in. wall thickness) containing UO_2 pellets in an effort to obtain uniform collapse, and at the same time to see whether the UO_2 would crack or spall enough to leave an area of the capsule wall unsupported. The specimen was subjected to an external pressure of 300 psi for 4 hr at 1900°F. The diametral clearance at room temperature between the UO_2 and the capsule wall was 0.016 in. Instead of collapsing uniformly, the capsule buckled in a one-lobe manner. The UO_2 pellets, however, remained intact and supported the capsule wall. The specimen was radiographed after the test, and no cracks in the UO_2 were detected.

Effect of Mid-plane Spacers

Spacers have been designed to be used at the axial mid-point of the EGCR fuel element to restrain movement caused by the asymmetrical

[8] GCR Semiann. Prog. Rep. Dec. 31, 1958, ORNL-2676, p 79.

temperature distribution. Therefore an investigation of the effect of spacers brazed to the capsule tubing has been initiated. Preliminary collapsing tests have been conducted on 6-in.-long, seamless, tubular specimens (0.750 in. OD, 0.020 in. wall thickness) containing no inserts to which central spacers of two sizes (1.245 and 0.914 in. OD) were brazed using GE-81 alloy. The brazing temperature was 2150°F and the time at temperature was 10 min. Collapsing tests were then carried out at 1500°F with an external pressure of 400 psi. A specimen without a spacer was also tested. All specimens ruptured in approximately 2 hr. The tubes with the spacers collapsed in a three-lobe mode, while the specimen without a spacer collapsed with the formation of two lobes. Failure in the tube with the larger spacer occurred underneath the spacer where the tube wall was pulled away. Failure of the other specimens occurred at the points where the tube wall collapsed around the end plugs.

It is important to note that none of the data that have been obtained on time to rupture, buckling characteristics, or strain cycling of tubes without mid-plane spacers can be considered to be applicable because of the metallurgical changes induced by brazing the spacers to the tubes. Additional tests will be necessary to obtain realistic design data.

Effect of Gaseous Environments on Properties of Type 304 Stainless Steel

Reactions of Type 304 Stainless Steel with Impurities in Helium

An all-glass apparatus was designed and constructed to permit the study of the effects on type 304 stainless steel of low concentrations of CO, CO_2, H_2, H_2O, and CH_4 singly and in combination in helium. A simplified, schematic drawing of the apparatus is shown in Fig. 4.6. This equipment provides for the replenishment of the impurity gas as it is consumed. Gaseous reaction products are to be removed by proper absorbents in either the humidity controller or the gas-metering

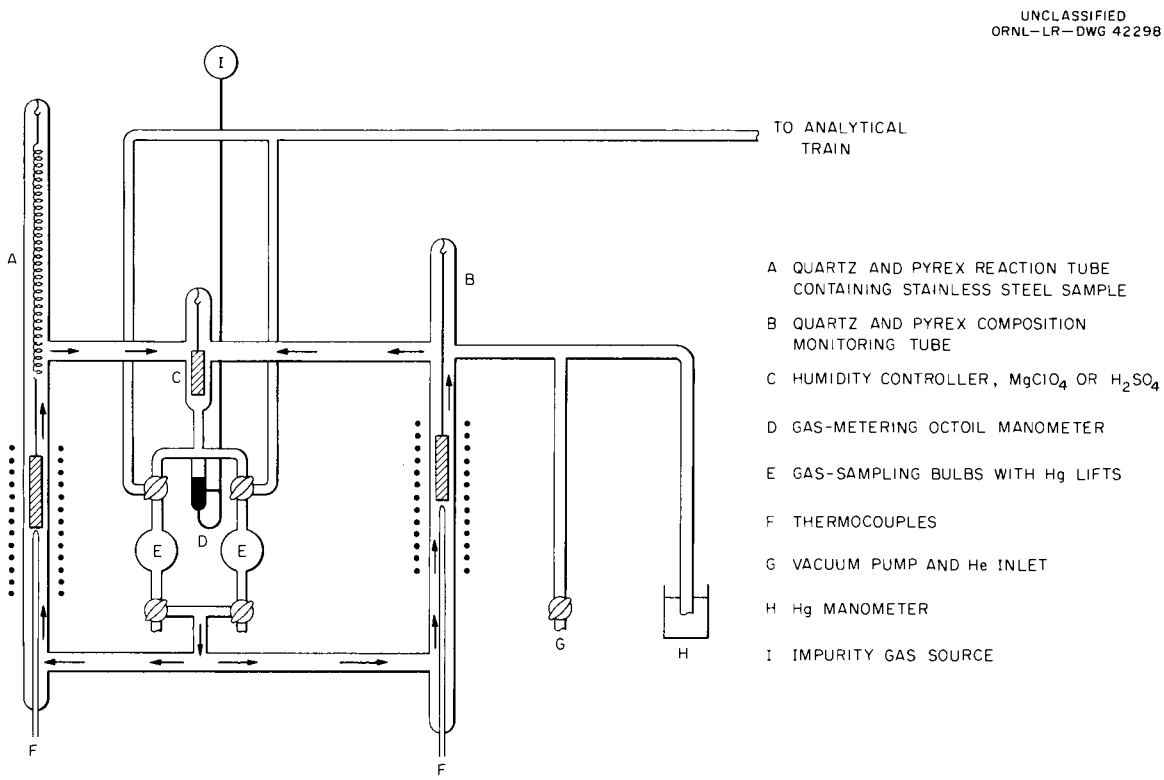

Fig. 4.6. Apparatus for Determining Reactions of Stainless Steel with Impurity Gases in Helium.

manometer. By proper selection of a compound, certain mixtures of gaseous impurities may be obtained; for example, by using CO_2 as the impurity in reservoir I and activated charcoal suspended in tube B, various CO/CO_2 ratios may be obtained by adjusting the temperature of tube B. If the atmosphere desired is CO_2, CuO will be used in tube B to convert the CO resulting from the reaction of CO_2 with stainless steel back to CO_2. The information obtained with this apparatus will be compared with the data obtained previously[9] on the reactions of type 304 stainless steel with CO_2 and CO at 1500°F for gas concentrations ranging from 0.6 to 100 vol % of the pure gases. It was found that these gases caused both oxidation and carburization.

Creep Tests in Various Gaseous Environments

The results of creep-rupture tests of type 304 stainless steel in pure gases, such as CO, CO_2, N_2, H_2, A, and air, as reported previously,[10] indicate that the creep strength is greater in air and nitrogen than in CO and CO_2. Since these results were unexpected inasmuch as both CO and CO_2 are carburizing to type 304 stainless steel at 1500°F, it was postulated that the compositional changes resulting from the carburization weakened and embrittled the metal matrix. To check this theory, specimens were carburized in CO and creep tested in argon.

A comparison of the creep rates of as-received and precarburized specimens tested in an argon environment and as-received specimens tested in the carburizing mediums is presented in Table 4.4. It is apparent from the data that substantial amounts of carbon in the matrix merely serve to strengthen the metal. More recent tests on a new heat of material have shown the expected improved creep properties in a CO environment. It is possible that the swaged thermocouples used in the early experiments were carburized and caused a constant increase in the test temperature that resulted in accelerated creep rates and early failures.

[9] GCR Semiann. Prog. Rep. June 30, 1959, ORNL-2767, p 114.
[10] GCR Semiann. Prog. Rep. June 30, 1959, ORNL-2767, p 107.

Table 4.4. Creep Rate of Type 304 Stainless Steel, Heat B, Tested at 3500 psi and 1500°F

Specimen History	Test Environment	Time to Produce Indicated Strain (hr)			Time to Rupture (hr)	Total Strain (%)	Final Carbon Content (wt %)
		1%	5%	10%			
As-received	Argon	12	150	290	346	14.5	0.04
Precarburized	Argon	66	660	1270	1400	12.4	0.15
As-received	CO	6	78	153	213	17.2	~1

Extensive carburization of specimens tested in pure CO_2 was observed previously,[11] and to confirm this unexpected phenomenon, a number of unstressed samples 0.020 in. thick were annealed in a ceramic tube at 1500°F in flowing CO_2. In about 140 hr the average carbon content of the samples had increased from 0.04 to 0.18%. The effect of flow rate was examined, and it was found that variations of from 0.75 to 1.5 cfh did not alter the results. Similar samples annealed in CO were carburized from 0.04 to 0.30% carbon in a comparable time. Preoxidation and thin copper films were found to reduce the rate of carburization in CO and CO_2, although neither one totally prevented carburization.

On the basis of the tests completed to date, the following tentative conclusions may be drawn concerning gas-metal reactions in the EGCR environment:

1. Capsules operating at 1500°F and above will tend to carburize.

2. Carburization will occur even if there is an oxide film on the metal.

3. Neither oxidation nor carburization appear to adversely affect the creep and rupture strength of type 304 stainless steel.

[11] GCR Semiann. Prog. Rep. June 30, 1959, ORNL-2767, p 109.

4. The creep data obtained in argon represent the most conservative values for design purposes.

Manufacturing Development

End-Closure Evaluation

The evaluation of the fuel capsule end closures delineated by the original development program has been completed. End-closure tests were made that consisted of room-temperature tensile tests, short-time tube-burst tests, and thermal-cycling tests. No significant differences among the three basic joint designs were found. In each method of testing, the end-cap weld joint was found to have greater strength than the tube wall.

In thermal-cycling tests,[12] capsules were thermally cycled 1000 times between room temperature and 1400°F while pressurized with helium to give hoop stresses of approximately 2600 psi at the highest temperature. The specimens were checked weekly for changes in pressure or dimensions and were found to maintain the helium-pressure originally applied. The outside diameters of the specimens increased by 0.001 to 0.0015 in., presumably because of buildup of oxide scale. After thermal cycling was completed, the specimens were leak tested at 1400°F, using a helium mass spectrometer, and found to be leaktight. Metallographic examinations of representative welds from the test capsules are being carried out.

Mid-plane Spacer

Restraint in the form of a mid-plane spacer has been found to be necessary to prevent catastrophic bowing and failure of the fuel elements because of uneven temperature distribution around the capsule perimeter. The proposed EGCR fuel element design incorporates a spacer in the form of a helical gear brazed at the center of each fuel capsule.

---

[12] GCR Semiann. Prog. Rep. June 30, 1959, ORNL-2767, p 120.

In order to determine the tolerable gap between the outer surface of the tube and the inner surface of the spacer, a series of brazing tests was run with diametral clearances between the tube and the spacer ranging from 0.001 to 0.013 in. The specimens were brazed in a hydrogen atmosphere at 1175°C for 30 min using GE-81 brazing alloy. A tube and spacer sample with the alloy applied in the slurry form before brazing and an as-brazed sample are shown in Fig. 4.7. It was found that clearances in excess of 0.006 in. on the diameter of the assembly caused incomplete flow of the brazing alloy and gaps between the spacer and the tube. Concentricity within the desired tolerance could be maintained between the tube and the spacer with clearances of 0.004 in. and less. The weight of alloy used for each joint was measured in order to determine the amount of alloy necessary for the manufacture of a precast brazing ring. No attempt was made to machine helical fins on the spacer because these would have no effect on the brazing variables.

Metallographic examination of the brazed joints indicated no dilution of the tube wall by the GE-81 alloy. The grain size of the tube wall increased by approximately a factor of 2 during the brazing operation.

Fuel Element Hangers

Modification of the fuel element hanger design from a joint requiring a longitudinal fillet weld to a joint requiring a circular fillet weld precipitated an investigation to determine whether cracking in the cast hanger material could be expected. Cast type 304 stainless steel material was obtained and machined to receive the end-cap hanger extension. Fillet welds of both the recessed and protruding type were made with type 308 stainless steel weld filler material. Metallographic examination indicated no cracks in either of the joints tested. Methods of making this weld by semiautomatic means are being investigated.

Helium Leak Testing of Fuel Capsules

The procedure specification for helium leak testing of fuel

capsules[13] has been revised to guard against the possibility of completely outgassing the helium from a capsule in the event of a gross leak. This specification has been designated RMIS-8 and will be available for use as soon as a final review is completed.

Inspection of Fuel Capsule Tubing

Eddy-Current Inspection

Reference Standards. An extensive investigation has been made of the problem of choosing a realistic reference-standard tube for use in the eddy-current inspection of tubing. The criteria for selection of a standard defect in the reference-standard tube are (1) that the response of the eddy-current tester should closely resemble that produced by a natural defect and (2) that the standard defect should be easily and reliably reproduced. Three types of standard defects have been examined: (1) longitudinal notches produced by a thin milling cutter, (2) transverse notches produced by a round file, and (3) longitudinal notches produced by electrical-spark-discharge machining.

The most common defect in tubing is a longitudinal crack, which can be simulated most easily by the two types of longitudinal notches listed above. Of the three types of notches, the spark-discharge notch is most reliably reproduced. The eddy-current trace of Fig. 4.8 illustrates the high degree of reproducibility achieved in the production of three sets of longitudinal notches on the outside surface of a 3/4-in.-dia, 0.020-in.-wall, type 304 stainless steel fuel capsule tube. The milled notches are not so easily reproduced, as may be seen by the eddy-current trace in Fig. 4.9 that was produced by a similar tube containing five notches which were intended to be 0.0025 in. in depth. The transverse filed notches are the most easily produced of the three standard defects examined, and, while filed notches cannot be as reliably reproduced as spark-discharge notches, the filed notches can

[13] GCR Semiann. Prog. Rep. June 30, 1959, ORNL-2767, p 121.

UNCLASSIFIED
Y 30813

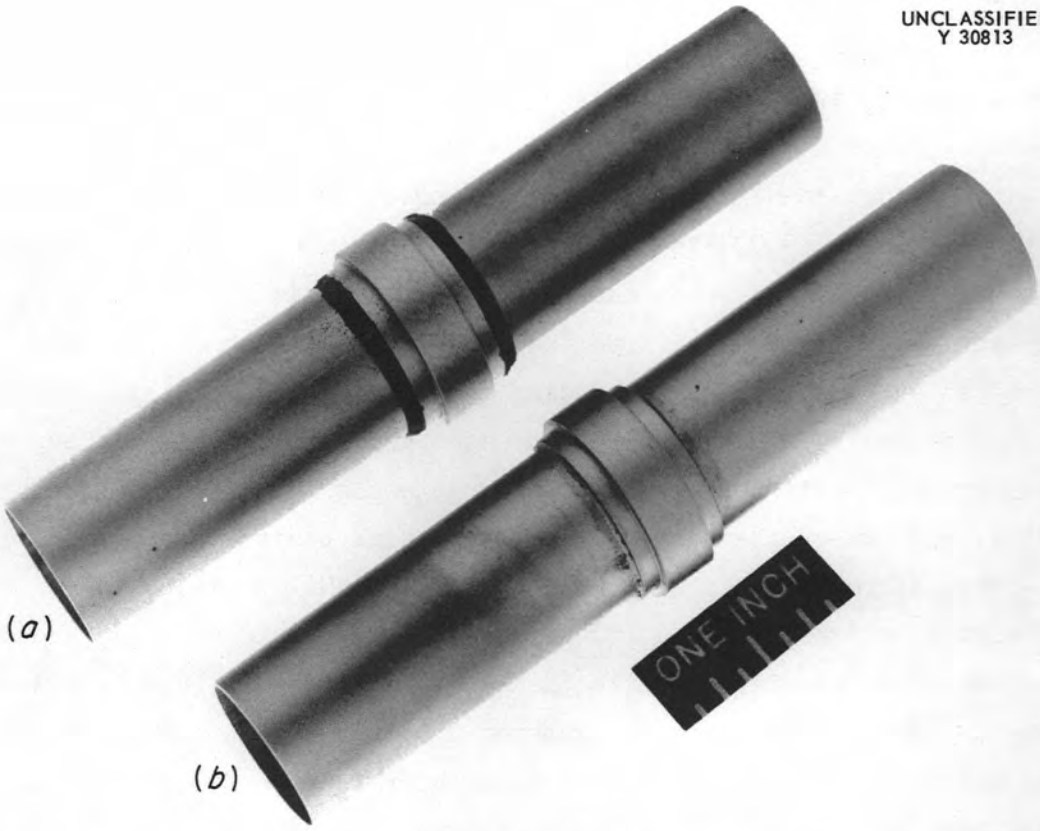

Fig. 4.7. Mid-Plane Spacer Brazing Test Specimens (a) with Alloy Applied as Slurry and (b) As Brazed.

UNCLASSIFIED
ORNL-LR-DWG 40700

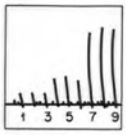

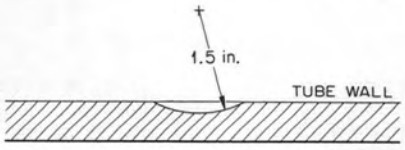

NOTCH	DEPTH
1	0.0029 in.
2	0.0032 in.
3	0.0030 in.
4	0.0054 in.
5	0.0053 in.
6	0.0051 in.
7	0.0098 in.
8	0.0104 in.
9	0.0100 in.

TUBING: 3/4-in. OD x 0.020-in. WALL, TYPE 304 SS
TYPE NOTCH: LONGITUDINAL
PRODUCED BY: ELECTRICAL SPARK DISCHARGE MACHINING WITH CIRCULAR TOOL 3-in. DIA x 0.005-in. WIDE
INSTRUMENT: MODIFIED RADAC MODEL 302
INSPECTION FREQUENCY: 64 kc

Fig. 4.8. Eddy-Current Signal Trace Illustrating Reproducibility of Notches Produced by Spark-Discharge Machining.

be more reliably reproduced than the milled notches. This is illustrated by the eddy-current trace of Fig. 4.10 produced by a 3/4-in.-dia, 0.020-in.-wall, type 304 stainless steel tube containing two sets of transverse filed notches intended to be 0.003 and 0.0035 in. in depth.

In conjunction with the development of a reference standard, 1500 ft of 3/4-in.-dia, 0.020-in.-wall, type 304 stainless steel tubing was inspected using eddy-current encircling-coil techniques with a longitudinally milled notch as a reference standard. The rejection point was chosen such that a tube producing a defect signal equal to the signal produced by a notch 0.0025 in. deep would be rejected. Several metallographic sections were taken through areas that produced defect signals, and two of the sections are shown with their corresponding eddy-current traces in Figs. 4.11 and 4.12. As may be seen, the 0.007-in.-deep crack (Fig. 4.12) produced a defect signal which greatly exceeded the reject level, while the 0.003-in.-deep lap (Fig. 4.11) produced a signal only slightly greater than the reject level. In all areas sectioned, no defects deeper than the reference standard were found which had not been rejected by the eddy-current inspection.

Although good correlation existed between the inspection and metallographic examination for the few samples examined, it is not felt that the optimum reference standard has been developed, and additional studies are being conducted. An interim standard consisting of a transverse-filed notch has been chosen, since it is easily fabricated and is fairly reproducible.

Test Parameters. The test parameters of greatest concern in the eddy-current inspection of tubing are the test frequency and coil configuration. After considerable experimentation, the following formula was empirically derived for determining the maximum permissible test frequency for the inspection of thin-walled austentic stainless steel tubing:

$$F_{max} = \frac{36.5}{D^2} ,$$

UNCLASSIFIED
ORNL-LR-DWG 38259R

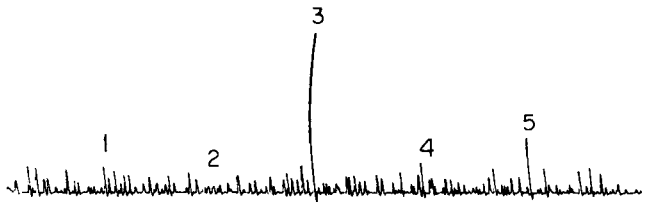

NOTCHES PRODUCED BY 2 ½-in. DIA x 0.010-in. WIDE MILLING CUTTER

NOTCH	DEPTH
1	0.0016 in.
2	0.0021 in.
3	0.0044 in.
4	0.0029 in.
5	0.0030 in.

INSPECTION FREQUENCY: 64 kc

INSTRUMENT: MODIFIED RADAC MODEL 302

Fig. 4.9. Eddy-Current Signal Trace Illustrating Reproducibility of Notches Produced by Milling.

UNCLASSIFIED
ORNL-LR-DWG 40701

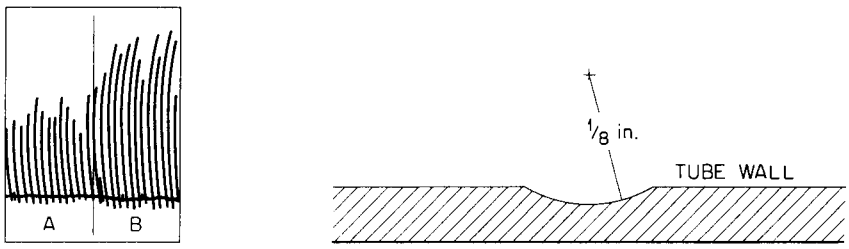

TUBING: 3/4-in. DIA x 0.020-in. WALL, TYPE 304 SS
TYPE NOTCH: TRANSVERSE
PRODUCED BY: 1/4-in. ROUND FILE
DEPTH: A ~0.003 in.
B ~0.0035 in.
INSTRUMENT: MODIFIED RADAC MODEL 302
INSPECTION FREQUENCY: 64 kc

Fig. 4.10. Eddy-Current Signal Trace Illustrating Reproducibility of Filed Notches.

UNCLASSIFIED
ORNL-LR-DWG 40696A

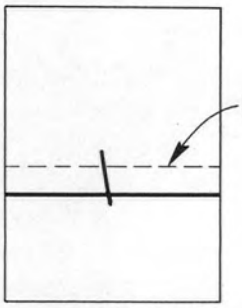

TUBING: 3/4-in. DIA. x 0.020-in. WALL, TYPE 304 SS
DEFECT: LAP 0.003-in. DEEP
INSTRUMENTATION: MODIFIED RADAC MODEL 302
INSPECTION FREQUENCY: 64 kc

AS POLISHED

EDDY CURRENT SIGNAL TRACE

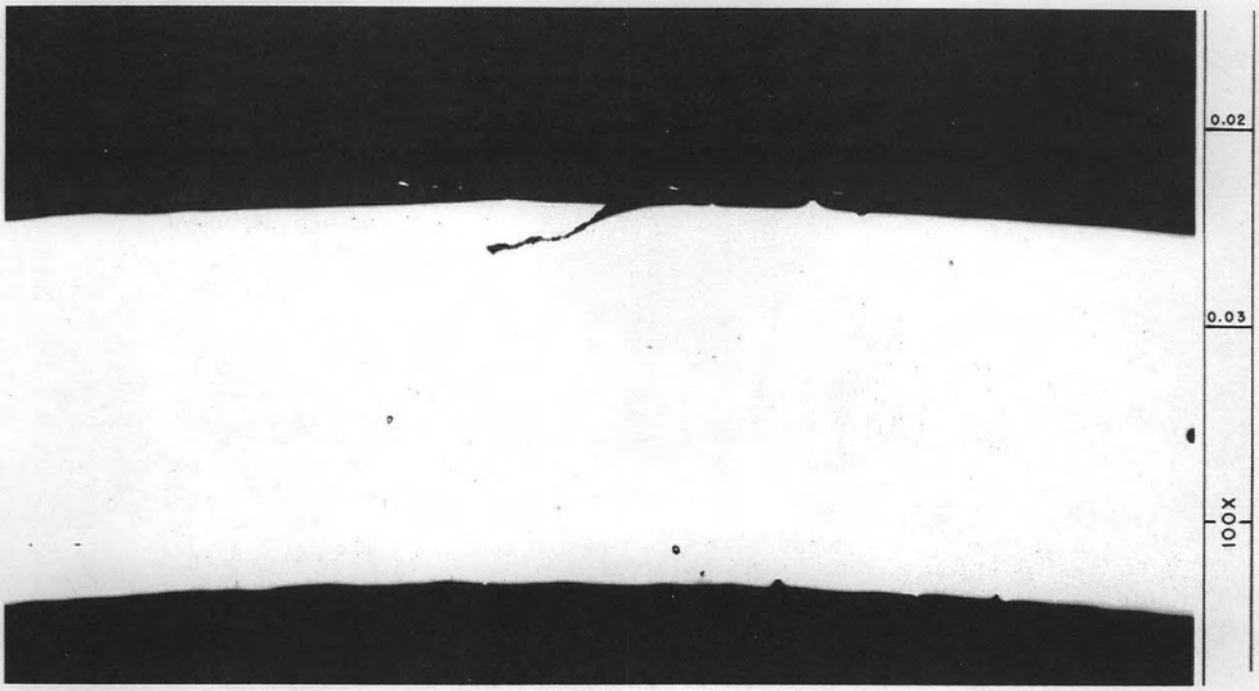

Fig. 4.11. Defective Tube with Lap 0.003 in. Deep and Eddy-Current Signal Trace by Which It was Detected.

UNCLASSIFIED
ORNL-LR-DWG 40699A

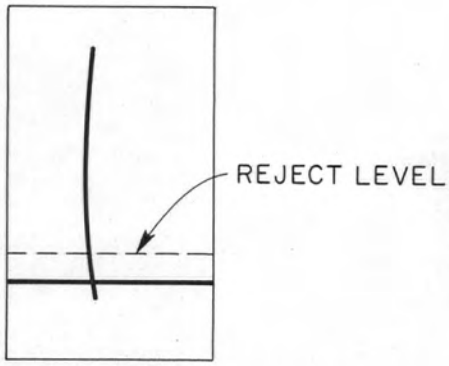

TUBING: 3/4-in. DIA. x 0.020-in. WALL, TYPE 304 SS
DEFECT: CRACK 0.007-in. DEEP
INSTRUMENTATION: MODIFIED RADAC MODEL 302 ENCIRCLING COIL
INSPECTION FREQUENCY: 64 kc

AS POLISHED

EDDY CURRENT SIGNAL TRACE

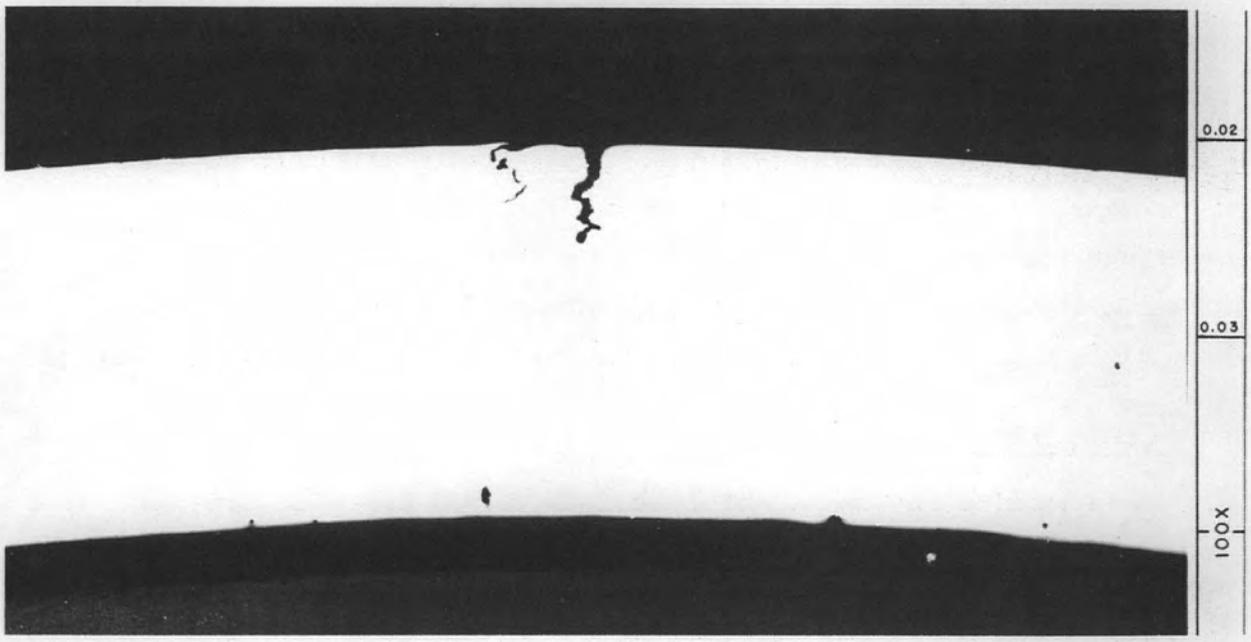

Fig. 4.12. Defective Tube with Crack 0.007 in. Deep and Eddy-Current Signal Trace by Which It Was Detected.

where F is frequency in kilocycles and D is diameter in inches. A lower test frequency is permissible if it gives adequate detection of the notches in the standard-reference tube.

The primary concern in the choice of a coil configuration is to obtain an optimum ratio between defect signals and background noise. The technique chosen for the inspection of EGCR tubing involves the use of two differential encircling coils. Investigations have been made to determine the effect of coil spacing in minimizing signals produced by insignificant variables within the tubing. The signal-to-noise ratio as a function of coil spacing is illustrated in Fig. 4.13. Although there is considerable scatter in the data, the trend toward a better signal-to-noise ratio with closer coupling between coils is apparent.

Inspection Procedure. The development effort on the eddy-current inspection of tubing has resulted in a major revision of RMIS-7, "Procedure Specification for the Eddy-Current Inspection of Thin-Walled Austenitic Stainless Steel Tubing." This specification is designed for the inspection of tubing at the vendor's plant. The standard defect chosen for use with this procedure is a transverse filed notch which has a depth of 12.5% of the wall thickness of the tubing. Improvements will be made to this specification as further information is gained.

Capsule Tubing Evaluation

Approximately 1500 ft of 3/4-in.-OD, 0.020-in.-wall, type 304 stainless steel tubing was procured from the Superior Tube Company for use in development work. This tubing was purchased to an inside diameter tolerance of 0.711 ± 0.001 in. and a wall-thickness tolerance of 0.020 ± 0.002 in., with no inspection requirements. A thorough evaluation was made of this tubing at ORNL using fluorescent penetrants, eddy currents, pulse-echo ultrasonics, resonance ultrasonics for wall-thickness determinations, and air gaging for inside-diameter measurements. The inspection results provide a quality reference for capsule tubing procured with no inspection requirements. The thoroughness of the evaluation served not only to give assurance that all flaws would

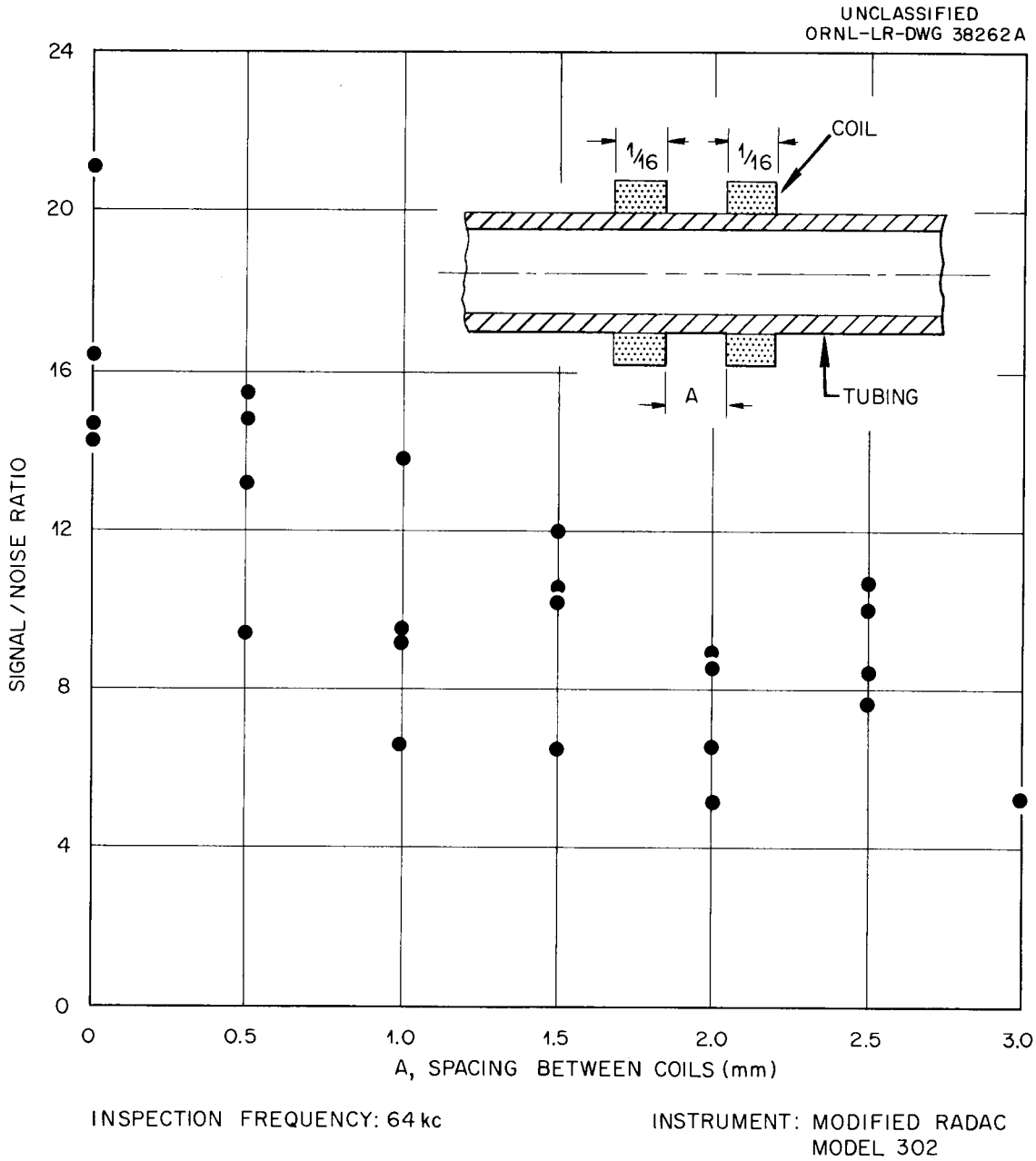

Fig. 4.13. Eddy-Current Signal-to-Noise Ratio as a Function of Spacing Between Differential Encircling Coils on 3/4-in.-dia, 0.020-in.-Wall Type 304 Stainless Steel Tubing.

be detected but also to aid in the establishment of confidence levels for the detection of the 0.0025-in.-deep discontinuities which are considered rejectable.

In the 100% inspection by the eddy-current technique, as described above, the total rejection was about 36%. Visual examination of the rejected areas revealed that about one-half of the rejection was caused by dents, nicks, or gouges. The penetrant inspection, which was conducted on about 1100 of the 1500 ft, resulted in a total rejection of about 3%. The pulse-echo ultrasonic technique detected the presence of several large crack-like indications for a total rejection rate of about 2%. Several of these defects, such as those shown in Figs. 4.11 and 4.12, were also detected by the eddy-current technique. Some of the smaller nonrejectable cracks and laps detected by the pulse-echo ultrasonic technique are similar to that illustrated in Fig. 4.14.

The resonance-ultrasonic technique was used to measure the wall thickness on about 100 ft of randomly selected tubing. All the tubing measured was within the prescribed tolerance of ±0.002 in. About one-third was within a tolerance of ±0.001 in. Air-gage measurements of the inside diameter of a small random sample indicated that about 12% of the measured tubing contained areas in which the inside diameter exceeded the ±0.001-in. tolerance.

The rejection rates given above were determined on the basis of the number of acceptable 30-in. lengths which could be derived from the 10 to 12 ft random lengths. Therefore, there may be shorter lengths of good tubing which were rejected. Since each inspection has been considered separately, the total rejection rate is not the sum of each rejection rate, but, with some coincident rejections, will fall between the sum and the highest individual rate, or about 45%.

Pressure Vessel Studies

Pressure Vessel Welding

A number of problems associated with the use of thick plates of

ASTM type SA-212, grade B steel for field fabrication of a large pressure vessel have been recognized. One of the more important problems is the determination of the pre- and postirradiation notch toughness of weldments prepared using field-erection welding procedures.

At the recommendation of the Chicago Bridge and Iron Company, a plate 144 × 48 × 4 in. conforming to ASTM specifications for type SA-212, grade B, and type A-300 steels was purchased from the Lukens Steel Company with a limit on the carbon content of 0.25% in order to promote good weldability. The plate and required test coupons were normalized at 1625/1675°F, water sprayed to 500°F, stress relieved at 1200/1250°F, and air cooled. The properties of the plate, as determined by the manufacturer, are presented in Table 4.5, along with the ASTM specifications for type SA-212, grade B steel.

The plate was delivered to the Chicago Bridge and Iron Company for preparation of three test weldments, as shown in Fig. 4.15. Two pieces of plate, 4 × 12 × 24 in. each, were reserved in the as-received condition and shipped to Rensselaer Polytechnic Institute for determination of the notch toughness of synthetic heat-affected zones. The welding procedure incorporates E7018 electrodes to fabricate the test weldments. The welding data are being used to select thermal cycles for preparation of Charpy V-notch specimens of heat-affected zones. Samples of the test weldments are currently being prepared for determination of the pre- and postirradiation properties of the parent plate, the weld deposits, and the heat-affected zones.

Inspection of Pressure Vessel Welds

Techniques for the inspection of thick test weldments in mild-steel plate for pressure-vessel applications are being developed. The most promising method for the inspection of the completed weldment makes use of pulse-echo ultrasound. Preliminary work on the three test weldments mentioned above has included the use of approximately 45-deg shear waves at 2.25 mc propagated into and through the weld both longitudinally and perpendicular to the weld axis. Four linear feet of weld fabricated by

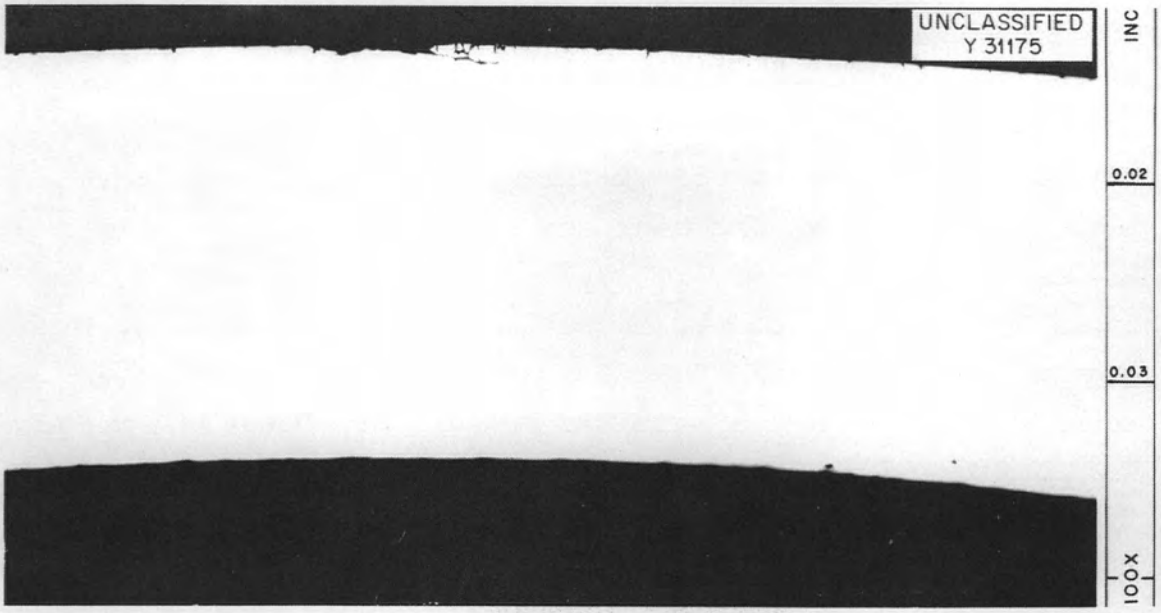

Fig. 4.14. Unrejected Discontinuities in Capsule Tubing.

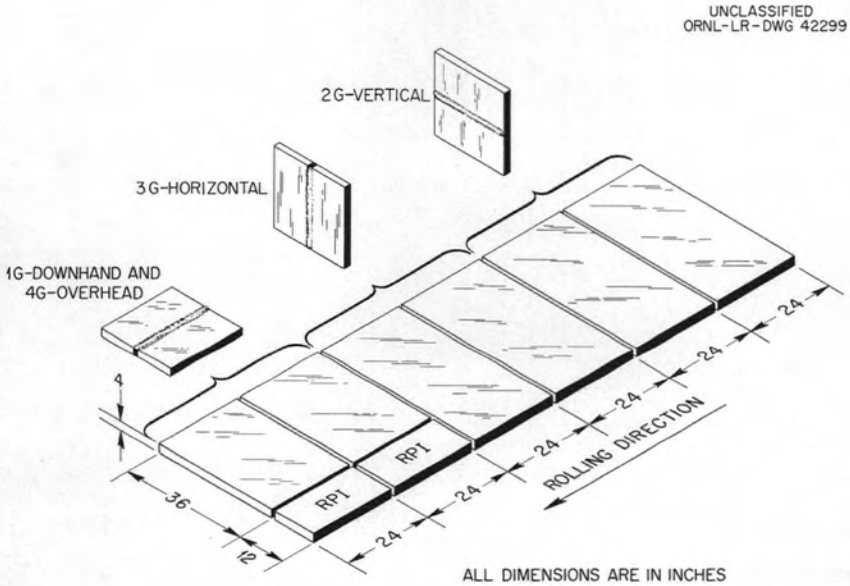

Fig. 4.15. Disposition of Type SA-212, Grade B, Steel Plate Rolled at Lukens Steel Company.

Table 4.5. Composition and Properties of 4-in.-Thick Plate Purchased from Lukens Steel Company

	Type SA-212, Grade B Steel	Lukens Heat 15900
Chemical Composition		
Carbon, max (%)	0.35	0.25
Manganese, max (%)	0.90	0.74
Phosphorous, max (%)	0.035	0.013
Sulfur, max (%)	0.040	0.025
Silicon (%)	0.15 to 0.30	0.020
Tensile Properties		
Tensile strength (psi)	70,000 to 85,000	82,500, 84,100
Yield strength, min (psi)	38,000	50,800
Elongation, min (% in 2 in.)	19	28
Impact Requirements (Type A-300 steel specifications)		
Charpy keyhold energy, min at -50°F (ft-lb)	15	24, 26, 23

the vertical welding technique was evaluated and a few small discontinuities were detected. While this plate is being cut for testing, certain selected areas will be obtained to assist in correlation of ultrasonic indications with the actual discontinuities within the weld.

Approximately 3 ft of weld fabricated in the overhead and downhand positions is now being ultrasonically examined by similar techniques. More and larger discontinuities are being located in this weldment. Although most, if not all, of these discontinuities are smaller than rejectable size, they aid in establishing confidence levels for inspection reproducibility, in determining the amount of inspection required to adequately detect objectionable discontinuities, and in developing precision in locating the discontinuities in three dimensions.

Beryllium Investigations

Welding and Brazing

Techniques for joining beryllium to itself and to other metals will be required in the preparation of specimens for the evaluation of physical properties and for in-pile testing. Joining methods other than fusion welding are being studied, since welds will probably be reliable only as seals.

Probably the most attractive method for joining beryllium is diffusion bonding. Using a molybdenum jig, a bond which was approximately 75% sound was produced between a beryllium tube and a solid beryllium plug placed inside the tube. The difference in the coefficients of thermal expansion of molybdenum (4.9 μin./°C) and beryllium (12.4 μin./°C) at elevated temperatures made the bonding possible after an extended length of time at temperature.

The brazing of beryllium is also being studied. An alloy consisting of 48% Zr-48% Ti-4% Be brazed at 1000°C was found to wet and flow on beryllium, but the joint was not sound. Cracks were found in the joint after cooling that resulted from the difference in the coefficients of thermal expansion of the beryllium and the brazing alloy (~7 μin./°C). Other alloy systems are being investigated which have expansion coefficients compatible with that of beryllium and which have the wetting and flowing properties necessary to produced brazed beryllium joints suitable for operation at approximately 600°C.

Beryllium-Tubing Evaluation

Approximately 28 ft of 3/4-in.-ID beryllium tubing obtained from England is currently being evaluated by nondestructive methods. The techniques which are being developed for beryllium-tubing inspection utilize resonance and pulse-echo ultrasonics, radiography, fluorescent penetrants, and eddy-currents. The resonance-ultrasonic technique revealed most of the wall-thickness variations to fall within the range 0.035 to 0.045 in., with occasional variations in a short length in

the range 0.040 to 0.050 in. Pulse-echo ultrasonic inspection has revealed the presence of several flaws, the nature of which has not been determined.

Radiographic inspection has detected numerous high-density particles and several pits, gouges, and longitudinal grooves. A few of the pits on the inner surface have diameters up to about 0.025 in., and they penetrate the wall as much as 75%. Thus far, the radiographic technique seems to be the most definitive for determining the quality of the tubing. It is thought that some of the high-density particles are present on the surface; a sulfuric acid etch will be investigated for removing these contaminants.

The fluorescent-penetrant technique has revealed the presence of many pits and pin holes in the outer surface, none of which seem to have much depth. This seems to be a common characteristic in all beryllium tubing examined to date.

Eddy-current techniques have not been used successfully thus far for the inspection of beryllium. Some of the difficulties are the surface roughness and probable ferritic contamination, which produce a high "noise" level, and the crookedness of the tubing, which hinders movement through the encircling coil.

Procurement of Beryllium Tubing

A thorough evaluation of beryllium as a capsule material will require the procurement of tubing from vendors experienced in fabricating the metal. At the present time, an attempt is being made to obtain 500 ft of 0.300-in.-ID, 0.040-in. wall tubing from each of three sources on a purchase order basis. One source is the Chesterfield Tube Company of Great Britain whose United States representative is Superior Tube Company. One hundred feet of tubing extruded from hot-pressed beryllium rod has been requested, with an estimated delivery schedule of 4 to 5 months. The remaining 400 ft of the order is to be extruded from virgin beryllium powder and can be supplied within 8 to 9 months.

Twenty feet of "off the shelf" tubing was recently received from the Chesterfield Tube Company through the Superior Tube Company.

Inquiries were made to the Pechiney Company of France, and their reply stated that beryllium tubing of the above-mentioned size is not currently available, but they are considering an attempt to produce tubing of this size. The smallest beryllium tubes on hand at present are 0.520 in. ID, 0.040 in. wall. A further inquiry has been made with regard to the procurement of 50 ft of the available tubing.

A third source, the Brush Beryllium Company of the United States, proposes to fabricate a total of 500 ft of beryllium tubing from their intermediate- or best-grade beryllium powder by the following methods: (1) machining from hot-pressed block, (2) warm extrusion, (3) hot extrusion, and (4) swaging powder and then sintering and extruding. The product delivered would represent the best results of variations of process conditions for each of these methods. It is felt that this approach would give a better product to evaluate, and it would provide the vendor with experience in the fabrication problems and in estimating the eventual manufacturing costs for large quantities. As soon as beryllium tubing is available, it will be evaluated nondestructively, and the degree of preferred orientation will be determined for correlation with the mechanical properties of the material.

Gas-Metal Reactions of Beryllium

The reactions between beryllium and low concentrations of CO_2, CO, CH_4, H_2, and H_2O in helium will be studied. The reactions of beryllium with O_2, N_2, and H_2 at reduced pressures have been studied by Gulbransen and Andrew.[14] The reaction with oxygen was studied over the temperature range 350 to 950°C at pressures ranging from 0.38 to 7.6 cm Hg. The experimental data may be fitted by the parabolic rate law, except for the initial period of the reaction. A comparison of the oxidation rates

[14]E. A. Gulbransen and K. F. Andrew, J. Electrochem. Soc. 97, 383 (1950).

showed that beryllium reacts at 825°C at about the same rate as zirconium does at 375°C. No reaction of beryllium with hydrogen was observed over the temperature range 300 to 882°C for a hydrogen pressure of 2.3 cm Hg.

Munro and Williams[15] found that the corrosion rate of beryllium prepared from electrolytic flake powder is negligible at 500°C in dry and wet CO_2 at atmospheric pressure. Extrapolation of the data showed that an oxide film 1 μ thick would be formed after three years at this temperature. The furface film formed at 600°C in wet CO_2 is not protective, but it is protective when formed in dry gas.

Experiments will be run to investigate the reaction of beryllium with CO_2 at 750°C, at which temperature carburization of the beryllium is expected. The reaction rate will be determined by observing the change in pressure in a closed reaction chamber. A sensitive octoil manometer will serve as the pressure-sensing device.

---

[15]W. Munro and J. Williams, Reaction of Beryllium with CO_2 in the Temperature Range 500 — 700°C, AERE-M/M-108 (1956).

5. IN-PILE TESTING OF COMPONENTS AND MATERIALS

Fuel Capsule Irradiation Program

Full-size (diameter only) single fuel rod specimens are being irradiated at both the ORR and ETR. Fabrication of a second set of experimental assemblies for irradiation in the ORR is complete, except for the fuel pellets, and assembly will be initiated shortly. Initial operation of the GETR helium loop revealed need for several design changes, including revision of the compressor housings and addition of a large heater. After effecting these changes and repairing numerous leaks, the loop now appears to be ready for irradiation testing. Thirteen miniature capsules have been irradiated in the LITR and six tests are now under way. Two of the capsules failed at thermocouple junctions, but the others completed the scheduled irradiation.

Full-Diameter Prototype Fuel Capsules

ORR Experiments. The irradiation of eight experimental capsules in the ORR has continued for about five months of the scheduled six-month period. The specified cladding temperatures, 1300°F (average for six thermocouples) for capsules 01, 03, 04, and 07 and 1600°F maximum for capsules 02, 05, 06, and 08, have been achieved on all except capsule 08 with the reactor at full power. It was necessary to reduce the power of the ORR from 20 to approximately 16 Mw during the summer period because of the high ambient temperature, and therefore the capsules have correspondingly lower burnup rates than would have accrued at 20-Mw operation. During an interim period of five weeks, the reactor power level fluctuated between 20 Mw at night and 14 to 18 Mw during the day, and thus there has been thermal cycling of the capsules. Increased concentrations of argon in helium have been used as the thermal barrier gas to maintain the desired capsule temperatures; however, even with pure argon, the required cladding temperatures are achievable only for capsules 01, 03, 04, and 05 when the reactor is operating at 16 Mw.

Capsule 07 experienced temperature oscillations on two occasions, having mean-to-peak amplitudes of 100°F with cycle periods of a few minutes which started and stopped abruptly without apparent cause. It is postulated that a mechanical instability is the cause, since an eccentricity in the position of the Nak-containing tube of as little as 0.0005 to 0.001 in. would change the gas annulus sufficiently to produce the observed temperature variation. It has not been possible to induce oscillation artificially by thermal cycling, and the capsule has been stable and apparently unaffected for over a month since the last period of oscillation.

Thermal cycles have been induced by changing the barrier gas during temperature adjustments and by using the cadmium shutters, in addition to those introduced by reactor power fluctuations. Bypassing of gases in the upper region of the capsule apparently prevents effective replacement of the gas mixture in the active region. Accordingly, it has been necessary to repeatedly pressurize and depressurize the barrier gas region to effect a change. This repeated forcing of gases of differing composition past the capsule produces thermal cycles. The capsules have now been redesigned, and future assemblies, including the second set for the ORR, will have provisions to minimize bypassing of the gas. A summary of all capsule thermal cycles by temperature range and source categories for ORR operating cycles X through XIV is given in Table 5.1.

ETR Experiments. The ETR capsule installed to verify flux predictions has been irradiated for a total of about 30 days. Its operating temperature after the first reactor cycle was increased from the 1200°F previously reported[1] to the design value of 1300°F by moving it to a new reactor reflector location. Six additional capsules were installed in the ETR during July and have operated satisfactorily, except that they too are in a low reactor flux and only one is at the design temperature. These capsules are to be moved at the next reactor shutdown to a higher flux region to obtain the desired temperature.

---

[1]GCR Semiann. Prog. Rep. June 30, 1959, ORNL-2767, p 134.

Table 5.1. Summary of Thermal Cycles of Prototype Fuel Capsules During ORR Cycles X Through XIV

Source and Magnitude of Cycle	Number of Thermal Cycles*							
	Capsule No.							
	01	02	03	04	05	06	07	08
Reactor Operation								
20-50°F	52	43	51	92	65	77	58	68
50-200°F	100	106	92	104	111	77	97	95
200-700°F	36	39	49	52	37	27	44	34
700+°F	67	66	72	69	70	70	49	59
Shutter Operation								
20-50°F	18	26	1	0	8	2	10	5
50-200°F	0	26	10	8	6	172	4	6
200-700°F	0	0	44	42	176	6	176	172
700+°F	0	0	0	0	0	0	0	0
Thermal Barrier Gas Adjustment								
20-50°F	181	225	172	96	199	55	156	88
50-200°F	165	187	167	109	236	101	276	81
200-700°F	24	57	38	18	48	42	21	9
700+°F	0	0	0	0	0	0	0	0
Total Cycles								
20-50°F	251	294	230	188	272	134	224	161
50-200°F	265	319	269	221	353	350	377	182
200-700°F	60	96	131	112	261	75	241	215
700+°F	67	66	72	69	70	70	49	59

*A cycle is defined as the total change in temperature in one direction prior to a stable period or reversal; only those changes occurring in a period of 10 min or less have been counted.

Reduced-Size Prototype Fuel Capsules

Initial operation of the helium-cooled loop in the General Electric Test Reactor (GETR) indicated the need for several modifications. It was not possible to achieve the design operating temperature because losses to the reactor pool and in some of the loop facility installation were greater than predicted. Accordingly, it has been necessary to install an additional electric heater of 300 kw capacity to obtain the loop design temperature of 800°F at the facility tube inlet. The heater is a bayonet-type, ribbon-element, nichrome unit manufactured by the Hines Electric Company.

Considerable difficulty was experienced with the compressors and the seals for the compressor motor shaft penetration into the compressor housing. These seals which were conventional commercial units failed repeatedly and so severely that helium pressure could not be maintained. Difficulty was also encountered with the compressor gear trains either from lack of lubrication due to the lubricating oils operating at too high a temperature, or from misalignment of the compressor shaft coupling and the seal connection. Accordingly, the compressor housings were extended to accommodate the drive motor and eliminate the seal. Special cooling was provided for the motor and the compressor lubricating oil. The compressors have operated without trouble for several hundred hours since this revision.

In an attempt to meet the short procurement and installation schedules required by the early loop operating target date, numerous flanged joints were installed in the loop, 45 of these joints being in valves. Considerable difficulty has been experienced in obtaining a leaktight system, and the flanged joints have been particularly troublesome when loop thermal cycles occur. It has been necessary to replace the flange bolts specified for 800°F operation with bolts of a different alloy steel capable of over 1000°F operation in order to obtain acceptable flange seal performance. Ten of the fifteen valves are being removed and replaced with welded-in pipe sections, and the remaining five are being removed to cooler locations to reduce leakage at flanges.

Numerous leaks in welds, joints, and other connections have been located and repaired for interim operation, and the additional leak testing and correction required probably can be conducted during operation and reactor shutdown periods.

With the exception of the leaks and minor difficulties in moving the neutron-absorbing thermal-cycling shutters, the loop now appears to be ready for nuclear operation. Fuel stringers have been installed in four of the five facility tubes, with the fifth tube being reserved for installation of a third thermocouple calibration test.

The first thermocouple test, which was conducted in a facility tube while in place in the reactor, was reported previously to be somewhat unsatisfactory.[2] A second test was therefore conducted in a facility tube outside the reactor pool using the loop compressors for circulation of helium. Sheathed thermocouples installed in accordance with the original design, bare-wire thermocouples attached to the outer surface of the fuel cladding, and thermocouples that penetrate the cladding wall were utilized in a test device employing a Globar heater. One of the internal thermocouples was defective, and there is considerable question concerning the comparison between temperatures indicated by the sheath thermocouples and the true cladding temperature. Thus, the results of this test are still somewhat inconclusive, although the thermocouples individually were more consistent than in the previous test. It is now planned to conduct a third thermocouple calibration test in the No. 1 facility tube at the next reactor shutdown.

In an effort to correlate indicated cladding temperatures with true cladding temperatures, a relationship was established as a function of gas velocity and power for the outside bare and sheathed thermocouples. The validity of the relationship has not yet been determined.[3]

---

[2] Ibid., p 143.

[3] For details see GCPR – Prototype Fuel Irradiation Program, Progress Report No. 12, General Electric Company, Vallecitos, GEAP 3233, August 1959.

Miniature Capsule Fission-Gas-Release Experiments

Irradiations of miniature capsules have continued in the LITR with increased emphasis on the achievement and measurement of high central pellet temperatures. Capsule irradiation experience to date is described in Table 5.2. The central pellet temperatures listed are those noted immediately after initial heatup and in all cases were the highest obtained. The point of failure for both capsules L-2a and L-20bx was at the braze of the thermocouple wire to the insulator seal pin.

Because of the difficulties previously reported with platinum-platinum-10% rhodium thermocouples,[4] rhenium-tungsten thermocouples have been installed in all recent LITR experiments. These thermocouples, except one mounted on a BeO ceramic insulator, have been sheathed with tantalum and insulated with granular BeO. Over extended periods these thermocouples show decreases in emf averaging an equivalent of 10°F per day, as shown in Fig. 5.1. This performance is to be compared with the larger drift of Pt-Pt-Rh thermocouples shown in Fig. 5.2. Although it is not readily apparent in Fig. 5.1, careful analysis of the thermocouple output, reactor power, and reactor control rod position indicates that the reduction in indicated temperature may be related to thermal cycling. There is no indication as to whether this effect may reflect changes in the fuel pellet or in the thermocouple. The thermocouple in one capsule initially indicated a temperature of approximately 3200°F, which dropped rapidly to about 2800°F. The rhenium-tungsten thermocouples are very fragile and require special handling to avoid early failure in operation, and only a fair degree of consistency has been obtained to date in their installation.

All the capsules presently being irradiated are designed with dual fuel specimens with a thermocouple in each section. Platinum-platinum-10% rhodium thermocouples are used in the upper chamber, and rhenium-tungsten thermocouples are used in the lower section where the temperatures are higher. To obtain still higher temperatures, a new capsule

---

[4] GCR Semiann. Prog. Rep. June 30, 1959, ORNL-2767, p 146.

Table 5.2. Operating Conditions for Miniature Capsules Irradiated in the LITR

Capsule	Date Installed	Present Status	Irradiation Time (hr)	UO_2 Pellet Theoretical Density (%)	Pellet Enrichment (% U^{235})	Pellet Central Temperature (°F)	LITR Core Facility
L-1a	10-23-58	Removed 2-25-59	2479	93.2	10	1850	C-47
-1b			2479	93.2	10	2100[a]	C-47
L-2a	2-25-59	Ruptured and removed 4-7-59	726	84.8	20	2480	C-47
-2b			726	84.8	20	2540[a]	C-47
L-3a	5-19-59	Removed 8-10-59	1820	75.0	10	(b)	C-28
-3b			1820	74.9	10		C-28
L-4a	9-30-58	Removed 4-28-59	4194	92.5	10	2350	C-42
-4b			4194	92.5	10	2500[a]	C-42
L-6a	10-23-58	Removed 5-18-59	4208	73.6	10	2250	C-28
-6b			4208	74.2	10	2500[a]	C-28
L-7a	3-17-59	Removed 6-8-59	1761	95.5	20	2160	C-57
-7b			1761	95.2	20	2600[a]	C-57
L-8a	4-28-59	Removed 6-29-59	1324	84.6	20	2660	C-47
-8b			1324	85.0	20	2800[a]	C-47
L-10a	8-18-59	Being irradiated		95.3	20	2750	C-44
-10b				95.2	20	3100	C-44
L-11a	7-7-59	Being irradiated		85.1	20	2460	C-47
-11b				85.2	20	2770	C-47
L-13a	11-11-58	Removed 6-8-59	4290	93.7	10	2230	C-46
-13b			4290	92.1	10	2560[a]	C-46

Table 5.2 (continued)

Capsule	Date Installed	Present Status	Irradiation Time (hr)	UO_2 Pellet Theoretical Density (%)	Pellet Enrichment (% U^{235})	Pellet Central Temperature (°F)	LITR Core Facility
L-14a	12-30-58	Removed 3-17-59	1565	94.7	20	2080	C-57
-14b			1565	94.7	20	2260[a]	C-57
L-15a	12-22-58	Removed 4-7-59	2155	91.6	20	1620	C-58
-15b			2155	89.7	20	2055[a]	C-58
L-16a	6-16-59	Being irradiated		94.4	30	1810	C-57
-16b				94.4	30	2040	C-57
L-17a	4-7-59	Removed 8-10-59	2695	93.7	30	2410	C-58
-17b			2695	93.8	30	2600[a]	C-58
L-18a	4-28-59	Removed 6-29-59	1324	84.9	30	(c)	C-42
-18b			1324	85.2	30		C-42
L-20xa	6-18-59	Ruptured and removed 6-18-59	1	95.4	15	(d)	C-28
-20xb			1	75.4	15		C-28
L-21a	8-11-59	Being irradiated		96.0	10	1500	C-58
-21b				96.2	10	1650	C-58
L-18xa	7-7-59	Being irradiated		84.7	30	2860	C-42
-18xb				84.6	30	3180	C-42

[a]Estimated from capsule wall and "a" capsule central temperature measurements.

[b]Calculated temperature 3000°F; tungsten-rhenium thermocouple failed during heatup.

[c]Calculated temperature 2760°F; tungsten-rhenium thermocouple failed during heatup.

[d]Capsule ruptured during startup and was removed from LITR core; temperature not established.

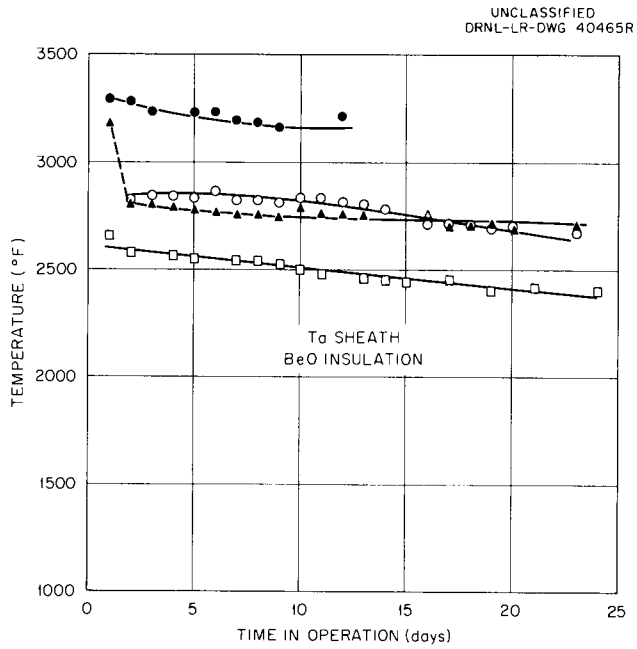

Fig. 5.1. Effects of Temperature and Environment on Accuracy of Tungsten-Rhenium Thermocouples.

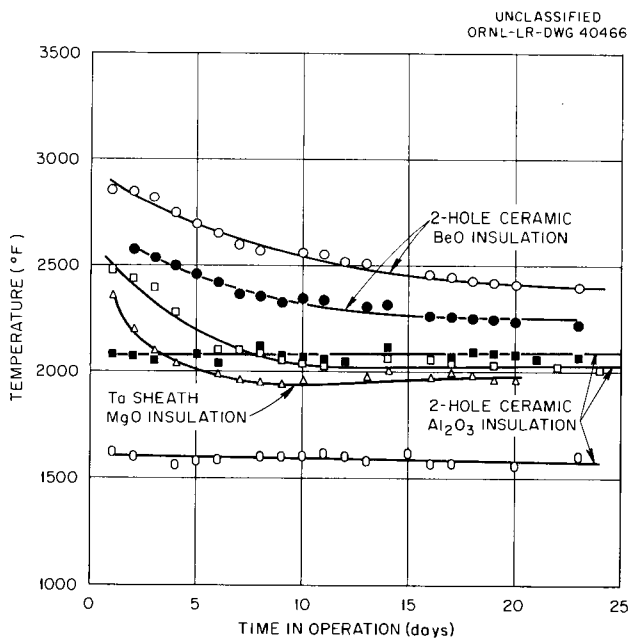

Fig. 5.2. Effects of Temperature and Environment on Accuracy of Platinum–Platinum-10% Rhodium Thermocouples.

has been designed which incorporates a hollow ceramic insulator around the UO_2 fuel. The designs of the current capsule and the new insulated capsule are shown in Fig. 5.3. The insulator material for initial experiments with the revised capsule will be made of depleted UO_2. Zirconium dioxide will be used later when fabrication techniques have been developed.

Fission-Gas-Release Studies

Instantaneous Fission-Gas-Release Experiment

The first experiment in the ORR C-1 facility for studying instantaneous fission gas release was terminated during the quarter, and a new experimental assembly was installed. Thin plates of UO_2, 0.030 in. thick, are being studied in the assembly shown in Fig. 5.4. The UO_2 material is 97% dense and generates 300 w/g in the highest flux position. The temperatures are being monitored by thermocouples between the plates and on the outer surface.

The gas evolved from the fuel sample irradiated previously contained too many fission products for quantitative analysis with a gamma-ray spectrometer, and therefore a system of charcoal adsorbers has been installed for the new experiment which will separate the xenon and krypton from the rest of the products in the sweep gas and then separate the xenon from the krypton. Quantitative measurements will then be made with the gamma-ray spectrometer.

The total activity of the sweep gas was measured previously, and it was concluded for the ThO_2-UO_2 sample that at temperatures above 1300°F the fission gases were released by a diffusion process and that recoil contributions were minor. The half life of the activity in the gas stream was about 2 min for normal operating conditions.[5]

---

[5] Ibid., p 164.

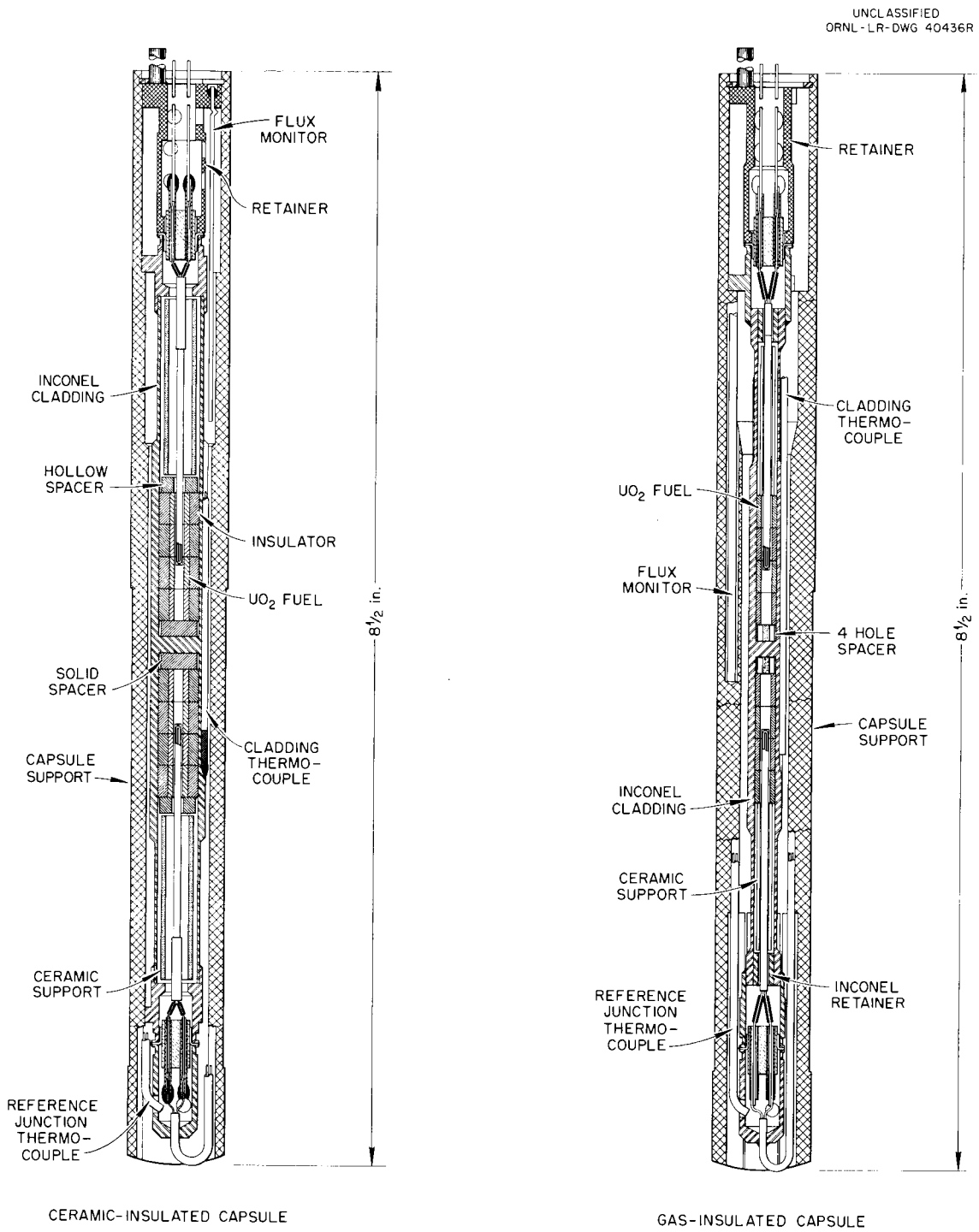

Fig. 5.3. Miniature Capsule Assemblies.

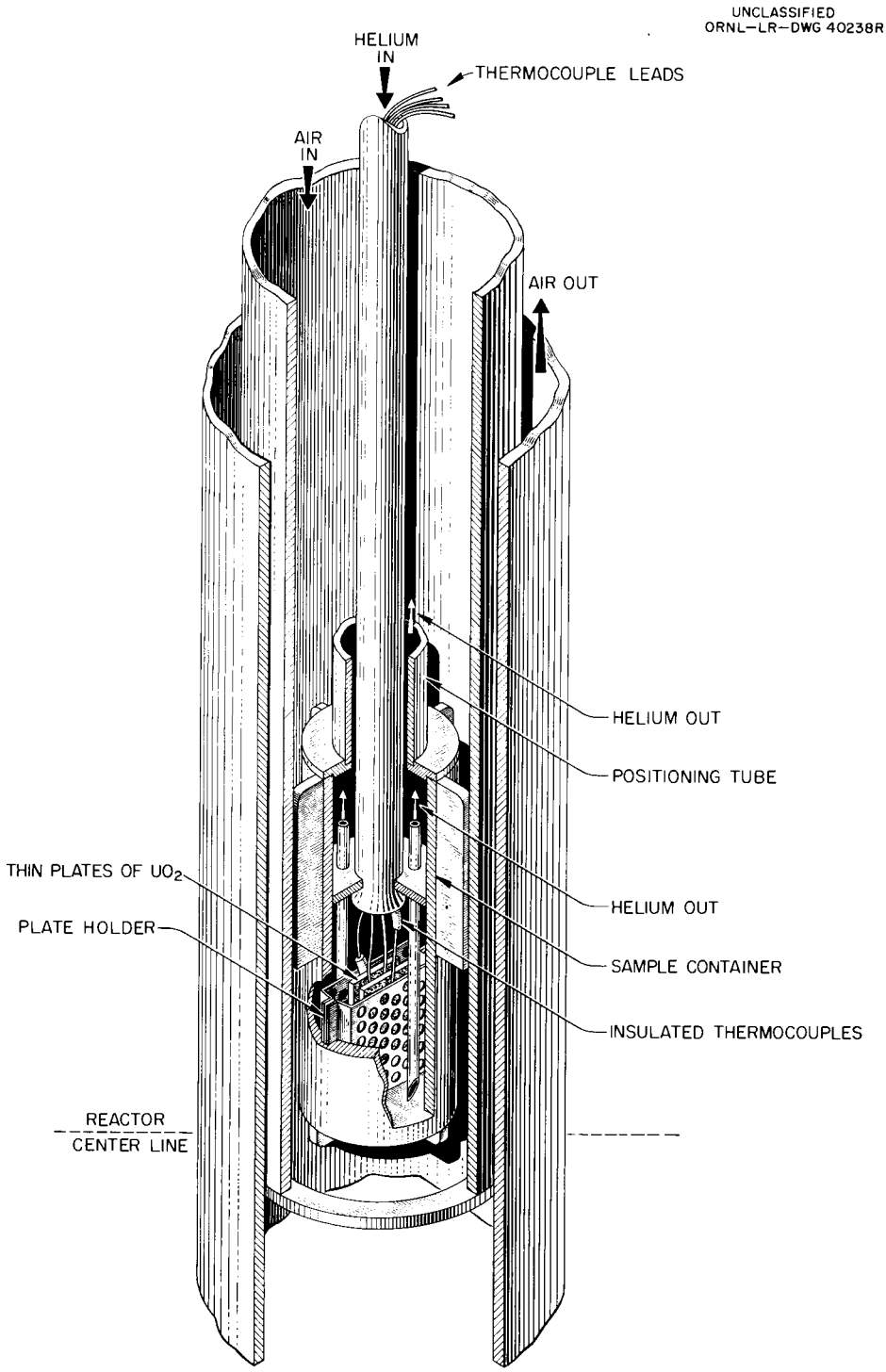

Fig. 5.4. Experimental Assembly for Instantaneous Fission-Gas-Release Studies of Thin Plates of UO_2.

Postirradiation Fission-Product-Release Studies

The summary of fission product release data has been brought up to date and is presented below in Table 5.3. Burnup calculations based on a cobalt monitor analysis have been corrected for flux depression. The wide range of results obtained at similar temperatures for capsules L-2, L-6, and L-13 may indicate that density has a major effect on fission gas release; however, the high oxygen-to-uranium ratio for capsule L-2 and other factors make it desirable to verify these data with other experiments before making any conclusive statements. Future postirradiation fission gas experiments will include capsule-pressure measurements at elevated temperatures and fission product evolution determinations at a series of temperatures up to 2500°F.

Stable Fission Gas Release

Mass spectrometer analyses of gas from four capsules were obtained. Two of the capsules, L-7b and L-13a, operated at too low a temperature to yield sufficient gas to obtain isotopic ratios. The xenon and krypton were separated from the other radioactive contaminants of the capsules and concentrated for analysis with the apparatus shown in Fig. 5.5. The mass spectrometer gives relative abundances only; therefore scans were made for Kr^{85} before the mass spectrometer analyses to furnish a basis for calculating absolute quantities of the stable gases. The results of the scans are not yet complete. The ratio of total krypton to xenon is approximately 1:7. The isotopic abundance of each element is indicated in Table 5.4.

Examinations of Irradiated Capsules

Hot Cell Examinations at GEVAL

Postirradiation examinations continued on five LITR-irradiated capsules, and six more LITR capsules were shipped to the General Electric Company at Vallecitos for examination. In general, the degree and type of fracture of the miniature pellets were similar to those observed

Table 5.3. Postirradiation Fission Gas Release From LITR Capsules

Capsule No.	UO_2 Density (% of Theoretical)	Central UO_2 Temperature (°F)	Burnup (Mwd/MT)	Fission Gas Evolved (% of existing fission gas)				Oxygen-to-Uranium Ratio	Carbon Content of UO_2 (ppm)
				Kr^{85m}	Kr^{88}	Xe^{133}	Xe^{135}		
UO_2-1-1	96	1760	4,000	0.026		0.0091	0.0024		
UO_2-1-2a	96	1770	11,000		0.01	0.033	0.012		
UO_2-1-2b	97	2000	11,000		0.02	0.033	0.012		
L-1a*	92.7	1600	9,000					2.016	6500
L-1b*	93.9	2100	9,000					2.016	6500
L-2a*	84.9	2400	4,000					2.130	2500
L-2b	84.4	2500	4,000			9.0		2.130	2500
L-3a	75.0				Being calculated			2.134	5200
L-3b	74.9				Being calculated			2.134	5200
L-4a	92.1	1600	14,000	0.011	0.021	0.028	0.0085	2.016	6500
L-4b	93.3	1900	14,000	0.012	0.020	0.04	0.0075	2.016	6500
L-6a	73.6	2200	14,000	0.091		0.29	0.049		
L-6b	74.2	2500	14,000	0.035		0.13	0.025		
L-7a*	95.5	2000	6,000					2.041	
L-7b	95.1	2200	6,000	0.019	0.033	0.066	0.035	2.041	
L-8a	84.6	2600	5,000		Being calculated			2.133	3000
L-8b	85.0	2900	5,000		Being calculated			2.133	3000
L-13a	93.7	2200	15,000			0.034		2.016	6500
L-13b	92.1	2550	15,000			0.057		2.016	6500
L-14a	94.1	2100	5,000	0.029	0.011	0.014	0.006	2.028	690
L-14b	95.4	2200	5,000	0.057	0.019	0.029	0.017	2.028	690
L-15a	91.6	1600	6,000	0.019	0.004	0.010	0.004	2.028	690
L-15b*	89.7	1900	6,000					2.028	690
L-17a	93.7				Being calculated			2.01	
L-17b	93.8				Being calculated			2.01	
L-18a*	84.9	~2850	9,000					2.082	3100
L-18b	85.2	~3150	9,000			15.9		2.082	3100

*Capsule L-1, which had lost its gas before removal from the reactor, was used only for the postirradiation heatup experiment; capsules L-2a, L-7a, L-15b, and L-18a had lost their gas.

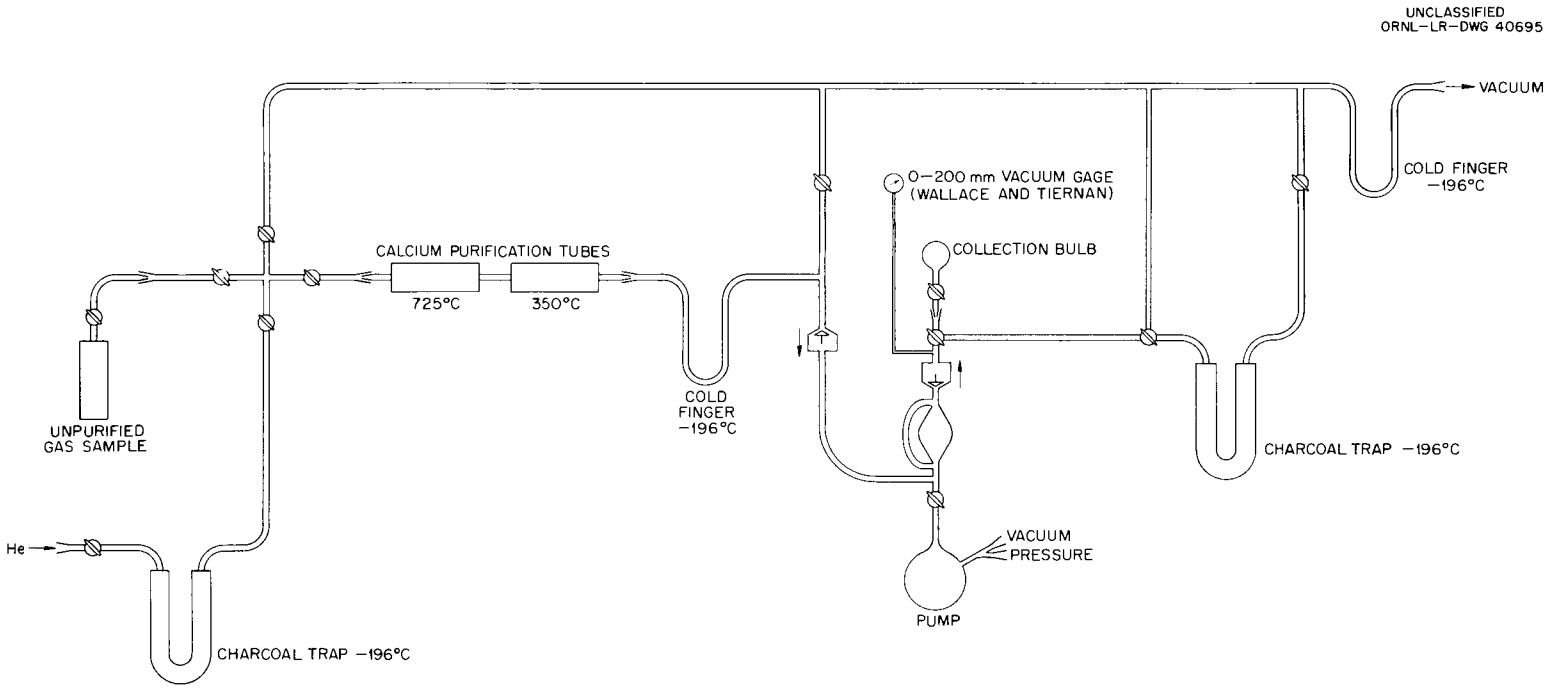

Fig. 5.5. Fission-Gas Purification and Concentration Apparatus for the Preparation of Mass Spectrometer Samples.

Table 5.4. Isotopic Abundances of Xenon and Krypton in Capsules L-6a and -6b

Isotope	Isotopic Abundance (%)	
	In L-6a	In L-6b
Kr^{83}	14.1	12.9
Kr^{84}	27.5	27.1
Kr^{85}	7.1	7.1
Kr^{86}	51.3	52.9
Xe^{131}	10.6	10.2
Xe^{132}	18.1	18.1
Xe^{134}	30.6	31.7
Xe^{136}	40.7	40.0

previously (many photomacrographs and photomicrographs have been received from GEVAL for inspection). In an effort to improve the burnup determinations, the cerium-to-uranium ratio is being investigated to be used along with the cesium-to-uranium ratio, and better sampling is being sought by crushing an entire pellet and then sampling the mixed powder.

The density measurements made in the hot cells are not yet satisfactory, and the equipment and method are being revised so that accurate density measurements may be made. Developmental work is also under way on means for obtaining oxygen-to-uranium ratios for the irradiated pellets.

Modifications of ORNL Cell 6

The contract construction phase of the cell 6 modifications has been completed. The remote cut-off machine is built, and all equipment layout design work is completed. Other cell equipment has been ready for some time. There are many small jobs remaining to be completed before the cell may be occupied, but it is planned to have the cell ready for postirradiation examinations in November 1959.

Closed-Cycle-Loop Irradiation Facility in ORR

Two coated graphite samples containing ThO_2-UO_2 fuel have been encapsulated and inserted in the B-9 facility of the ORR, and operation of the loop has been started. Two special Joy compressors were installed in the basement cubicle to replace ones which had excessive seal leakage.

Thermocouple Irradiation Studies

Further investigations of irradiation effects on platinum-platinum-10% rhodium thermocouples were carried out. It was found that the error in emf output of the irradiated thermocouples depends on the location of the thermal gradient with respect to rhodium transmutation, as well as upon the total neutron exposure.

The results for the normal method of calibration are shown in Fig. 5.6 and Fig. 5.7. A 24-in. tube furnace with 12-in. thermocouple immersion was used for postirradiation calibration. A summary of error emf's as measured at 1900°F in a 7-in. tube furnace with 3 1/2 in. immersion is presented in Fig. 5.8.

The furnace temperature gradient for the measurements presented in Fig. 5.9 occurred in a region of higher rhodium transmutation than that used in obtaining the data for Fig. 5.7. The Leeds & Northrup Co. thermocouples received a uniform high neutron dosage throughout their length, while the Sigmund Cohn & Corporation thermocouple had a comparable high dosage only near the junction. Additional Cohn thermocouples were therefore irradiated in the ORR to a dose of 4×10^{20} neutrons/cm^2 and will be calibrated when their activity has decayed to a lower level.

Radiation Effects on Structural Materials

Steels

The previous report on this study indicated specimen size effects, relation of impact transition temperature change with fast neutron dose,

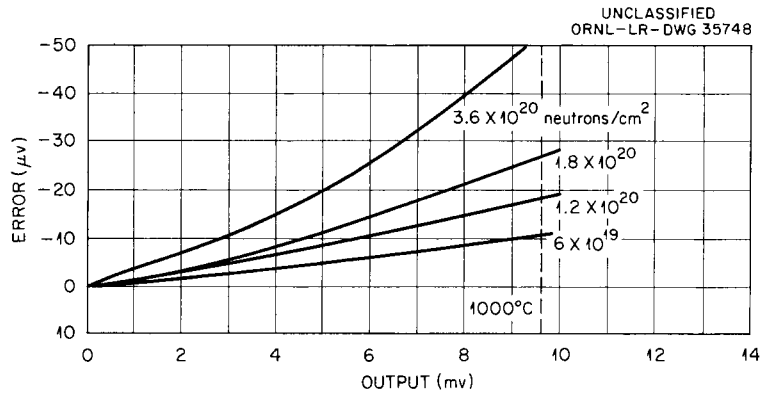

Fig. 5.6. Effect of Neutron Irradiation on Platinum–Platinum-10% Rhodium Thermocouples. J. Bishop & Company wire measured in a 24-in. tube furnace with 12-in. immersion.

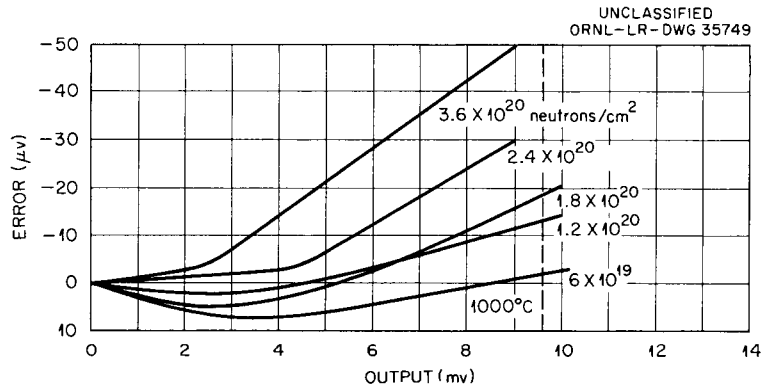

Fig. 5.7. Effect of Neutron Irradiation on Platinum–Platinum-10% Rhodium Thermocouples. Sigmund Cohn & Corporation wire measured in a 24-in. tube furnace with 12-in. immersion.

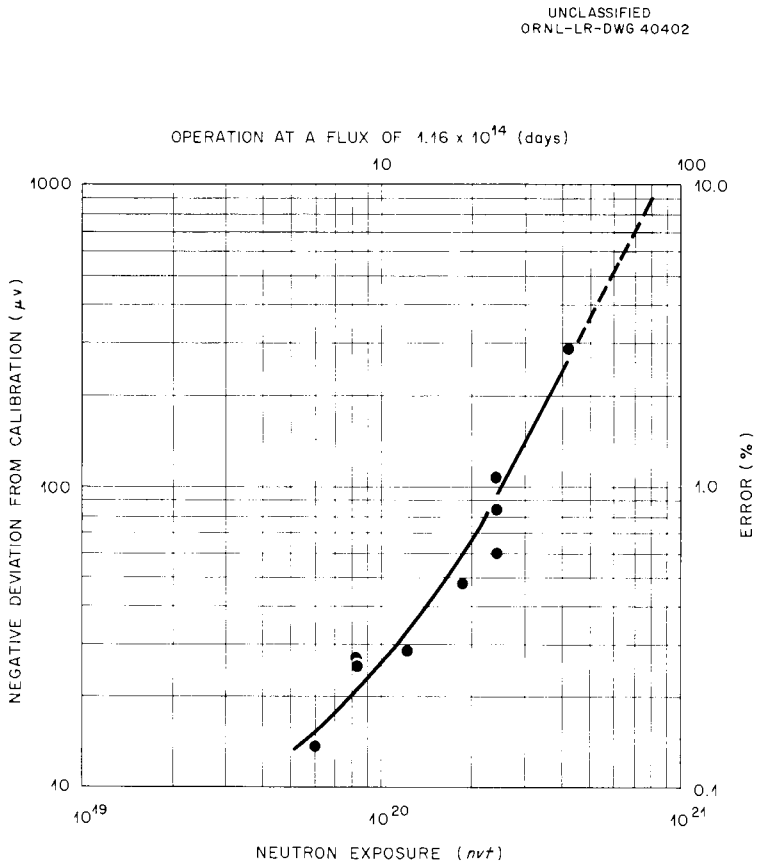

Fig. 5.8. Errors of Platinum–Platinum-10% Rhodium Thermocouples in 7-in. Tube Furnace with 3 1/2-in. Immersion at 1900°F as a Function of Neutron Exposure.

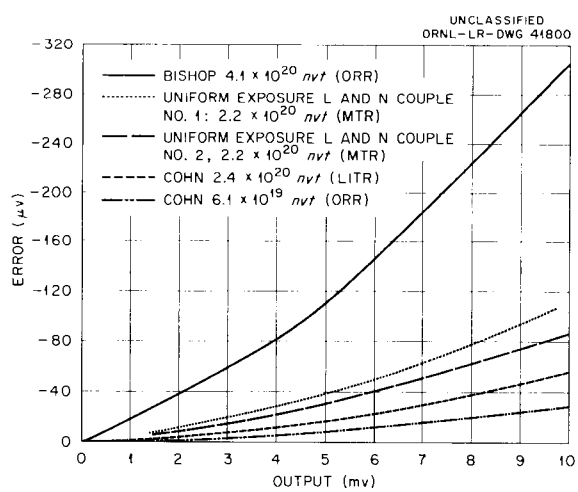

Fig. 5.9. Errors of Platinum–Platinum-10% Rhodium Thermocouples in 7-in. Tube Furnace with 3 1/2-in. Immersion as a Function of Temperature.

temperature effects, and preliminary information on postirradiation annealing.[6] Data obtained during this quarter have been reported elsewhere[7] and serve primarily to substantiate the results reported previously. The first two irradiation experiments in the ORR were completed, the apparatus has been removed, and testing of specimens is in progress. These experiments were designed to add to the information on the effects of elevated-temperature irradiation and on the kinetics of postirradiation annealing.

The comparison of the experimental results obtained in various reactors by several investigators[7] is a problem of increasing significance and difficulty. Analyses of the results obtained by the group at ORNL indicate that, although general trends in properties are being determined, greater accuracy in flux monitoring is required for future studies. Efforts are being made to improve the precision of neutron flux measurements by threshold detectors and to compare property changes in identical specimens in the various reactor experimental facilities.

The Charpy V-notch impact properties of several steels at temperatures from 175 to 330°F exposed to fast neutron doses of up to 10^{20} neutrons/cm^2 (>1 Mev) show the now familiar rise in impact transition temperature and decrease of ductile energy absorption with increasing irradiation dose.[7]

Results of the effect of elevated-temperature irradiation on the brittle fracture properties of steel have also been reported.[7] These data have substantiated the conclusion that irradiation at 575°F leads to less change than irradiation at lower temperatures and that a variation in the magnitude of the effect is found even in steels of similar types. Other data[8,9] have indicated a greater change in transition

---

[6] GCR Semiann. Prog. Rep. June 30, 1959, ORNL-2767, p 176.

[7] O. Sisman *et al.*, Solid State Div. Ann. Prog. Rep. Aug. 31, 1959, ORNL-2829 (in press).

[8] R. C. Burnett, J. M. N. Allen, and D. R. Harries, The Effects of Neutron Irradiation on the Ductile-Brittle Transition Temperatures of Weldable Structural Steel Plates, AERE-M/R-2536 (1958).

temperature for irradiations at 270 and 440°F than at 100°F. Irradiation effects in the temperature range from 200 to 500°F, on the basis of the little information available, are an undertermined function of the material, irradiation dose, and irradiation temperature, and may be either larger or smaller than the effects observed at irradiation temperatures less than 200°F, for which the largest body of data exists.

Beryllium

Beryllium is a potential cladding material for future gas-cooled reactor fuel elements. A program has been initiated, in collaboration with General Nuclear Engineering Corporation, to study the effects of irradiation on beryllium. Gas is produced in beryllium by an (n,2n) reaction resulting in two atoms of helium and an (n,α) reaction resulting in two atoms of helium and one of tritium. Experiments are planned for measuring the quantity of gas produced and the disposition of the gas at elevated temperatures. Stress-rupture experiments are also planned. Several kinds of beryllium will be studied.

---

[9]J. C. Wilson *et al.*, *Solid State Div. Ann. Prog. Rep. Aug. 31, 1958*, ORNL-2614, p 98.

6. OUT-OF-PILE TESTING OF MATERIALS AND COMPONENTS

Materials Compatibility Tests

The program of out-of-pile tests of reactor materials compatibility and the structural integrity of fuel elements was continued with the use of the test facilities described previously.[1-3] Test operation of static pot No. 12, which contained a metal specimen that was heated to 1600°F was completed. Two similar tests of metal specimens heated to 1700°F (pot No. 15) and 1800°F (pot No. 14) are under way. A low-pressure thermal-convection loop (test No. 9) has been in operation for 4000 hr of a scheduled 5000-hr period. The first high-pressure thermal-convection loop (test No. 1A) was operated for 1000 hr at 325 psig with a maximum gas temperature of approximately 1225°F. High-pressure test No. 2, scheduled for 5000 hr, and test No. 3, scheduled for 1000 hr, have completed approximately 1500 and 200 hr, respectively. Operation of the forced convection loop (test No. 2) was prematurely terminated after 145 hr because of a compressor bearing failure. The compressor used in test No. 1 has been installed in the loop and the test section is being prepared for test No. 3. The operating conditions for these tests and the results obtained during the quarter are summarized in Table 6.1. Results of earlier tests were reported previously.[2,3]

Static Helium Tests

Test assembly No. 12 operated with AGOT graphite at 1100°F and with a heated specimen temperature of 1600°F near the top and 1560°F near the bottom. Additional metal specimens were located above the

---

[1] The ORNL Gas-Cooled Reactor – Materials and Hazards, ORNL-2505, p 12, (May 22, 1958).

[2] GCR Semiann. Prog. Rep. Dec. 31, 1958, ORNL-2676, p 138.

[3] GCR Semiann. Prog. Rep. June 30, 1959, ORNL-2767, p 188.

Table 6.1. Summary of Conditions and Metallurgical Results of Materials Compatibility Tests

Test No.	Maximum Specimen Temperature (°F)	Maximum Graphite Temperature (°F)	Type of Graphite	Total Elapsed Time of Test (hr)	Maximum Observed Impurity Concentration of Gas (vol %)	Specimens Included and Metallurgical Results
				Static Pot Tests		
12	1600	1100	AGOT	1000	5.7	Stainless and low-alloy steels and Fe-Al base alloys exposed at 1100°F: Stainless steel specimens (types 304, 310, 316, and 410) showed weight gains ranging from 0.07 to 0.11 mg/cm^2. Weight gains of 0.24 to 1.6 mg/cm^2 were found on the low alloy steels; the Fe-Al base alloy specimen gained 0.05 mg/cm^2. A type 304 stainless steel assembly that was heated to 1600°F independently of the pot had a bright green surface film on the upper portion, and two removable sleeves near the bottom were dark gray.
14	1800	1100	AGOT	400	7.1	Specimens same as those in static pot test No. 12; heated section at 1800°F. Test in progress.
15	1700	1100	AGOT	150	4.0	Specimens same as those in static pot test No. 12; heated section at 1700°F. Test in progress.
				Low-Pressure Thermal-Convection Loop Tests		
8	1400	1400	AGOT	2754	19.6	Stainless and low-alloy steels and Fe-Al base alloys: Loop failed because of catastrophic oxidation of cold leg. Weight gains ranging from 0.3 to 1.0 mg/cm^2 were found on types 304, 310, 316, and 410 stainless steel specimens. Gains of 4.0 to 14.0 mg/cm^2 occurred on the low-alloy steels and 0.1 mg/cm^2 on the Fe-Al base alloy specimens. A total of 1.3 g of carbon was found deposited in a 6-in. cold-leg section.
9	1400	1400	TSF	4000	5.5	Specimens same as those in low-pressure thermal-convection loop test No. 8. Test in progress.

Table 6.1 (continued)

Test No.	Maximum Specimen Temperature (°F)	Maximum Graphite Temperature (°F)	Type of Graphite	Total Elapsed Time of Test (hr)	Maximum Observed Impurity Concentration of Gas (vol %)	Specimens Included and Metallurgical Results
				High-Pressure Thermal-Convection Loop Tests		
1A	~1225	~1225	AGOT	1000	1.5	Specimens same as those in low-pressure thermal-convection loop test No. 8. The types 304, 310, and 316 stainless steel specimens had a tightly adherent gray-green oxide film; the weight gains ranged from 0.07 to 0.15 mg/cm^2. The type 410 stainless steel specimens had a tightly adherent silvery gray oxide film, and the weight gains ranged from 0.22 to 0.29 mg/cm^2. The Fe-Al base alloy specimen showed the usual iridescent oxide film and a 0.07 mg/cm^2 weight gain. The low-alloy steels showed heavy attack in the form of a silvery gray oxide which spalled and revealed a black bulk oxide beneath the surface. In the case of one alloy specimen the black oxide also spalled. The weight gains for those specimens where spalling had not progressed significantly ranged from 0.7 to 8.0 mg/cm^2. The fuel element mockup showed an adherent gray-green oxide over all surfaces. There was no soot deposit found in loop.
2	~1225	~1225	AGOT	1500	2.6	Specimens same as those in low-pressure thermal-convection loop test No. 8. Fuel element mockup included. Test in progress.
3	1225	1225	AGOT	200		Specimens same as those in low-pressure thermal-convection test No. 8. Fuel element mockup included. Test in progress.
				Forced-Convection Loop Tests		
1	1400	1400	TSF	1000	3.3	Fuel element mockup showed a black oxide over all surfaces.
2	1400	1400	AGOT	145	8.9	Test prematurely interrupted by a compressor bearing failure.

graphite assembly and were subjected to the same temperature conditions as the graphite. The stainless steel specimens suspended in the 1100°F gas environment showed light gray surface films and relatively small weight gains. Similarly exposed low-alloy steel specimens showed somewhat larger weight gains than the stainless steels and had dark gray surface films. A Fe-Al alloy specimen showed the usual irridescent surface film and an almost negligible weight gain. The surface appearance of the type 304 stainless steel heated element assembly varied noticeably along the length of the element. The upper portion of the assembly had a bright green surface film, while two removable sleeves near the bottom were dark gray. Specimens of both types of films have been submitted for electron diffraction analysis.

Test assemblies Nos. 14 and 15, which contain AGOT graphite at 1100°F and type 304 stainless steel specimens heated to 1800°F and 1700°F, respectively, have been placed in operation. Test assembly No. 14 has operated approximately 400 hr, and test assembly 15 has operated approximately 150 hr. The heated specimens in these assemblies consist of 3/4-in.-OD, 0.020-in.-wall, type 304 stainless steel tubes 24 in. long which form the heater section of a direct-resistance heater circuit.

A summary of gas analyses obtained from these tests indicates that the temperature of the heated specimen has no appreciable effect on the gaseous impurity concentrations. A comparison of impurity concentrations for static tests with heated specimens at various temperatures is shown in Fig. 6.1.

Low-Pressure Thermal-Convection Loop Tests

The operating conditions and results of low-pressure thermal-convection loop tests Nos. 8 and 9 are presented in Table 6.1. Test No. 8, which was scheduled for 5000 hr, was interrupted after 2754 hr because of a gas leak in the loop cold leg.[2] The weight gains for the stainless steel and Fe-Al base alloy specimens tested were of the order of a fraction of a milligram per square centimeter, while the low and

medium alloy steels showed somewhat larger weight gains. All the weight gains were several times larger, however, than those found in preceding tests. Correspondingly, the total concentration of gaseous impurities, as determined from gas analyses made during the test, was considerably higher throughout test No. 8 than for any thermal-convection loop test operated previously. A comparison of the total impurity concentration found in this test with that found in test No. 6, which was run with type AGOT graphite under temperature conditions identical to those of test No. 8, is shown in Fig. 6.2. It may be seen that the impurity concentration during both tests reached a maximum shortly after the hot-leg temperature reached 1400°F, and a steady decrease in concentration occurred throughout the remainder of the test. The concentration of mass 28 components (N_2 and CO) contributed most significantly to the high impurity levels in test No. 8. The results of a mass-spectrographic analysis of a gas sample taken at the time of maximum impurity concentration are presented below:

Gas	Composition (vol %)
He	80.381
H_2	1.380
CH_4	0.195
H_2O	0.038
N_2 + CO	15.102
O_2	0.001
A	0.003
CO_2	2.900
Hydrocarbons	None
Total impurities	19.619

The data show that N_2 and CO constitute approximately 77% of the total impurities present. Several samples analyzed by gas chromatography indicate the ratio of CO to N_2 in these samples to be about 4 to 1. Thus it is indicated that the maximum CO concentration reached during this test was almost 12 vol %.

Examination of the cold leg of test assembly No. 8 showed an appreciable amount of carbon mass transfer. As much as 0.2 g of material

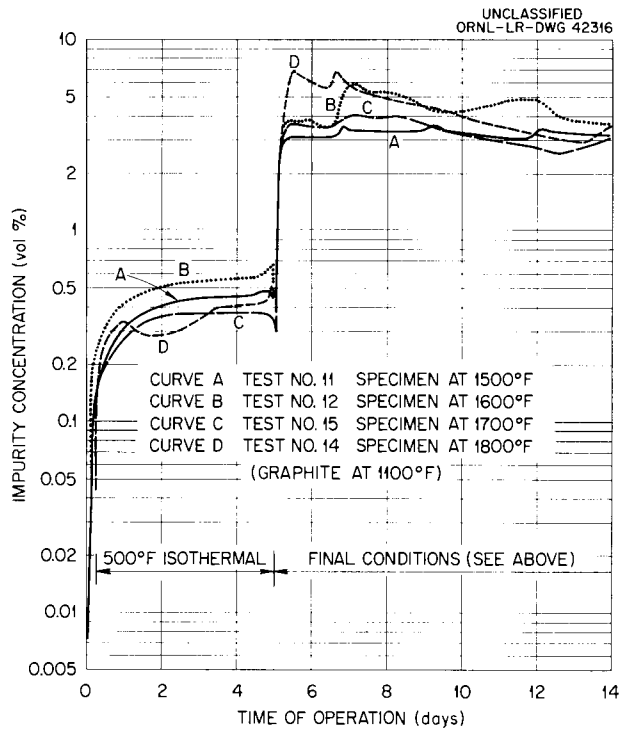

Fig. 6.1. Comparison of Total Gaseous Impurity Concentrations in Helium Used in Static Pot Tests Nos. 11, 12, 14, and 15. Test system contained type AGOT graphite, stainless and low-alloy steels, Fe-Al base alloys, and an independently heated type 304 stainless steel section.

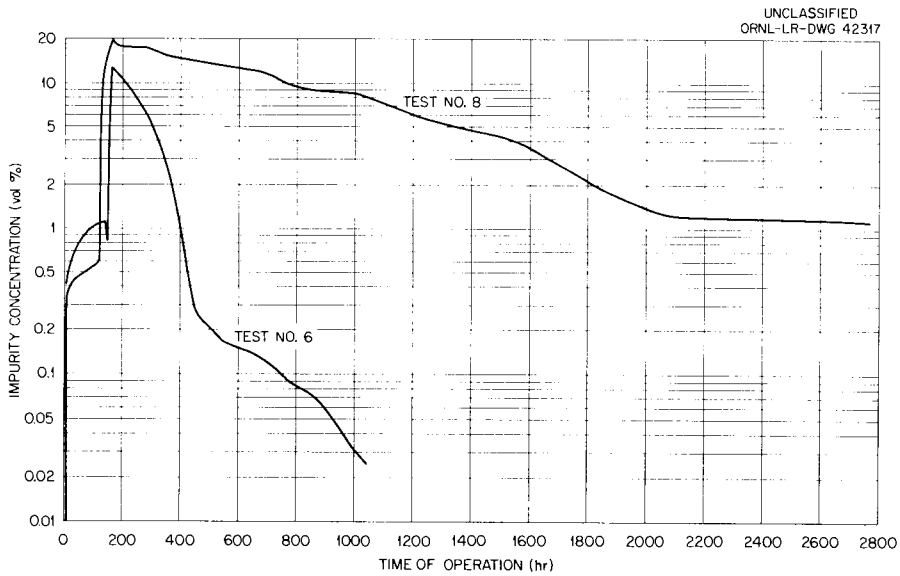

Fig. 6.2. Comparison of Total Gaseous Impurity Concentrations in Helium Used in Low-Pressure Thermal-Convection Loop Tests Nos. 6 and 8. Test system contained type AGOT graphite and metal specimens, and it operated at a maximum temperature of 1400°F.

per inch of pipe was found in some areas of the cold leg. In view of the extremely high CO concentration in proportion to CO_2, carbon deposition in the cold leg would be expected, since CO cooled in such a mixture would decompose to form CO_2 and carbon.

Test assembly No. 9, which contains TSF graphite and metal specimens at 1400°F, has completed approximately 4000 hr of a scheduled 5000-hr run. An impurity addition program which is planned for this facility is progressing on schedule. A system for continuously monitoring and adding impurities is being designed.

High-Pressure Thermal-Convection Loop Tests

Operation of the first high-pressure thermal-convection loop, described previously,[3] was terminated after 1000 hr. The system contained type AGOT graphite, and the system gas pressure was 325 psig. The intended loop hot-leg temperature was 1400°F. Unfortunately thermocouple failures prevented a direct measurement of the gas temperature, and it was necessary to establish the temperature by means of thermocouples attached to the outer wall of the hot-leg section. However, direct measurements of the maximum gas temperature in subsequent test runs under conditions identical to those of test No. 1A have indicated a hot-leg temperature of 1225°F. It has therefore been concluded that the fuel element, metal specimens, and graphite in test No. 1A were at approximately 1225°F instead of 1400°F, as originally assumed. Upon completion of tests Nos. 2 and 3, the loops will be modified in an effort to increase the fuel element and metal specimen temperatures. A summary of the results of these tests is included in Table 6.1.

The EGCR fuel element mockup contained in the loop showed an adherent gray-green oxide over all surfaces. The metal specimens in the gas stream of test 1A showed attack of a somewhat different nature than has been common in these materials compatibility tests. The type 304, 310, and 316 stainless steel specimens had tightly adherent gray-green oxide films, and the type 410 stainless steel specimen had a tightly adherent silvery gray bulk oxide coating. The Fe-Al base alloy

specimen characteristically showed a thin irridescent oxide film. However, the low-alloy steels showed heavy attack in the form of a silvery gray bulk oxide which spalled badly and revealed a black oxide layer beneath the surface. In the case of several specimens, spalling of the black oxide was also evident (see Fig. 6.3). None of these reaction films have, as yet, been identified.

Test assemblies Nos. 2 and 3, which contain type AGOT graphite and EGCR fuel element mockups, have now completed approximately 1500 and 200 hr, respectively, at conditions similar to those of test 1A.

Forced-Circulation Loop Tests

The EGCR fuel element mockup tested in the initial forced-circulation loop test (No. 1), has been removed from the system. The system operated for 1000 hr with TSF graphite at a test section temperature of 1400°F and a gas velocity of 300 fps. The mockup showed a tightly adherent black oxide over all surface.

A bearing in the gas compressor of the forced-circulation test facility[3] failed near the beginning of the second 1000-hr run (test No. 2). This was a new compressor installed for test No. 2. The compressor used in test No. 1 was subsequently reinstalled and operated for a 100-hr period to assure proper functioning. Following this qualification run, which included one thermal cycle, a leak check of the compressor and loop revealed a recurrence of a gas leak around the seals for the gas heater electrical leads. A redesigned seal has been installed, and the loop has been rechecked for leak tightness. The metal specimens and type AGOT graphite installed for test No. 2 are currently being replaced in preparation for test No. 3.

Evolution of Gases from Graphite

The experimental methods employed in the degassing of graphite and the results of the previous studies have been reported.[4] In more recent studies additional data have been collected for several of the

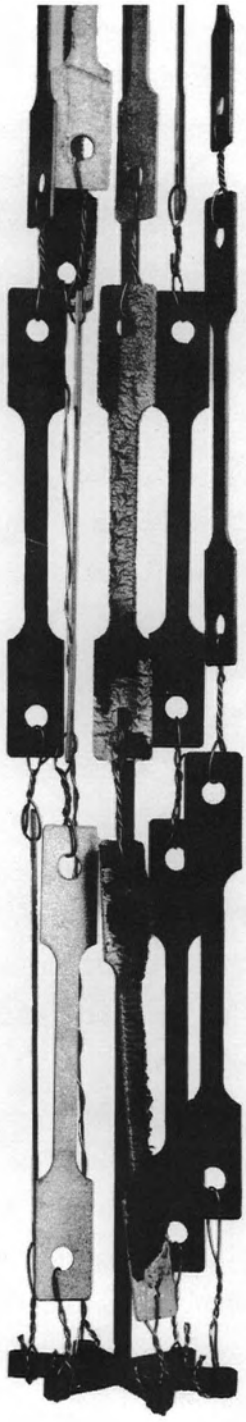

UNCLASSIFIED
PHOTO 34713

Fig. 6.3. Specimens Exposed in High-Pressure Thermal-Convection Loop Test No. 1A. Severe spalling of film on low-alloy steel specimens may be seen.

types of graphite previously examined, and, in addition, three types of graphite not previously studied have been degassed. Characterization of the various graphite specimens through ash content, porosity, surface area, and loss in weight upon degassing has been initiated.

The following specimens have not been described previously: (1) National Carbon Company Porous No. 60, having a density of 1.02–1.09 g/cm^3, that had been subjected to open indoor storage for two years; (2) Great Lakes Carbon Company H4LM, with a density of 1.60–1.65 g/cm^3, that had been stored for two years under unknown conditions; (3) Great Lakes Carbon Company H4LM reimpregnated, having a density of 1.78–1.82 g/cm^3, that had been subjected to outdoor storage for two years.

Results of the degassing studies on these specimens, as well as results of studies at temperatures up to 1000°C of Speer Moderator Nos. 1 and 2, are presented in Tables 6.2 and 6.3. Speer Moderator No. 2, which was gas purified by a proprietary process, is characterized by a low gas content. The low-density Porous No. 60 graphite, which might be expected to have a high gas content, evolved volumes of gases not much different from those found for type AGOT graphite. The Great Lakes H4LM graphite appears to be similar to the Great Lakes sample previously examined, the volumes and composition of evolved gases from the two being quite similar. The high-density reimpregnated H4LM specimen evolved considerably more gas than the plain H4LM specimen, and the relative composition of the evolved gases was also quite different. Apparently the reimpregnation process changed the relatively clean H4LM to something similar in behavior to AGOT.

The evaluation of these three types of graphite brings the total of different types of graphite studied to nine, with more than one specimen of some types of graphite having been examined. The maximum variation found in the total volume of gases evolved is approximately a factor of 3. Considering the difference in the relative composition of the gases evolved, however, the volume of $CO + CO_2$ evolved shows a somewhat larger variation.

---

[4]GCR Semiann. Prog. Rep. Dec. 31, 1958, ORNL-2676, p 147 and GCR Semiann. Prog. Rep. June 30, 1959, ORNL-2767, p 190.

Table 6.2. Volume and Composition of Gases Evolved by 1 1/2-in.-dia, 2-in. Long Specimens of Various Types of Graphite at 300, 600, and 1000°C

Type of Graphite	Temperature (°C)	Time (hr)	Gas Volume (cm^3/100 cm^3 of graphite)	Gas Constituents													
				H_2		Hydrocarbons		H_2O		CO_2		Mass 28		N_2		CO	
				vol %	cm^3	vol %	cm^3	vol %	cm^3	vol %	cm^3	vol %	cm^3	vol %	cm^3	vol %	cm^3
Speer Moderator No. 1	300	6	0.3			5		76	0.2	4		15	0.1				
	600	6.5	2.9	3.8	0.1	10	0.3	20	0.6	11	0.3	55	1.6	21	0.6	34	1.0
	600	12	1.4	3.2		5	0.1	6	0.1	9.3	0.1	76	1.1	53	0.8	23	0.3
	1000	6.75	9.4	61	5.7	2	0.2	1		1.2	0.1	34	3.2	6	0.6	28	2.6
	1000	10	3.0	55	1.6	1				0.1		43	1.3	26	0.8	17	0.5
	1000	11.5	0.8	61	0.5	1				0.2		38	0.3	24	0.2	14	0.1
	1000	15.75	1.6	50	0.8	1				0.1		49	0.8	31	0.5	18	0.3
	1000	8	0.9	51	0.5	1				0.2		47	0.5	30	0.3	17	0.2
	Total		20.3		9.2		0.6		0.9		0.5		8.9		3.8		5.0
Speer Moderator No. 1	300	3.5	0.7	1.9		9	0.1	61	0.4	6.5	0.1	18	0.1	17	0.1	1	
	600	5.25	2.8	6.0	0.2	17	0.5	23	0.6	15	0.4	38	1.1				
	600	11.75	0.9	8.4	0.1	9	0.1	8	0.1	12	0.1	62	0.6				
	1000	8.5	8.4	59	5.0	2	0.1	1	0.1	1	0.1	37	3.1	5	0.4	32	2.7
	1000	12.5	2.7	78	2.1	1						20	0.5	1		19	0.5
	Total		15.5		7.4		0.8		1.2		0.7		5.4				
Speer Moderator No. 2	300	1.5	0.3			1		27	0.1	5		67	0.2				
	600	3.5	1.9	13	0.3	27	0.5	21	0.4	9	0.2	30	0.6				
	600	64	1.6	29	0.5	27	0.5	9	0.1	1.9		33	0.5	28	0.4	5	0.1
	1000	4.25	3.2	70	2.3	3	0.1	1		0.3		26	0.8				
	1000	21	2.2	72	1.6	0.5				0.1		27	0.6	13	0.3	14	0.3
	Total		9.2		4.7		1.1		0.6		0.2		2.7				
Speer Moderator No. 2	300	6.75	0.5	1.2		5		77	0.4	4		13	0.1	9	0.1	4	
	600	7	2.2	14	0.3	24	0.5	18	0.4	14	0.3	30	0.7	4	0.1	26	0.6
	600	15	0.9	Not analyzed													
	1000	2.5	4.7	74	3.5	2	0.1	1		0.3		23	1.1	2	0.1	21	1.0
	1000	5	1.9	75	1.4	2				0.1		19	0.3	7	0.1	12	0.2
	Total		10.2		5.2		0.6		0.8		0.3		2.2		0.4		1.8

Table 6.2 (continued)

Type of Graphite	Temperature (°C)	Time (hr)	Gas Volume (cm^3/100 cm^3 of graphite)	Gas Constituents													
				H_2		Hydrocarbons		H_2O		CO_2		Mass 28		N_2		CO	
				vol %	cm^3	vol %	cm^3	vol %	cm^3	vol %	cm^3	vol %	cm^3	vol %	cm^3	vol %	cm^3
Porous No. 60	300	4.5	0.9	5.9	0.1	17	0.2	49	0.4	9	0.1	19	0.2	15	0.1	4	
	600	6.75	11.6	9.0	1.1	13	1.5	7	0.8	50	5.8	20	2.4	12	1.4	8	1.0
	600	15	2.2	53	1.2	8	0.2	1		15	0.3	24	0.5	4	0.1	20	0.4
	1000	6.25	11.8	42	5.0	2	0.2	1	0.1	1	0.1	54	6.3	1	0.1	53	6.2
	1000	17.25	3.6	52	1.9	1		1		0.2		45	1.6	8	0.3	37	1.3
	Total		30.1		9.3		2.1		1.3		6.3		11.0		2.0		8.9
Porous No. 60	300	6	0.9	2.3		1		74	0.7	6	0.1	16	0.1	15	0.1	1	
	600	9	14.8	12	1.7	16	2.3	8	1.1	48	7.1	17	2.6	3	0.5	14	2.1
	1000	6.25	14.8	47	7.0	3	0.4	1	0.1	1	0.1	48	7.1	1	0.1	47	7.0
	1000	6.25	3.0	60	1.8	4	0.1			0.1		36	1.1	2	0.1	34	1.0
	Total		33.5		10.5		2.8		1.9		7.3		10.9		0.8		10.1
Great Lakes H4LM	300	5.5	0.6	1.8		5		71	0.4	5		16	0.1	11	0.1	5	
	300	17	0.16	Not analyzed													
	600	7.25	3.4	16	0.6	37	1.2	17	0.6	7	0.2	23	0.7	4	0.1	19	0.6
	600	10.75	0.5	Not analyzed													
	1000	6	8.1	74	6.0	5	0.4	5	0.4	1	0.1	15	1.2	3	0.2	12	1.0
	1000	15.5	2.5	89	2.2	1				0.1		10	0.3	1		9	0.3
	Total		15.3		8.8		1.6		1.4		0.3		2.3		0.4		1.9
Great Lakes H4LM	300	5.25	0.6	4		5		73	0.4	5		13	0.1	9	0.1	4	
	600	9	3.3	16	0.5	30	1.0	23	0.8	9	0.3	22	0.7	7	0.2	15	0.5
	1000	11.5	10.3	81	8.3	4	0.4			1	0.1	14	1.4				
	Total		14.2		8.8		1.4		1.2		0.4		2.2				
Great Lakes H4LM reimpregnated	300	4.25	0.8	3.8		2		73	0.6	14	0.1	7	0.1	5		2	
	600	6.25	7.5	7.8	0.6	9	0.6	5	0.4	39	2.9	39	2.9				
	600	11.5	2.8	Not analyzed													
	1000	9.75	7.7	19	1.4	0.5		0.6		0.5		79	6.0	12	0.9	67	5.1
	1000	12.5	3.0	58	1.7	24	0.7	1		0.2		18	0.5	3	0.1	15	0.4
	Total		21.8		3.7		1.3		1.0		3.0		9.5				

Table 6.2 (continued)

Type of Graphite	Temperature (°C)	Time (hr)	Gas Volume (cm^3/100 cm^3 of graphite)	Gas Constituents													
				H_2		Hydrocarbons		H_2O		CO_2		Mass 28		N_2		CO	
				vol %	cm^3	vol %	cm^3	vol %	cm^3	vol %	cm^3	vol %	cm^3	vol %	cm^3	vol %	cm^3
Great Lakes H4LM reimpregnated	300	5.25	1.0	2.2		4		66	0.7	15	0.2	13	0.1	7	0.1	6	0.1
	300	6	0.2	Not analyzed													
	600	10	19.4	7.3	1.4	9	1.6	3	0.6	69	13.4	12	2.3	2	0.3	10	2.0
	600	5	1.0	Not analyzed													
	1000	8.25	15.1	40	6.0	4	0.6	1	0.1	2	0.3	54	8.1	4	0.6	50	7.5
	1000	9	3.0	58	1.7	2		1				40	1.2	6	0.2	34	1.0
	Total		39.7		9.1		2.2		1.4		13.9		11.7		1.2		10.6
Great Lakes H4LM reimpregnated	300	6.75	0.9	1.5		2		70	0.7	14	0.1	13	0.1				
	600	6.25	10.1	8.5	0.9	9	0.9	14	1.5	50	5.1	18	1.8	8	0.8	10	1.0
	600	10.5	2.1	22	0.5	5	0.1	5	0.1	50	1.0	18	0.4	3	0.1	15	0.3
	1000	5.25	11.6	27	3.1	4	0.4			2.2	0.3	64	7.4				
	1000	15.5	4.7	78	3.6	2	0.1					20	1.0	2	0.1	18	0.9
	Total		29.4		8.1		1.5		2.3		6.5		10.7				

Table 6.3. Volume and Composition of Gases Evolved by 1 1/4-in.-dia, 2-in. Long Specimens of Various Types of Graphite in the Temperature Range 1000–1800°C

Type of Graphite	Temperature (°C)	Time (hr)	Gas Volume (cm^3/100 cm^3 of graphite)	Gas Constituents													
				H_2		Hydrocarbons		H_2O		CO_2		Mass 28		N_2		CO	
				vol %	cm^3	vol %	cm^3	vol %	cm^3	vol %	cm^3	vol %	cm^3	vol %	cm^3	vol %	cm^3
Porous No. 60	1000	2	48.7	36	17.4	5	2.3	0.7	0.3	3.7	1.8	55	26.8	1.4	0.7	54	26
	1400	2.25	5.6	11	0.6	0.3		0.8		0.6		87	4.9	33	1.9	54	3
	1800	1	1.0	58	0.6							42	0.4	27	0.3	15	0.2
	Total		55.3		18.6		2.3		0.3		1.8		32.1		2.9		29.2
Porous No. 60	1000	3	51.5	38	19.6	1.6	0.9	5	2.6	2.6	1.3	52	26.6	1.2	0.6	51	26
	1400	2	3.0	15	0.4							85	2.6	39	1.2	46	1.4
	1800	1.75	1.5	67	1.0	0.5						33	0.5	29	0.4	4	0.1
	Total		56.0		21.0		0.9		2.6		1.3		29.7		2.2		27.5
Great Lakes H4LM	1000	2.75	22.8	48	10.9	0.5	0.1	4.2	0.9	0.3	0.1	47	10.7	2	0.5	45	10.2
	1400	5.25	9.5	61	5.8	0.7	0.1			0.4		36	3.4	2	0.2	34	3.2
	1800	1.5	3.2	27	0.9							73	2.3	11	0.3	62	2.0
	1800	2.0	1.1	Not analyzed													
	Total		36.6		17.6		0.2		0.9		0.1		16.4		1.0		15.4
Great Lakes H4LM	1000	2	17.7	82	14.5	1	0.2			0.6	0.1	17	2.9	2	0.3	15	2.6
	1400	5.5	6.9	63	4.3	0.3				0.3		37	2.5	3	0.2	34	2.3
	1800	1.5	2.3	21	0.5	0.2				0.1		78	1.8	12	0.3	66	1.5
	1800	1.75	0.8	Not analyzed													
	Total		27.7		19.3		0.2				0.1		7.2		0.8		6.4
Great Lakes H4LM reimpregnated	1000	1.25	57.2	22	12.6	0.4	0.2	3.7	2.1	2.7	1.5	71	40.8	1	0.6	70	40.2
	1000	1.5	4.5	Not analyzed													
	1400	4.0	10.0	44	4.5	0.7	0.1			0.3		54	5.4	5	0.5	49	4.9
	1800	2.75	6.6	81	5.4	0.3						17	1.1	13	0.9	4	0.2
	Total		78.3		22.5		0.3		2.1		1.5		47.3		2.0		45.3

Table 6.3 (continued)

Type of Graphite	Temperature (°C)	Time (hr)	Gas Volume (cm^3/100 cm^3 of graphite)	Gas Constituents													
				H_2		Hydrocarbons		H_2O		CO_2		Mass 28		N_2		CO	
				vol %	cm^3	vol %	cm^3	vol %	cm^3	vol %	cm^3	vol %	cm^3	vol %	cm^3	vol %	cm^3
Great Lakes H4LM reimpregnated	1000	2.75	41.8	46	19.0	2.4	1.0	1.3	0.5	1.4	0.6	49	20.6	2	0.9	47	19.7
	1000	1.0	2.9	Not analyzed													
	1400	5.25	12.1	22	2.7	1.2	0.1	0.9	0.1	0.7	0.1	75	9.1	5	0.6	70	8.5
	1800	1.5	4.1	63	2.6	1.7	0.1					35	1.4	15	0.6	20	0.8
	1800	2.25	1.8	67	1.2	0.8						32	0.6	10	0.2	22	0.4
	Total		62.7		25.5		1.2		0.6		0.7		31.7		2.3		29.4
Great Lakes H4LM reimpregnated	1000	4.75	63.2	50	31.6	1.2	0.8	1	0.6	2.2	1.4	46	28.9	1	0.6	45	28.3
	1400	3.5	10.3	23	2.4	0.9	0.1			0.1		75	7.7	12	1.2	63	6.5
	1800	3.25	9.2	67	6.2	0.6				0.1		32	2.9	19	1.7	13	1.2
	Total		82.7		40.2		0.9		0.6		1.4		39.5		3.5		36.0

It is believed that with the data available for the several gas purified and thermally purified types of graphite from several sources, the volumes and composition of the gases evolved at various temperatures can be predicted with a fair degree of certainty for commercially available graphite. Special materials, such as high-density and/or low-permeability graphite would, however, have to be examined experimentally to determine degassing behavior.

Characterization of the various types of graphite through ash content (also analyses for impurities), surface area, porosity, permeability, and loss of weight upon degassing has been initiated. Aside from ash content and the loss in weight on degassing, it is not expected that any correlation between these properties and the volume of gas released will be found. A few runs have been made to establish what effect the degassing has on porosity. Preliminary results show little, if any, change in the porosity of AGOT-III when degassed at 1000°C. Specimens are being degassed at 1800°C for porosity determinations. The losses in weight of a number of specimens of various types of graphite have been determined in connection with the degassing studies. The results are given in Table 6.4. Specimens 1 1/4 × 1 in. were subjected to a maximum degassing temperature of 1800–2000°C by induction heating, whereas the 1 1/2 × 2 in. specimens were degassed at a top temperature of 1000°C, using external resistance heating. The first four types of graphite listed in Table 6.4 evolve considerably more gas than the others. There appears to be some correlation between the weight loss and the volume of gas evolved, with the first four types of graphite showing larger weight losses at both 1000°C and 1800–2000°C. The weight losses are, in general, less at the lower temperature. Inconsistencies are apparent, and a rough correlation is all that is possible.

No systematic study of evolution rates has been made during the quarter, although data have been collected as a byproduct of the degassing studies. The rate of evolution is known to be strongly dependent upon both the temperature and the partial pressures of the gases over the specimen. Some revisions are to be made in the equipment to

Table 6.4. Losses in Weight Produced by Degassing of Various Graphite Specimens

Type of Graphite	Loss in Weight (wt %)	
	1 1/4 × 1 in. Specimen Degassed at 1800–2000°C	1 1/2 × 2 in. Specimen Degassed at 1000°C
AGOT-II	0.07	
AGOT-III	0.2 0.2	0.04 0.02
Porous No. 60	0.2 0.1	0.04 0.04
H4LM impregnated	0.1 0.1	0.03 0.02
TSF-II	0.07 0.03	0.02 0.02
TSF-III	<0.001 0.01	
H4LM	0.04 0.02	0.006 0.005
Speer Moderator No. 1	0.004 0.04	0.01 0.007
Speer Moderator No. 2	0.003 0.03	0.005 0.007

permit better control of the partial pressures of the cover gases, and, if these modifications are satisfactory, rate studies will be performed on selected types of graphite.

Transport of Gases Through Graphite

Removal of the fission-product krypton and xenon diffusing from unclad fuel elements by purging with a "sidestream" of the coolant helium through an annulus between the fuel element and a graphite sleeve has been proposed. Evaluation of such proposals requires knowledge of the process by which krypton and xenon diffuse "upstream" in helium flowing through the graphite sleeve under a driving force consisting of a differential pressure. Apparatus for study of these flow processes has been constructed and given very preliminary testing. It will first be used to determine the effective diffusion coefficients of argon, for example, by streaming helium past one face of a graphite system and a dilute solution of argon in helium past the other face at the same total pressure. An untested relationship between the variables of interest has been proposed by Carman.[5]

Viscous flow experiments, in which the rate is proportional to the pressure gradient, are necessary adjuncts to the study of true diffusional flow of gases through such media. Parameters to be determined from viscous flow measurements include pore diameters, molecular slippage of gas at the graphite interface, and the tortuosity factor. Values for porosity of the graphite are also required if diffusion behavior is to be evaluated.

A basic property of graphite from the standpoint of gas-cooled reactor applications is its volumetric capacity to hold gases within interconnected voids. This property is frequently referred to as the open-pore porosity and is defined as 100 [1 - (fraction of solid material + enclosed voids)]. Porosity data have been of particular value

---

[5]P. C. Carman, Flow of Gases Through Porous Media, p 79, Butterworths Scientific Publications, London, 1956.

in previous investigations as a parameter for correlating data on gaseous diffusion rates in graphite.[5,6] Accordingly, the open-pore porosities of several reactor-grade graphite specimens have been determined by means of a well-established procedure[7] wherein helium is utilized as the test fluid. It appears that the reproducibility of the method is ±3% based on repeat determinations performed on different days. The possibility of porosity variations due to sampling position and outgassing procedures was studied.

The open-pore porosity and total porosity values for the several specimens tested are listed in Table 6.5. The total porosity is defined as 100 [1 - (w/2.25V)], where w is the sample weight in grams, V is the sample volume in cubic centimeters, and 2.25 is the theoretical density of graphite in grams per cubic centimeter. Specimens were taken in each case from different portions of large blocks of each type of graphite. The porosity remained, in general, independent of sample position, but for Speer Moderator No. 2 and for TSF-II and -III variations of 4 to 6% were observed.

The change in porosity of two specimens of AGOT upon outgassing at elevated temperatures is shown in Table 6.6. Outgassing at 1000°C resulted in a marginal 1–3% porosity increase over that of the control specimen. No additional effect was observed for the single sample given an additional heat treatment at 1800°C.

Purification of Cooling Gas

Methods of removing impurities, including fission gases, from coolant gases of gas-cooled reactors are being investigated. In the case of removal of short-lived fission gases by adsorbents, such as

---

[6]H. L. Weissberg and A. S. Berman, Diffusion of Radioactive Gases Through Power Reactor Graphite, ORGDP-KL-413 (April 6, 1959).

[7]C. G. Rall, H. C. Hamontre, and D. B. Taliferro, Determination of Porosity by a Bureau of Mines Method: A List of Porosities of Oil Sands, Bureau of Mines Report of Investigations 5025, July 1953.

Table 6.5. Porosity of Reactor Grade Graphites

Graphite Type	Open-Pore Porosity (%)		Total Porosity (%)
	Experimental*	Mean	
AGOT-II	20.2 19.8 19.9	20.0	24.1
AGOT-III	22.0 22.1 22.2	22.1	25.7
Speer Moderator No. 1	17.6 17.8 17.8 18.1	17.8	23.2
Speer Moderator No. 2	20.4 20.2 18.9 21.0 20.9	20.6	29.4
Great Lakes H4LM	20.6 20.9 21.4	21.0	24.6
TSF-II	26.8 25.7 25.7 26.3 24.2 26.7 28.4	25.9	28.4
TSF-III	19.0 18.1 20.1	19.1	25.1

*Each value represents average of three determinations.

Table 6.6. Open-Pore Porosities of Type AGOT Graphite Samples Before and After Outgassing

Sample	Open-Pore Porosity (% of total volume)		
	As Received	After Outgassing	
		At 1000°C	At 1800°C
A	22.0	22.7	22.6
B*	22.2 22.4 22.4		
C	22.2	22.7	

*This specimen served as a control. It was not outgassed but its porosity was determined each time determinations were made on specimens A and C.

charcoal, which is highly useful for this purpose in certain applications, the thermal conductivity of the adsorbent and carrier gas combination is of considerable importance in adsorber design. This is because the design must provide for dissipation of the heat produced in the adsorbent by radioactive decay of fission gases. Consequently, measurements of thermal conductivity have been made for Columbia G activated carbon, 8/14, by both a direct and by an indirect method. In the indirect method, heat generation in the charcoal resulting from radioactive decay is simulated by resistance heating of the charcoal. Also, in effect, krypton retention times are used to evaluate temperature profiles in the charcoal. Then, by assuming uniform heat generation, values of thermal conductivity are calculated. This method probably yields low values for traps of small diameter, since the effect of the wall on packing probably results in a disproportionately high amount of heat being generated in the central zone of the charcoal. With oxygen as the carrier gas and with traps having inside diameters of 0.64, 1.03, and 2.29 in., thermal conductivities of 0.06, 0.07, and

0.08 Btu/hr·ft^2(°F/ft), respectively, were obtained. The corresponding values were 0.12, 0.13, and 0.15 Btu/hr·ft^2(°F/ft) with helium carrier gas.

In the direct method, the Columbia G charcoal was contained in the annular space between copper or aluminum pipes with the ends well insulated. Known quantities of heat were applied to the inside pipe and temperatures of both pipes were measured to provide, together with the pipe dimensions, the necessary information for calculating the thermal conductivities. The results obtained, for a variety of carrier gases, are shown as a function of the thermal conductivities of the pure gases in Fig. 6.4. A comparison of curve 1 with curve 2 indicates that the wall effect is probably applicable with regard to thermal conductivity, as well as electrical conductivity, as would be expected. Furthermore, all the results obtained by the two different methods appear reasonably compatible when wall effects are considered.

Retention of krypton and xenon by Linde molecular sieves has been measured at room temperature with helium as the carrier gas. Molecular sieve type 5A was observed to be the most effective, with types 10X and 13X being about equal in this respect. This behavior was similar to that observed previously for krypton with oxygen as the carrier gas. Sieve type 4A was not tested because the previous work showed that its pores were too small to admit appreciable amounts of krypton or, therefore, xenon.

Measurement of High Temperatures

Attachment of Thermocouples for Measurement of Surface Temperatures in High-Velocity Cooling Gas

When the surface temperatures of the fuel elements in a gas-cooled reactor are measured by thermocouples attached to the surface, it is necessary to correct for the cooling effects of the gas stream on the temperature of the thermocouple. The magnitude and reproducibility of the correction depend upon details of the thermocouple fabrication

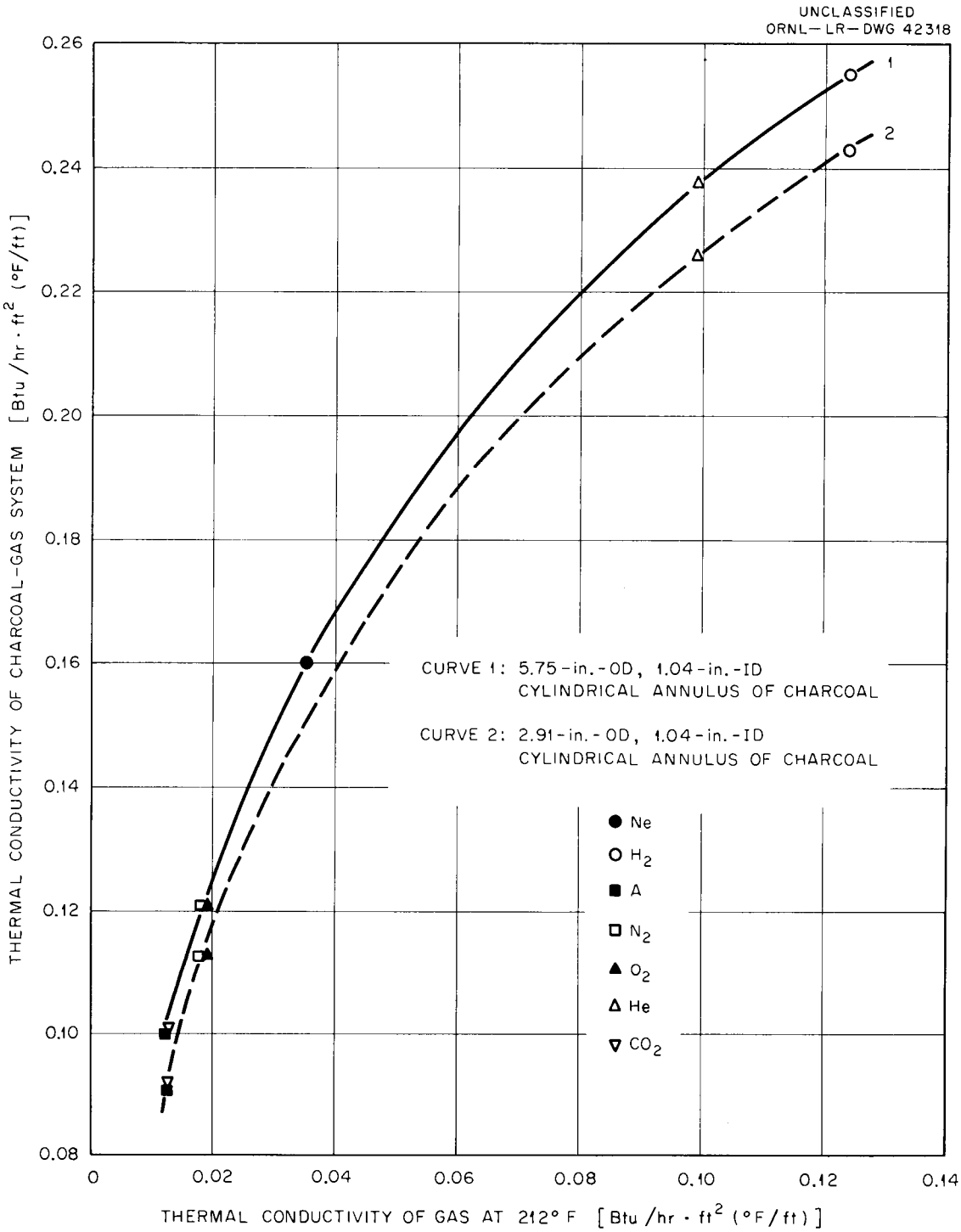

Fig. 6.4. Thermal Conductivity of Columbia G Activated Carbon-Gas Systems.

operation which influence the shape of the thermocouple in the vicinity of its effective junction and the location and distribution of that junction. A previous study of the relationship between fabrication technique and thermocouple performance has been reported.[8] The magnitude of the thermocouple correction also depends upon the factors which affect heat transfer in the vicinity of the thermocouple, such as the heat flux through the gas-metal surface, the cooling annulus thickness, gas velocity, identity of cooling gas, gas temperature relative to surface temperature, and obstructions in the coolant channel by the thermocouple and lead wire. An experimental investigation is being made of the effects of these factors on the thermocouple correction.

Experimental measurements of the thermocouple cooling correction are made using a metal tube simulating a fuel element electrically resistance heated and cooled by gas flowing over the metal tube through an annular space, the outer boundary of which is defined by a quartz tube, which also serves as an observation window for an optical pyrometer. The temperature indicated by thermocouples attached to the heated metal surface is compared with the corresponding temperature obtained by observation of the metal surface at the thermocouple, using the optical pyrometer. The heated test specimen is short enough that only a small temperature rise occurs in the cooling gas. Entrance and exit temperatures and pressures of the gas are observed so that the fluid system may be adequately described. Tests have been run with air and with helium as the cooling gas at pressures varying from 15–75 psia with gas annulus thicknesses of 0.050 and 0.0875 in. The heating element was 0.1875 in. diameter and 1 in. long. The heating power was varied from 60–600 watts. Preliminary analyses of the results of these tests indicate that the necessary temperature correction for gas cooling of the thermocouple at constant heat flux and temperature is relatively independent of gas pressure but that it depends upon the identity of

---

[8] W. E. Browning and H. L. Hemphill, ANP Quar. Prog. Rep. March 10, 1955, ORNL-1864, p 146 (classified).

the coolant gas and thickness of the coolant channel. Greater corrections are required for thermocouples in air than in helium. Thermocouples used in a larger coolant channel require greater corrections. The thermocouple correction in general increases with heat flux. The thermocouple corrections range from 10 to 100°C at 800°C for the conditions tested. Calculations are being made of the heat transfer conditions at the thermocouple during these tests in order to separate and identify the specific factors which define thermocouple performance in a coolant gas stream.

Stability of Rhenium-Tungsten Thermocouples

Tests have been conducted on rhenium-tungsten thermocouples at temperatures ranging from 1500–2000°C (2700–3600°F) to determine the stability of these thermocouples and to develop experience with thermocouple materials and other materials of construction needed for in-pile thermocouple tests in the 1500–3000°F (2700–5400°F) temperature range.

A small resistance-tube furnace has been developed and put into operation. This furnace consists of a thin tube of a refractory metal, such as tantalum, electrically heated in a helium atmosphere with provision for inserting thermocouples within the tube in such a way that the temperature of the thermocouple may be determined with optical pyrometer viewing through a quartz window. This furnace has been operated for periods up to several days at 2000°C (3632°F) and for shorter periods as high as 2600°C (4712°F). Using this furnace, rhenium-tungsten thermocouples showed a change in calibration curves after operating periods of 29 hr at 1900°C (3452°F). This effect is being investigated further. Thermal cycling to room temperature and to intermediate temperatures produced no significant change in thermocouple calibration curves. The calibration curves obtained were consistent with those reported by Lachman.[9] These tests will be continued for

[9]J. C. Lachman, Calibration of Rhenium-Tungsten Thermocouples, APEX-365 (April 30, 1958).

longer times and at higher temperatures and will culminate in similar in-pile tests.

Chromel-Alumel Thermocouple Drift Problem

Data obtained by the Instrument Division have shown Chromel-Alumel thermocouples to be unstable under certain exposure conditions. Errors as great as -70°C were noted after exposure for 24 hr at 1040°C in stagnant air in a tube containing chromium powder. Fresh Inconel filings caused rather large errors also. Exposures in stagnant helium atmospheres showed smaller errors, the largest (-33°C) being noted in a couple exposed to fresh Refrasil tape.

Data accumulated during the past quarter show relatively small drifts in stagnant air, flowing air, and flowing helium, with exposure of the thermocouple to the following materials at 1000°C: Inconel filings, oxidized Inconel filings, chromium filings, and fresh and prebaked Refrasil tape. After exposure in flowing air at 1000°C for 120 hr, all thermocouple readings were within 1% of the reference thermocouple reading. In stagnant air the thermocouple emf's drifted negatively, and errors as great as 3% were noted after 120 hr at 1000°C. Drifts were relatively minor in flowing helium. All thermocouples measured within 1.5% of the reference thermocouple after 120 hr at 1000°C. The recent experiments have all been carried out using tight-fitting ceramic insulators around the thermocouple wires extending from the bead to the outside of the furnace. Under such conditions, contamination of the thermocouple wires in the thermal gradients is unlikely, and any drifts should be small.

Experimentation is under way to determine the reproducibility and statistical significance of the data. Further thermocouple exposures will be made with broken insulators to allow contamination of the wires in thermal-gradient regions.

Theoretical Effects of Transmutation on Thermocouples

Calculations are being continued of the amount of various

impurities produced in thermocouple materials by transmutation reactions under various conditions of neutron flux and duration of exposure. The results of these calculations will be used to predict the relative sensitivity of various thermocouple materials to radiation under various conditions of exposure and will be used to interpret the results of the in-pile experiments on thermocouples.

Automatic Continuous Analysis of Helium from Test Loops

In order to maintain the desired control of the concentration of impurities in the atmosphere of the low-pressure thermal-convection loop for testing materials compatibility, continuous monitoring of the following constituents of the helium stream is required:

Impurity	Concentration Range (vol%)
H_2O	0.001–1.0
H_2	0.1–10
CO	0.01–10
CO_2	0.01–10
N_2	0.01–1
O_2	0.01–1

A system to provide automatic determination of each contaminant has been designed in which the concentration of water is continuously determined with a Consolidated Electrodynamics Corp. moisture monitor by measuring the current consumed by the quantitative electrolysis of the water which is absorbed by anhydrous phosphorous pentoxide from a sample gas stream at a flow rate of 20 cm^3/min. The remaining contaminants are determined by means of a Greenbrier Chromamatic-112 dual-column gas chromatograph that can be programmed to analyze a dry gas stream at intervals from 20 min to 1 hr.

At preselected intervals a reproducible volume of the sample gas is injected into a stream of helium carrier gas which is directed through two columns packed with activated silica gel and Linde molecular sieve,

type 5-A, respectively, and then through a thermal-conductivity detector equipped with thermistor elements. The silica-gel column serves to separate CO_2; the molecular sieve column fractionates the other gases in the following order: H_2, O_2, N_2, CH_4, and CO. When these lighter constituents have entered the molecular sieve column, a dual-column valve is actuated to isolate this column and route CO_2 directly to the detector. As soon as the CO_2 has been eluted, the dual-column valve is returned to its original position, and the components absorbed on the molecular sieve column are eluted and measured. By using this technique, each contaminant is absolutely isolated, except oxygen, which will be accompanied by any argon that may be present. Except for hydrogen, which can be detected down to concentrations of only 1000 ppm, the limit of detection of the contaminants is expected to be less than 50 ppm.

A stepless attenuator which can be adjusted to record data in terms of percentage or other appropriate concentration units in either bar-graph or spectrum form is provided for each of the six components. A programed timer is also provided to perform all functions in proper sequence, for example, balancing of the thermal-conductivity bridge, actuation of sampling and dual-column valves, and selection of attenuator circuits so that the instrument can be operated unattended.

Design of the sampling system is complete and installation is in progress. The moisture monitors have been delivered and are being calibrated. Delivery of the gas chromatograph is expected during the last week of September. Following application engineering, including selection and installation of appropriate columns and setting of programing circuits, the system is expected to be in operation early in October. At a later date, an ionization detector will be installed to provide increased sensitivity, particularly for hydrogen, and a means to distinguish between oxygen and argon.

7. DEVELOPMENT OF TEST LOOPS AND COMPONENTS

ORR Gas-Cooled In-Pile Loops

Design work on a gas-cooled loop for experimental evaluation of clad fuel elements was completed. The loop, which was described previously,[1] is now designated GCR-ORR loop No. 1. Design work has been initiated on GCR-ORR loop No. 2, in which the fission product technology and performance of unclad fuel elements can be investigated.

GCR-ORR Loop No. 1

The detailed design of all loop No. 1 components was completed, and fabrication was initiated. Instrumentation and control layouts were completed, instruments were ordered, and detailed panel and wiring design work was initiated. Installation design and site preparation work were started. Tests to assure adequate performance of the heater and cooler were completed,[2] as were tests for the selection of suitable insulation and determination of heat losses to the environment.[3]

Fabrication was initiated on a test apparatus in which to calibrate thermocouples for measuring surface temperatures of fuel element cladding under prototype conditions of temperature, pressure, and flow, in helium. Performance tests of the prototype heater and cooler will also be made in the thermocouple-calibration loop.

An underwater checkout test was planned in which to prove the operation of the fuel element transfer mechanism. A facility was prepared in which to perform this work. The loop in-pile section and fuel element transfer station will be installed and tested when fabrication of these components is complete. Tests will be conducted with a dummy

---

[1] GCR Semiann. Prog. Rep. June 30, 1959, ORNL-2767, p 205.

[2] W. H. Kelley, Jr. and E. Storto, Test of Heater and Cooler Concepts for GCR-ORR Loop, Design 4, ORNL CF 59-7-31, July 31, 1959.

[3] R. B. Knight and R. E. Helms, Determination of Suitable Insulation for a 1-5/16" Helium Filled Annulus in the ORR Helium In-Pile Loop, Design No. 4, ORNL CF-59-8-57, Aug. 17, 1959.

element and with helium at prototype pressure (400 psig). Construction of a compressor test facility, and procurement of loop compressors, drive equipment, and controls were initiated.

The loop arrangement in the ORR and a schematic diagram of the test section are presented in Figs. 7.1 and 7.2, respectively. The loop is being fabricated of type 304 stainless steel, throughout, and the design specifies concentric-tube construction. The pressure wall (see Fig. 7.2) will be exposed externally to the reactor ambient temperature, and it will be protected internally by a thermal barrier consisting of an insulation-filled annulus. Temperature profiles of the coolant gas stream are indicated in Fig. 7.3 for maximum gas temperatures of 1500, 1300, and 1000°F. The maximum fuel element cladding temperature will be 1800°F; the pressure in the test section will be maintained at 400 psig, and the mixed mean temperature of the gas will be 300°F below the maximum cladding temperature at all temperature levels of operation. The loop is scheduled to be installed and ready for startup by August 1, 1960.

GCR-ORR Loop No. 2

The use of unclad or ceramic-clad fuel elements capable of operation with high surface temperatures (1800°F and above) has been considered as a means of improving the efficiency of gas-cooled reactor cycles.[4] Little information is available, however, on the release and deposition of fission products from such unclad fuel elements and on the activity to be expected in the primary coolant stream under reactor operating conditions. Therefore GCR-ORR loop No. 2 is being designed as an experimental facility for the development of unclad fuel element technology. The loop consists of a circulating gas flow system in which representative unclad fuel elements or clusters may be exposed to radiation under simulated reactor operating conditions. The loop will

[4]W. B. Cottrell et al., The HGCR-1, A Design Study of a Nuclear Power Station Employing a High-Temperature Gas-Cooled Reactor with Graphite-UO_2 Fuel Elements, ORNL-2653 (July 14, 1959).

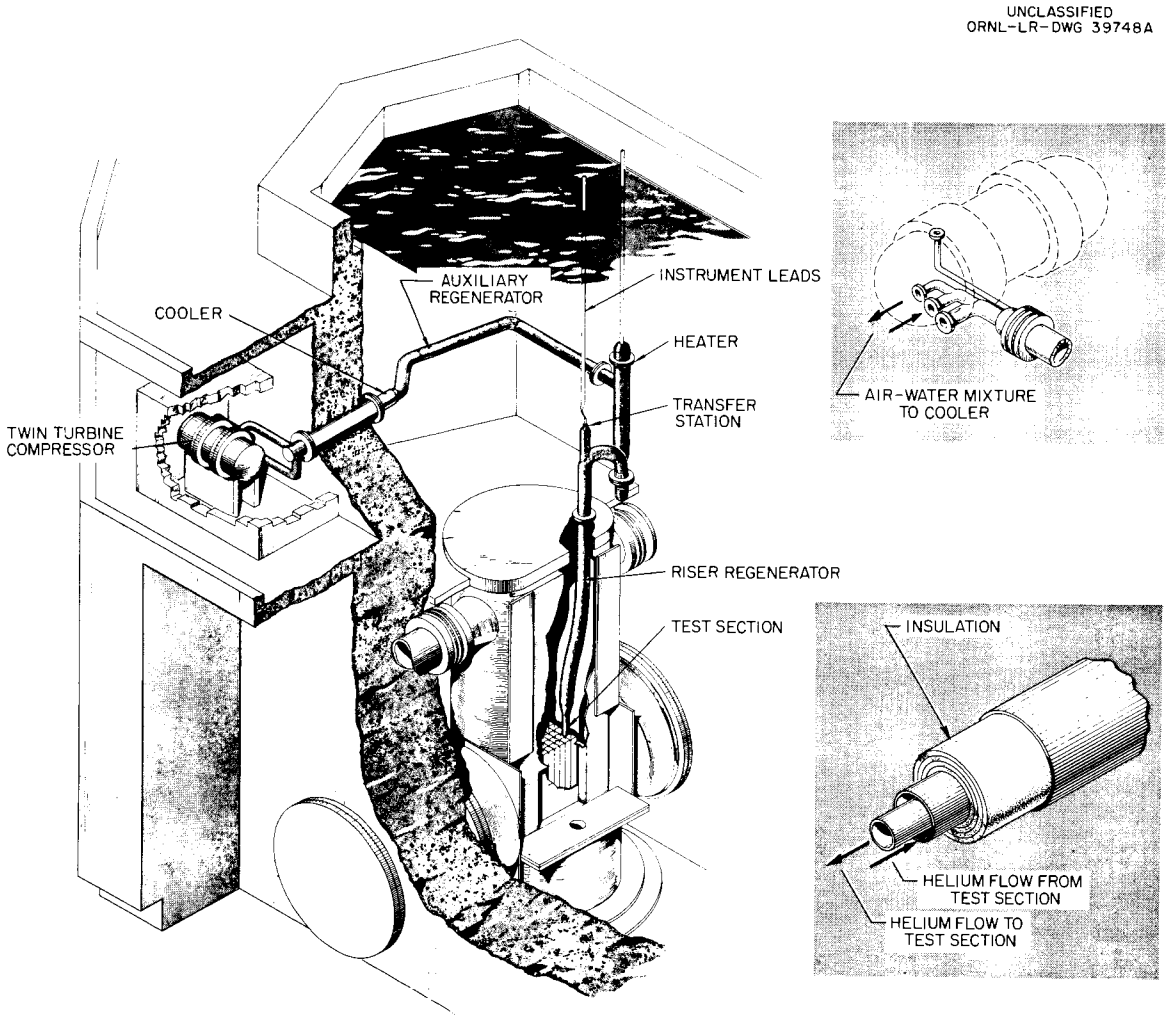

Fig. 7.1. Arrangement of GCR-ORR Loop No. 1 in ORR.

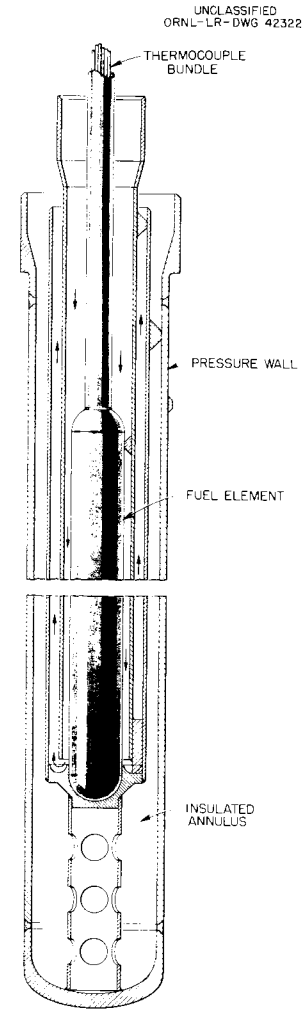

Fig. 7.2. Detail of Test Section of GCR-ORR Loop No. 1.

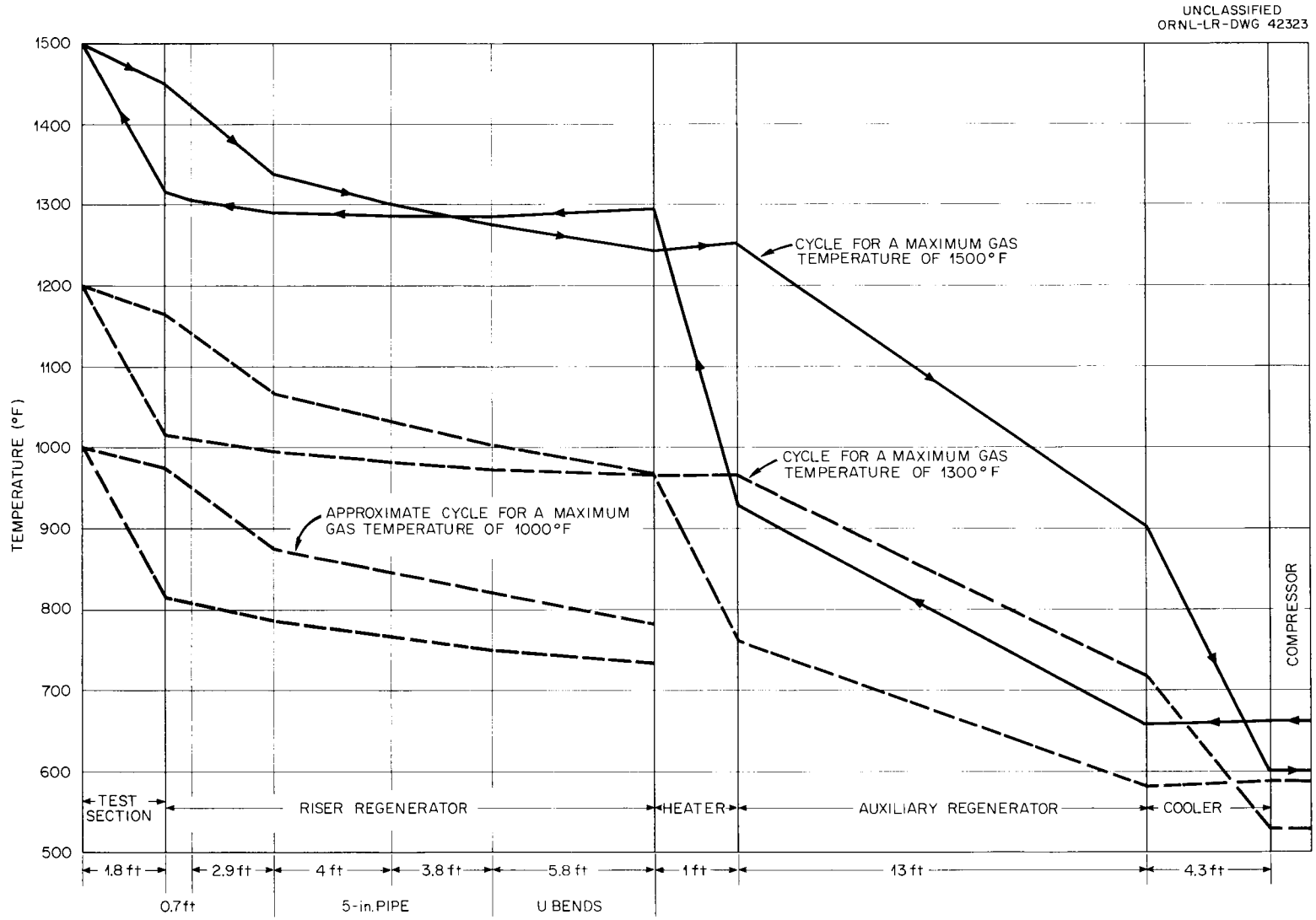

Fig. 7.3. Temperature Profiles of GCR-ORR Loop No. 1.

serve as an intermediate step in the selection of unclad fuel systems for future testing in EGCR experimental loops. A flow diagram of the loop is shown in Fig. 7.4. The loop is being designed for operation in the large south beam hole of the ORR.

Operation of the loop will provide data on the production of fission products in unclad fuel elements, their release from the fuel element, and their behavior after release into the gas stream. Information will be obtained on fission-product deposition and on gas stream activation. Techniques for activity level control (for example, cleanup of recycle side streams) and semiremote methods for maintenance, replacement, and decontamination of equipment will be studied. Tests of the unclad fuel elements under various simulated reactor operating conditions will also provide information on the mechanical and thermal stability of unclad fuel elements and fuel materials.

Special Gas Compressors and Electric Motors

Grease-Lubricated Centrifugal Compressors

As mentioned in the previous report,[5] the impeller of the grease-lubricated centrifugal compressor (HECC-1) rubbed against the casing during the second cold shakedown test. Therefore several running clearances were increased, that is, those between the bearing races and grease shields, between impeller and labyrinth at the suction plate, and between impeller periphery and main housing; procedures for assembling the unit were revised; provisions were made for checking all critical clearances; and the compressor was reassembled. The unit was given a cold shakedown test and then installed in the hot-test loop. The pressure vessel which encapsulates the compressor was seal-welded at the girth joint to attain a positive seal.

Compressor performance data were taken at several impeller speeds and at (1) 240 psig and 170°F and (2) 400 psig and 600°F. Curves of

[5] GCR Semiann. Prog. Rep. July 30, 1959, ORNL-2767, p 206.

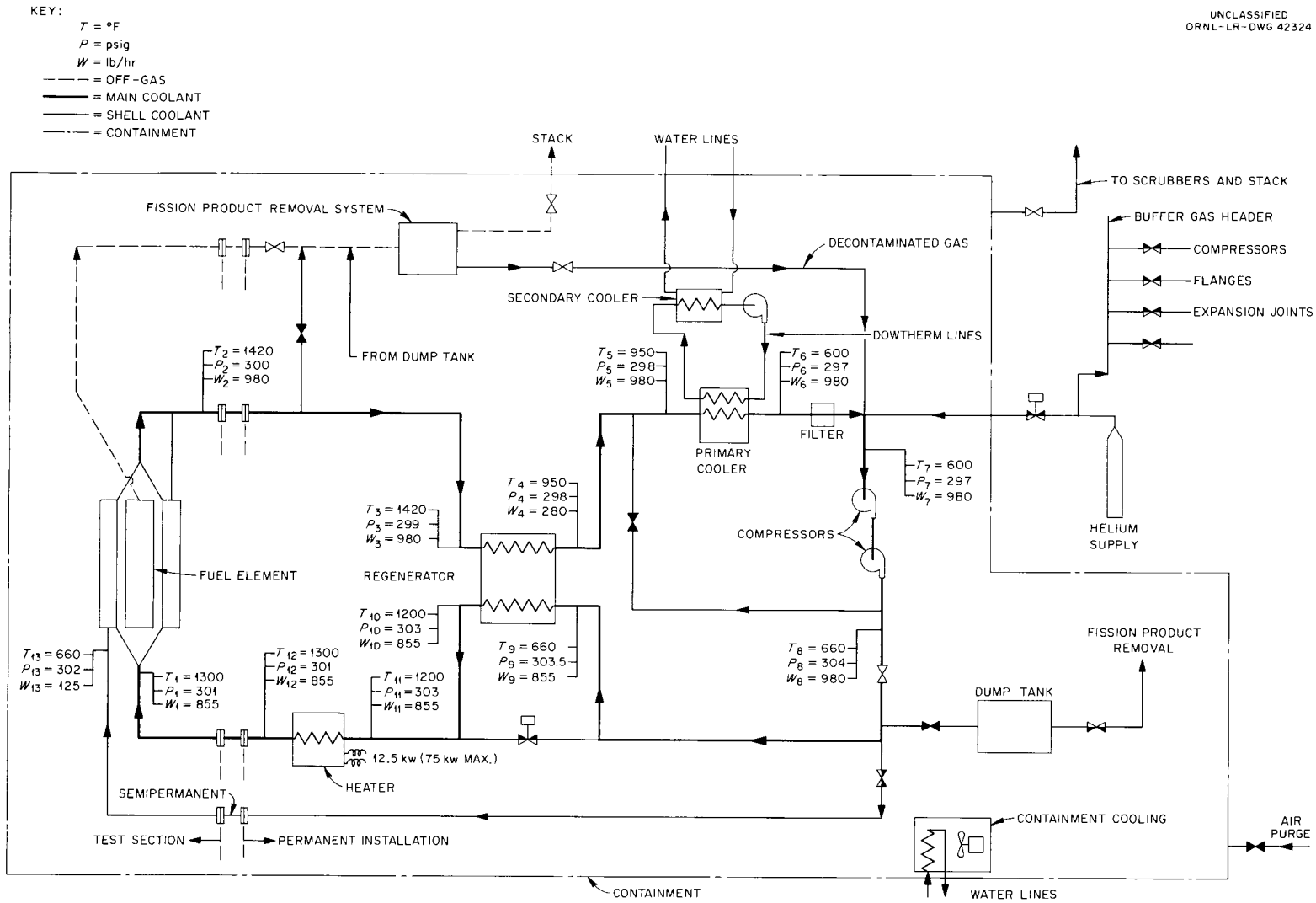

Fig. 7.4. Preliminary Flow Diagram of GCR-ORR Loop No. 2.

head vs flow for various impeller speeds are given in Figs. 7.5 and 7.6. The hot test was continued for 456 hr until halted by a failure of the overvoltage protection device in the electrical supply. During the shutdown, modifications were made to the loop to conserve helium and to provide additional loop heater capacity. The endurance test of the compressor at 400 psig and 600°F suction will be resumed after completion of the modifications.

Regenerative Compressors

The first unit of the regenerative gas compressor (HECT-2, Fig. 7.7) for use in the ORR-GCR in-pile loop was assembled, operated in a cold shakedown test stand, and is presently being prepared for test operation at 600°F. Prior to assembly, a detailed assembly procedure was prepared in which actual dimensions and measurements of the compressor components were recorded and compared with the assembly drawing dimensions.

The impeller disk in this type of compressor is separated from the casing by small running clearances that are established during assembly. As the suction temperature increases, the impeller and casing are subject to relative motion in the axial direction from the common anchor point, the front bearing, which is caused by the difference in thermal expansion of the shaft and of the casing support. In order to measure the impeller-to-casing running clearances (0.003 to 0.015 in.) under dynamic conditions (speed, temperature, pressure, and load) four capacitance probes were installed. The probes were mounted about 90-deg apart on both the front and back impeller housings. A discrepancy of approximately 0.001 in. was noted between the capacitance readout and feeler gage readings in the measurement of impeller-casing clearance at zero speed. Both measurements indicated the axial runout of the impeller face to be approximately 0.0005 in. Measurements of impeller running clearances at 600°F with capacitance probes should be adequate to forewarn of impending rubbing and to indicate the proper distribution of axial running clearance for assembly procedures.

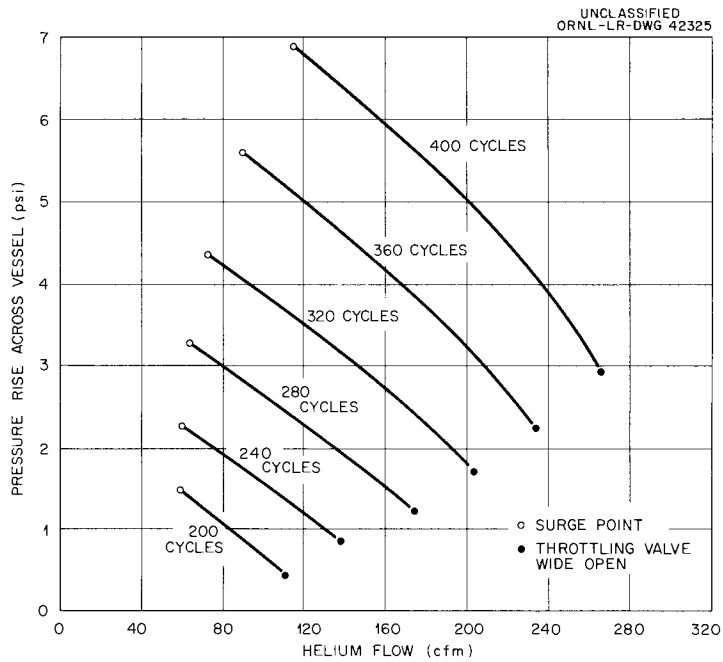

Fig. 7.5. Performance Data for a Grease-Lubricated Centrifugal Compressor (HECC-1) Operating With Helium (Density, 0.1507 lb/ft^3) at 170°F and 240 psig at Various Impeller Speeds.

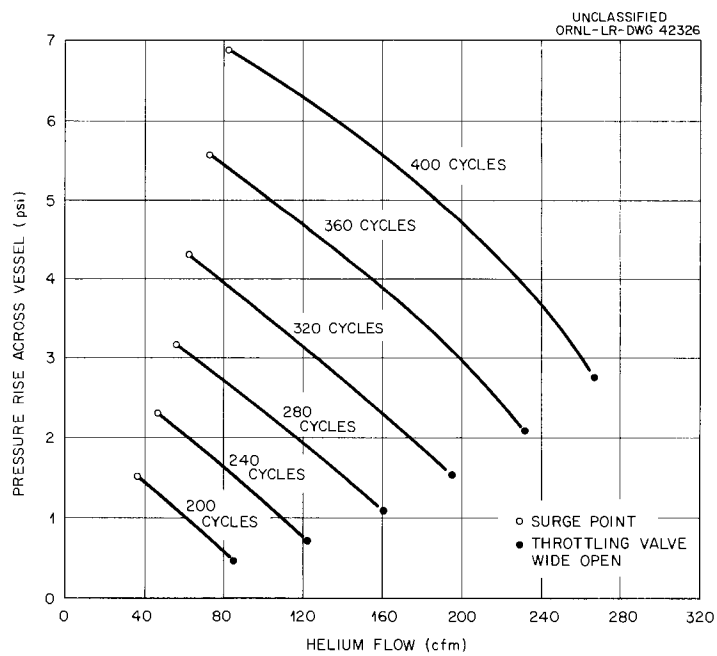

Fig. 7.6. Performance Data for a Grease-Lubricated Centrifugal Compressor (HECC-1) Operating With Helium (Density, 0.1457 lb/ft^3) at 600°F and 400 psig at Various Impeller Speeds.

Several preliminary cold test runs with the compressor in the vertical position (impeller up) were made in air at impeller speeds from 6,000 to 12,000 rpm. The compressor operated satisfactorily over this range of speed. Extrapolation of the cold-test data indicated relative axial movement between casing and impeller of 0.0095 to 0.010 in.

Preparations are under way to install the first unit in the hot-test loop (horizontal orientation) to check out the effect of cantilever support on mechanical performance and to obtain running clearance and aerodynamic data at suction conditions of 300°F and 600°F at 400 psia. The second unit (the first A-Tool and Gage Co. unit) is being assembled. Fabrication of the other three units at A-Tool and Gage Co. has been delayed about three weeks because of labor difficulties, which have been resolved. The tentative delivery data for the first of these three units has been set as the second week of November 1959.

Compressors with Gas-Lubricated Bearings

A gas-bearing tester is being assembled, and design work has been started on a loop for testing the compressor ordered from Bristol-Siddeley Engines, Ltd. The bearing load and torque measuring system (strain gages) for the gas-bearing tester have been assembled, and the readout system for the strain gages is being assembled and calibrated. The eccentricity of the bearing with respect to the journal will be measured by using capacitance gages. The gas-bearing tester will first be used to check load-carrying capacity computations and whirl characteristics for the bearings of a tester for high-temperature electric motors.

The test loop for the Bristol-Siddeley compressor is being designed to operate with the design mass flow at suction temperatures ranging from 150 to 1000°F and pressures up to 400 psia. The compressor was assembled and operated at 3000 rpm under atmospheric conditions by Bristol-Siddeley.

Electric Motors for High-Temperature Service

Two sizes of electrical motors having stators equipped with ceramic insulation are available for high-temperature testing. One size is rated 12 hp, 24,000 rpm, 3 phase, and the other is rated 1 hp, 3600 rpm, 3 phase. A tentative test program includes building a tester locally for long-term tests and obtaining proposals from the manufacturer and two firms concerned with producing gas-lubricated bearings for short-term testing.

A design layout (Fig. 7.8) for a long-term tester for the 12 hp motor has been completed and detailed designing started. The tester will provide for operation in helium at temperatures ranging from 60 to 1000°F, and pressures ranging from 15 to 30 atm. The Louis-Allis Company of Milwaukee, Wisconsin, is studying a method for performing a short-term test to determine motor characteristics at room temperature and at 600°F in air of the 12-hp motor. Analogue Controls, Inc., and Tribonetics, two firms that produce gas-lubricated bearings, have been requested to study methods for determining the motor characteristics of the 1-hp motor in helium at room temperature and 600°F.

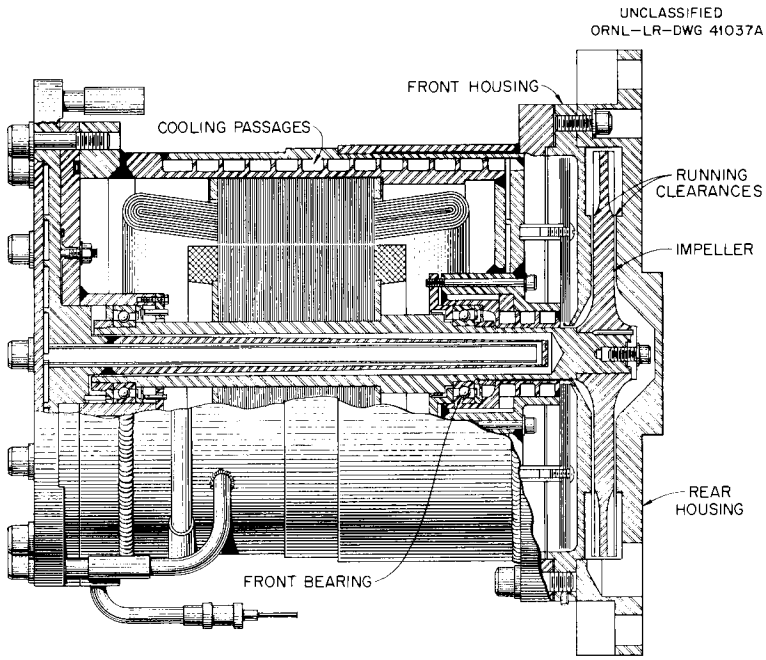

Fig. 7.7. Regenerative Gas Compressor (HECT-2).

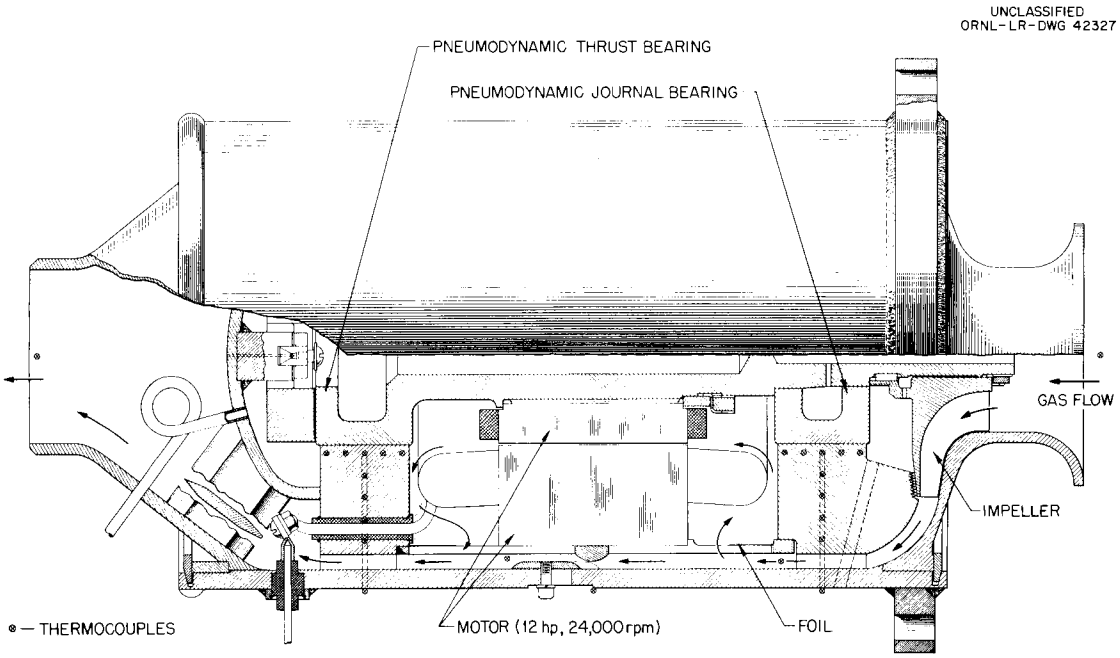

Fig. 7.8. Diagram of GABE-1 Compressor.

ORNL-2835

Reactors – Power
TID-4500 (15th ed.)

INTERNAL DISTRIBUTION

1. J. W. Allen
2. S. A. Beall
3. M. Bender
4. D. S. Billington
5. E. P. Blizard
6. A. L. Boch
7. C. J. Borkowski
8. W. F. Boudreau
9. G. E. Boyd
10. E. J. Breeding
11. R. B. Briggs
12. C. E. Center (K-25)
13. R. A. Charpie
14. T. E. Cole
15. J. H. Coobs
16. J. A. Conlin
17. W. B. Cottrell
18. J. A. Cox
19. F. L. Culler
20. H. N. Culver
21. J. H. DeVan
22. L. M. Doney
23. D. A. Douglas
24. L. C. Emerson
25. L. B. Emlet (K-25)
26. E. P. Epler
27. H. L. Falkenberry
28. J. Foster
29. A. P. Fraas
30. J. H. Frye, Jr.
31. G. A. Garrett (K-25)
32. J. M. Googin (Y-12)
33. B. L. Greenstreet
34. W. R. Grimes
35. E. Guth
36. R. F. Hibbs (Y-12)
37. M. R. Hill
38. H. W. Hoffman
39. A. Hollaender
40. A. S. Householder
41. W. H. Jordan
42. P. R. Kasten
43. C. P. Keim
44. M. T. Kelley
45. J. J. Keyes
46. R. B. Korsmeyer
47. J. A. Lane
48. S. A. Levin (K-25)
49. R. S. Livingston
50. H. G. MacPherson
51. W. D. Manly
52. E. R. Mann
53. H. C. McCurdy
54. W. B. McDonald
55. H. F. McDuffie
56. F. R. McQuilkin
57. H. J. Metz
58. A. J. Miller
59. J. G. Morgan
60. K. Z. Morgan
61. J. P. Murray (Y-12)
62. F. H. Neill
63. M. L. Nelson
64. L. G. Overholser
65. P. Patriarca
66. F. S. Patton (Y-12)
67. A. M. Perry
68. D. Phillips
69. M. E. Ramsey
70. P. M. Reyling
71. M. W. Rosenthal
72. A. F. Rupp
73. G. Samuels
74. H. W. Savage
75. A. W. Savolainen
76. O. Sisman
77. E. D. Shipley
78. M. J. Skinner
79. A. H. Snell
80. E. Storto
81. R. D. Stulting
82. C. D. Susano
83. J. A. Swartout
84. E. H. Taylor

85. D. B. Trauger
86. E. Von Halle (K-25)
87. C. S. Walker
88. J. L. Wantland
89. A. M. Weinberg
90. J. C. White
91. E. A. Wick
92. G. C. Williams
93. C. E. Winters
94. J. Zasler
95-98. ORNL – Y-12 Technical Library
Document Reference Section
99-168. Laboratory Records Department
169. Laboratory Records Department, ORNL R.C.
170-172. Central Research Library

EXTERNAL DISTRIBUTION

173. Richard Kirkpatrick, AEC, Washington
174. Donald Stewart, AEC, Washington
175. Division of Research and Development, AEC, ORO
176-178. W. F. Banks, Allis-Chalmers Mfg. Co.
179-181. P. D. Bush, Kaiser Engineers
182-183. H. Lichtenburger, General Nuclear Engineering Corp.
184. H. B. Rahner, Savannah River Operations Office
185-186. W. L. Webb, East Central Nuclear Group. Inc.
187-763. Given distribution as shown in TID-4500 (15th ed.) under Reactors – Power category (75 copies – OTS)

Previous reports in this series are:

ORNL-2500	Parts 1-4, issued April 1, 1958
ORNL-2505	Issued June 19, 1958
ORNL-2510	Issued September 18, 1958
ORNL-2676	Period Ending December 31, 1958
ORNL-2767	Period Ending June 30, 1959